A CHEMICAL STUDY OF THE SILICATE MINERALS OF THE GREAT GOSSAN LEAD AND SURROUNDING ROCKS IN SOUTHWESTERN VIRGINIA

by

Walter Thomas Staten

Thesis submitted to the Graduate Faculty of the

Virginia Polytechnic Institute and State University

in partial fulfillment of the requirements for the degree of

MASTER OF SCIENCE

in

Geological Sciences

APPROVED:

Dr. D.A. Hewitt, Chairman

Dr. M.C. Gilbert

Dr. L.T. Taylor

Dr. J.R. Craig

December, 1976
Blacksburg, Virginia

ACKNOWLEDGEMENTS

This research was supported in part by the Earth Sciences Section, National Science Foundation, NSF Grant DES74-22499 to D.A. Hewitt, and is gratefully acknowledged. Special assistance from Professor D.A. Hewitt in the form of many fruitful discussions and for serving as my committee chairman is also appreciated. M.C. Gilbert, J.R. Craig and L.T. Taylor are also acknowledged in their capacity as members of my committee and for critically reviewing the manuscript. My wife, Ruth Erwin Staten is also acknowledged for her patience and encouragement, without which this study would not have been completed.

TABLE OF CONTENTS

Introduction

Sulfide-silicate equilibria have been the subject of several recent investigations. Qualitative aspects of sulfide-silicate relationships were described by Kullerud and Yoder (1963, 1964). Quantitative equilibrium studies have been published on Fe-Ni olivines - Fe-Ni monosulfide solid solution (Naldrett and Brown, 1968); pyroxene-pyrrhotite (Naldrett and Brown, 1968); biotite-pyrrhotite (Hammarback and Lindquist, 1972; Tso and Gilbert, 1976); and amphibole-pyrrhotite (Popp and others, 1974; Popp, 1975).

Sulfide-silicate relationships suggested by the experimental studies have assisted in the determination of the origin, emplacement, and metamorphism of sulfide ore bodies. Studies published on sulfide-silicate interactions in some natural sulfide ore bodies include Naldrett (1966), Fullagar et al (1967), Craig and Gilbert (1974), and Staten and Hewitt (1976). The current study was undertaken in order to document the extent of the sulfidation of silicates around the Great Gossan Lead in southwestern Virginia, and to place some limits on the conditions of ore emplacement.

The Great Gossan Lead district in Carroll and Grayson counties in southwestern Virginia, is a zone of massive pyrrhotite ore deposits that Kinkel (1967), and Ross (1935) considered to be similar to a number of other massive sulfide ore deposits in the Appalachians. Figure 1, from Kinkel (1967), shows the location of a number of these deposits.

Two cores that penetrate a portion of the Gossan Lead, numbered 117 and 142, and drilled by Freeport Sulfur Company, were made available to the Department of Geological Sciences at Virginia Polytechnic

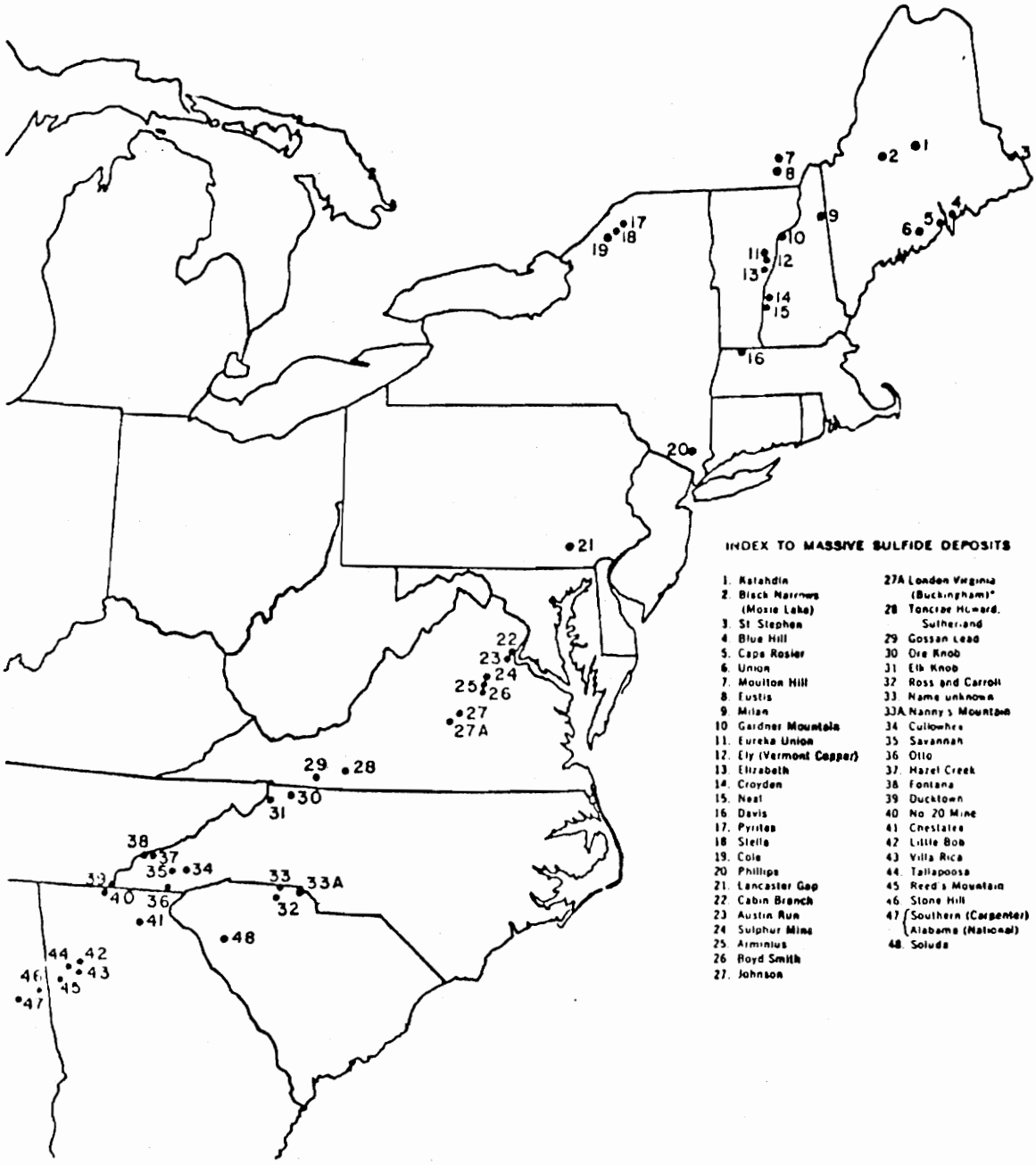

Figure 1. Massive sulfide deposits in the Appalachians (from Kinkel, 1967.

Institute and State University by Freeport Sulfur Company for detailed petrologic studies. The locations of these two cores are shown on figure 2. Both cores appear to have penetrated the Ashe formation at nearly right angles to the foliation. Samples were taken from both cores and analyzed petrographically. Microprobe analyses of the major silicate minerals were conducted on selected samples with special attention placed on the ferromagnesian minerals occurring in the ore as well as the country rock.

Figure 2. Location map of the Great Gossan Lead in Carroll and Grayson counties, southwestern Virginia. Names of the individual segments are A) Betty Baker, B) Little Vine, C) Reed Island, D) Cranberry, E) Wildcat, F) Sarah Ellen, G) Copperas, H) Chestnut Creek, I) The Great Outburst.

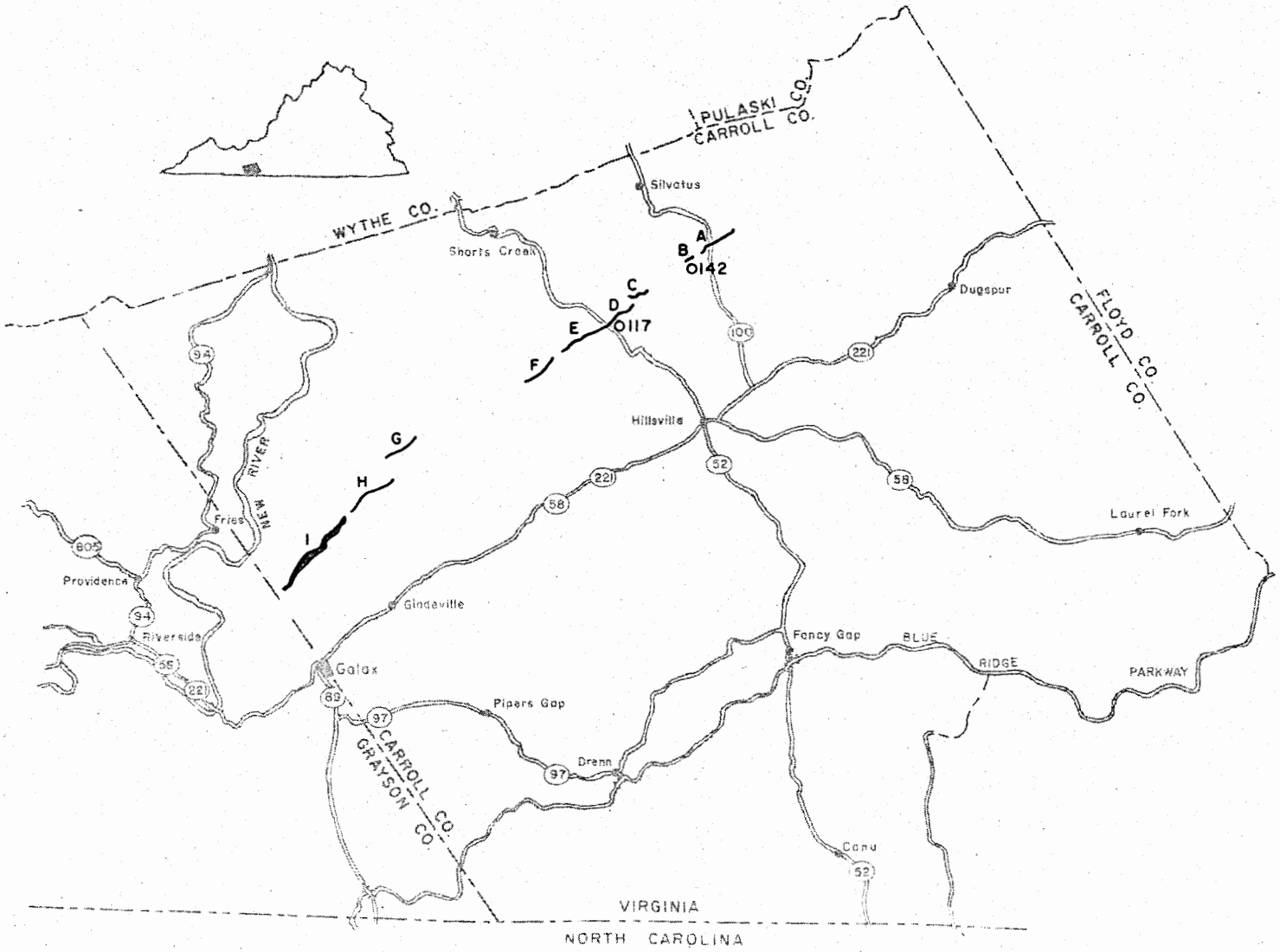
PULASKI CO.
CARROLL CO.
WYTHE CO.
Silvatus
Shorts Creek
A
B
0142
C
D
E
0117
F
G
H
I
Dugspur
FLOYD CO.
CARROLL CO.
Hillsville
Fries
NEW RIVER
Providence
Riverside
Galax
Gladeville
Laurel Fork
Fancy Gap
BLUE RIDGE PARKWAY
Pipers Gap
Drenn
CARROLL CO.
GRAYSON CO.
Cana
VIRGINIA
NORTH CAROLINA
94
100
221
58
52
59
805
55
89
97

Previous Work

C. R. Boyd (1881), in his description of the geology and mineral resources of Carroll and Grayson counties, described the pyrrhotite lodes, calling them the "Great Northern Lode." In other early studies of the area, T. L. Watson (1907) described the copper mines along the Gossan Lead, and R. O. Curry (1907) discussed the general geology of the area. C. S. Ross (1935) related the Gossan Lead to similar ore bodies occurring in the Blue Ridge province of the southern Appalachians. The most complete study of the area was published by Stose and Stose (1957). In their lengthy volume, Stose and Stose described the geography, stratigraphy, structural geology, and economic geology of the Great Gossan Lead district. These early investigators believed that the Great Gossan Lead ore body resulted from hydrothermal solutions localized along shear zones formed after the major metamorphism of the area. More recently, Rankin (1970) and Rankin et al (1973), have described the general geology of much of southwestern Virginia and northwestern North Carolina, including the Gossan Lead district. Recent studies of the ore zone, and, in particular, the relations between the ore and the country rock, have been published by Craig et al (1971), Henry et al (1976), and Staten and Hewitt (1976).

A fairly detailed chemical study of wallrock alteration has been conducted by Fullagar et al (1967) on the Ore Knob sulfide deposit in North Carolina; a deposit similar in occurrence, form, and mineralogy to the Great Gossan Lead.

General Geology

The Great Gossan Lead of Carroll and Grayson counties in southwestern Virginia, occurs as podiform deposits roughly conformable with the foliation of the enclosing schists and gneisses of the Ashe formation. As early as 1927, A. Jonas, mapping in northern Virginia, suggested that the Lynchburg formation of that area may be equivalent to the Carolina Gneiss in North Carolina (Jonas, 1927). Fullagar and Dietrich (1976) considered the Lynchburg formation of Virginia, the Ashe formation of North Carolina and Virginia, and the Great Smokey Group of the Ocoee Supergroup in Tennessee and North Carolina to all be at least in part correlative. Rankin (1970), in his definition of the Ashe Formation, considered the Ashe formation at least in part correlative with the Lynchburg formation. However, he defined the Ashe formation as a new formation because of the large unmapped region between Lynchburg, Virginia, and Ashe county, North Carolina, and because the Ashe formation may also include rocks correlative with units overlying the Lynchburg. For the same reasons, this study uses the terminology of Rankin (1970). Formation names for the rocks enclosing the Gossan Lead that are now considered obsolete include the Carolina Gneiss and the Roan Gneiss (Keith, 1903).

The Ashe formation near Galax and Sylvatus, Virginia, is predominately metagreywacke, metapelite, minor amphibolite layers, and rare thin marble lenses. It is similar to the descriptions of the Lynchburg by Brown (1958), and the description of the Ashe formation by Rankin (1970) and Rankin et al (1973). The majority of the rocks are fine- to medium-grained phyllites, schists, gneisses, and some quartzite. The

mineralogy of the schists and gneisses around Sylvatus does not change significantly. However, the modal compositions, as indicated in table 1, show significant variability. Mild lithologic variations observed in the schists and gneisses are consistent with what can be expected from the metamorphism of relatively rapidly accumulated clastic sediments with comparatively minor deposits of volcanic origin.

Rankin et al (1973, figure 3) show the metamorphism of the Ashe formation as increasing from biotite grade near Fries and Sylvatus, through staurolite and kyanite grades, and reaching sillimanite grade south of Stuart, Virginia. The isograds roughly parallel the northeast-southwest structural trend.

The Fries Thrust Fault forms the northwestern boundary of the Gossan Lead district (Stose and Stose, 1957). Large-scale thrust faulting displaced the Precambrian metasedimentary and plutonic rocks of the Blue Ridge and the Paleozoic sedimentary rocks of the Valley and Ridge to the northwest (Rankin et al, 1973). Rankin et al (1973) reports a minimum of 65 km of displacement along the Fries Thrust, thrusting the rocks of the Blue Ridge over Valley and Ridge province sedimentary rocks. The age of the thrusting is probably late Paleozoic and after the peak of regional metamorphism since some isograds are displaced by the thrust faults (Rankin et al, 1973).

K-Ar and Rb-Sr isotopic studies (Kinkel et al, 1965; Fullagar and Bottino, 1970; and Fullagar and Dietrich, 1976) conducted on some Appalachian sulfide ore bodies included samples from the Gossan Lead. These studies indicate dewatering or metamorphic events at 520-583 million years and 350-402 million years, correlating with the Virgilina and/or

Figure 3. Metamorphic map of the Winston-Salem 2° sheet showing the location of the Great Gossan Lead (adapted from Rankin et al, 1973).

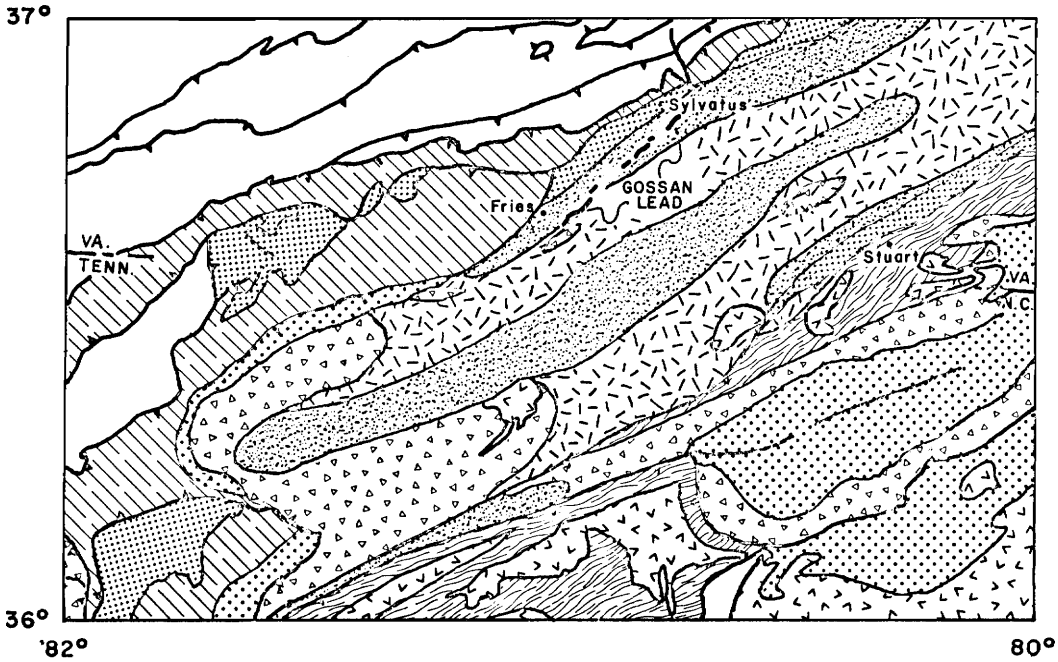

Paleozoic Igneous Rocks

Undifferentiated Metamorphic Facies

Greenschist

Amphibolite

0 20
Miles

0 30
Kilometers

Zones of Paleozoic Regional Metamorphism

Weakly to nonmetamorphosed

Biotite

Garnet

Staurolite

Kyanite

Sillimanite

Avalonian deformation and the mid-Paleozoic Acadian Orogeny respectively (Fullagar and Dietrich, 1976).

Analytical Methods

Thin sections of 109 samples from the two cores were studied using standard transmitted-light petrographic techniques. Modal analyses of 800-1000 counts per analysis were made on selected samples From these samples, a number of polished thick sections were made for investigations by reflected-light ore microscopic techniques, and electron microprobe analysis.

Electron microprobe analyses were made using the Krisel Control automated three-channel ARL-EMX microprobe at Virginia Polytechnic Institute and State University. The average of three to five analyses with ten second counting time on each element per mineral grain were made at 15 kV operating potential, 0.150 mA beam current, and a focused beam of approximately 5-10 microns in diameter. Well-characterized silicates were used as standards. Data were reduced according to the method of Bence-Albee (1968). Formulae were calculated by the SUPERECAL computer program of Rucklidge (1971) with H_2O calculations based on the number of hydrogen ions present in the idealized mineral formula.

Lithologies and Mineral Chemistry

The overwhelming majority of samples from both cores studied are sulfidic metagreywacke and metapelite schists, gneisses, and fels of slightly varying composition. Most are quartz-muscovite schists with varying amounts of garnet, biotite, chlorite, and plagioclase. Other lithologies include the massive sulfide ore of the Great Gossan Lead, hornblendic amphibolite, and thin marble lenses.

Descriptions of the different lithologies are given below. Logs of both cores are given in detail in Appendix A and shown somewhat less completely in Fig. 4 . Modal analyses of a number of samples of each lithologic type are included in Table 1. Microprobe analyses of the minerals described are given in Appendix B.

Quartz-Muscovite Schists and Gneisses

Close to 90% of the rocks intercepted by both drill holes are fine- to medium-grained quartz-muscovite schists with well-developed schistosity. Modal analyses given in Table 1 indicate that quartz, plagioclase, and muscovite are virtually ubiquitous and generally quite abundant, with garnet, biotite and chlorite frequently occurring as major phases, but in varying quantities. Mica-rich bands of muscovite, biotite, and chlorite are often segregated with respect to nonmicaceous, quartz- and plagioclase-rich mineral bands. This banding rarely exceeds a quarter millimeter. Lithologic variations of the original greywacke and pelite are reflected by the distinct variation in the relative amounts of the major minerals, particularly quartz, muscovite, and plagioclase.

Muscovite forms discrete plates as well as more or less continuous bands or aggregates. Analyses of several characteristic muscovites

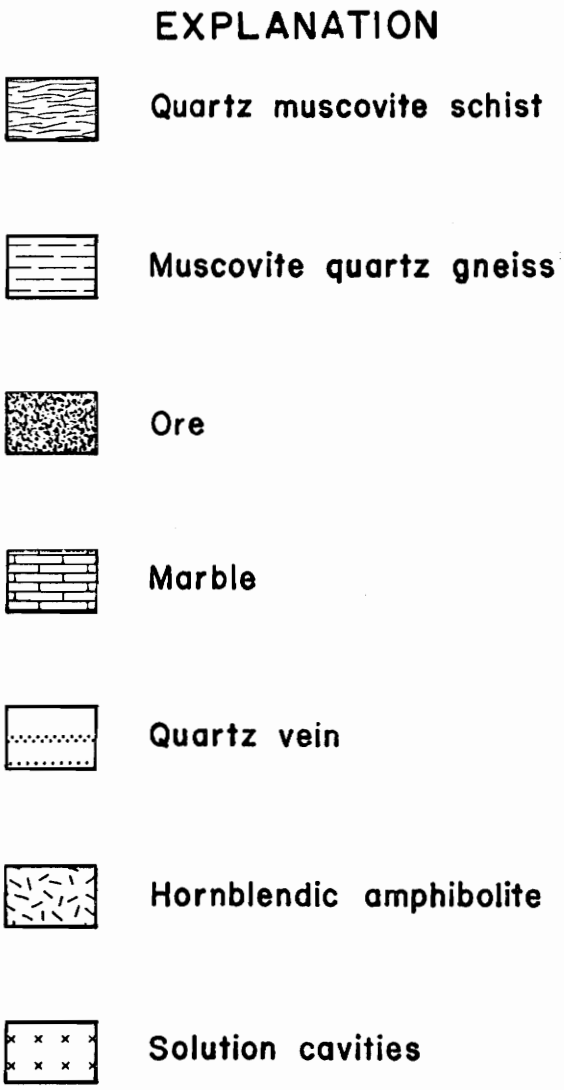

Figure 4A. Explanation of symbols used on the core logs

Figure 4B. Log of Core 117.

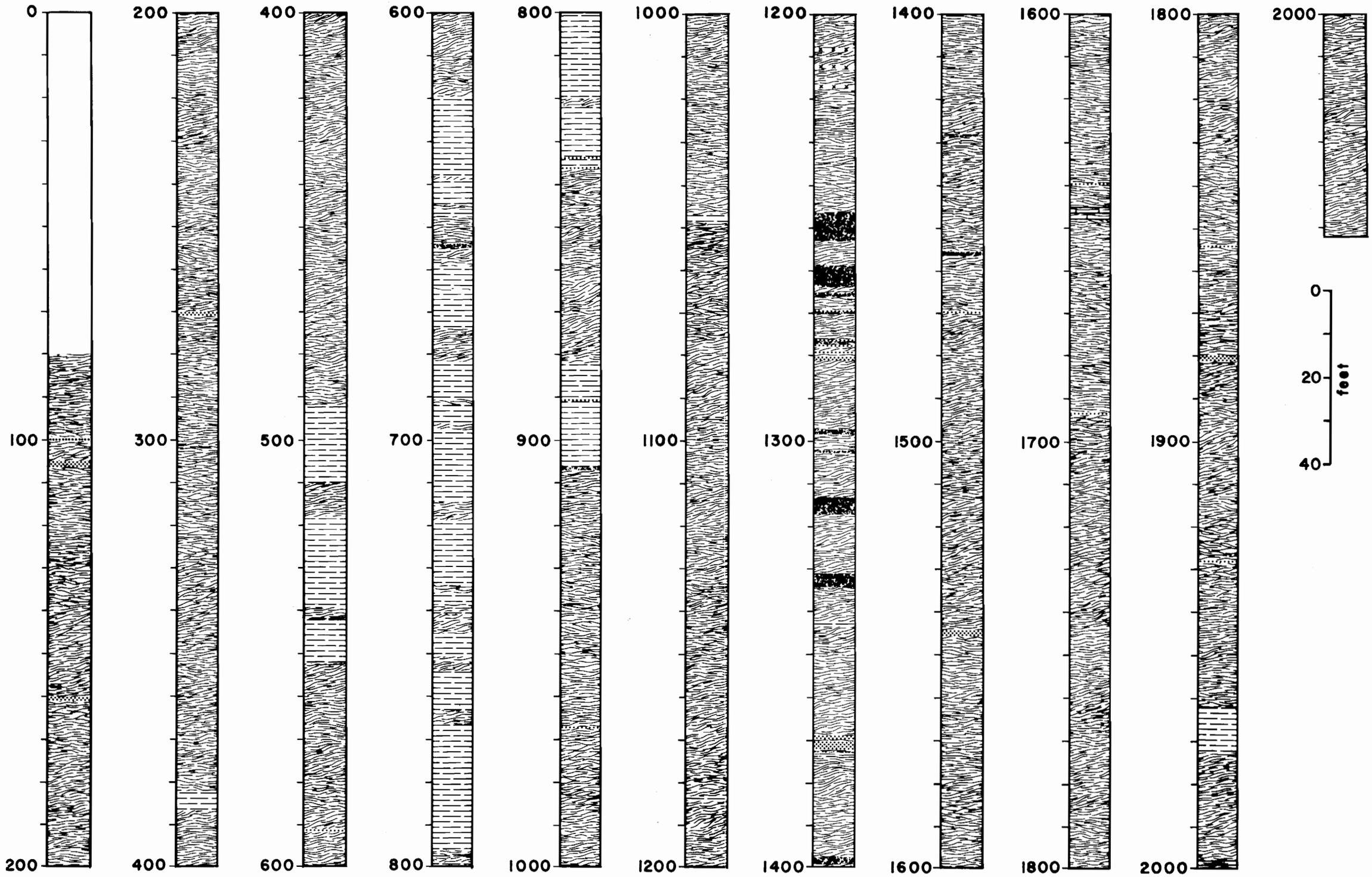
0
100
200
200
300
400
400
500
600
600
700
800
800
900
1000
1000
1100
1200
1200
1300
1400
1400
1500
1600
1600
1700
1800
1800
1900
2000
2000
0
20
40
feet

Figure 4C. Log of core 142.

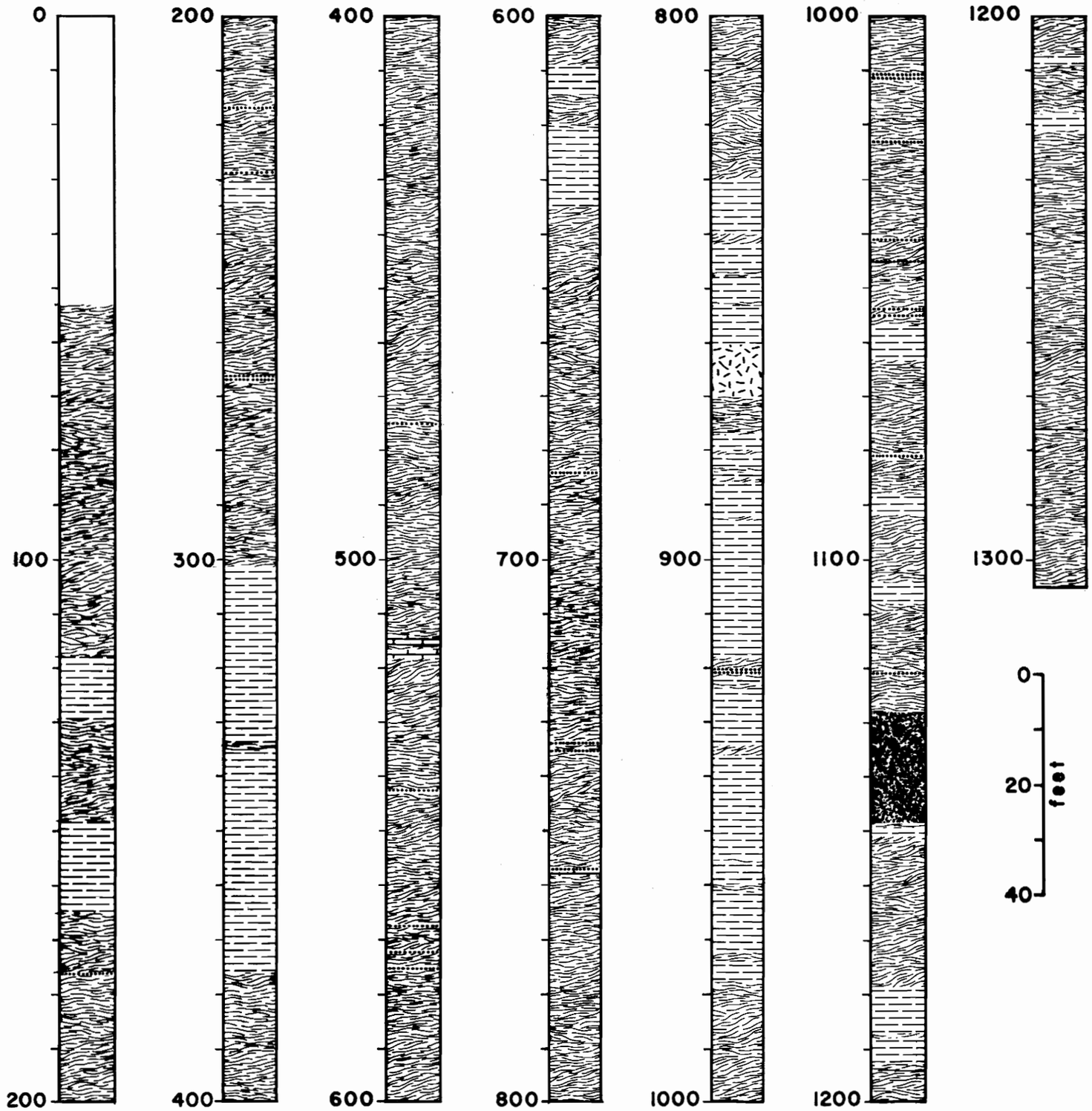
0
100
200
200
300
400
400
500
600
600
700
800
800
900
1000
1000
1100
1200
1200
1300
0
20
40
feet

Table 1 - Modal Analyses (%) of selected core samples

Sample Depth - Core 117

	494	654	822	1168	1178	1223	1238	1243	1249	1253	1271	1356	1376
Quartz	43	31	23	20	48	10	31	15	35	7	15	1	15
Muscovite	19	20	53	47	25	64	44	69	tr	2	1	81	50
Plagioclase	21	7	2	10	7	11	6	3	tr			1	17
Biotite	13	32	18	13	7	3	6	1	12	4	1	1	4
Chlorite	3	1	tr	6	8	7	8	7	26	32	19	7	11
Garnet	2	5	1	2	2	2	1	2	3			1	1
Opaques	1	3	1	1	2	3	4	4	24	51	59	1	2
Clinozoisite		1	2				1	1	tr				1
Apatite	tr	1	1	1	1	1	1	1		1	tr	1	1
Zircon	tr	tr	tr	tr	tr	tr	tr	tr	tr	tr	tr	tr	tr
Calcite										5	5	tr	
Sphene													
Amphibole										1			

Table 1 (continued)

Sample Depth - Core 142

	72	294	345	490	799	870	898	899	1094	1112	1149	1203	1265	977
Quartz	30	19	29	7	7	25	18	12	50	48	26	18	30	40
Muscovite	27	66	37	74	54	9	9	43	19	27	43		54	tr
Plagioclase	20	tr	7	7	5	27	61	14	11	8	4	35	3	29
Biotite	21	9	11	1	17	25	5	8	9	6	10	20	1	9
Chlorite	1	2	5	8	14	9	5	11	6	7	8	11	6	3
Garnet		1	9	2	1	1	1	2	3	2	2	8	1	1
Opaques	tr	4	2	2	2	1	1	10	2	2	7	1	6	1
Clinozoisite		1	1		1	7	1	1	1	1		7	1	1
Apatite	1			1		1			1	1	1		1	
Zircon	tr	tr	tr	tr	tr	tr	tr	tr	tr	tr	tr	tr	tr	
Calcite	1													
Sphene	1													
Amphibole														16

are given in Appendix B and are shown in figures 5 and 6. Muscovites contain a relatively low phengite component indicative of the near amphibolite facies assemblages observed in the region. Experimental work of Velde (1965) and field investigations of Butler (1967) indicate that phengitic micas are stable at low temperatures and relatively high pressures, breaking down to more aluminous muscovite, biotite, feldspar, and quartz with increasing temperature.

As in Butler's (1967) investigations in Scotland, the muscovites are deficient in alkalis; Na + K being significantly less than 2.00 in all samples (figure 6). Powder x-ray diffraction studies of muscovites from a number of samples indicate that there is only one mica present. Therefore, metamorphic temperatures must have exceeded the muscovite-paragonite solvus. Figure 6 shows the alkali content of analyzed muscovites as well as the temperature of coexisting muscovite-paragonite pairs as determined by Eugster et al (1972). From figure 5 it appears that temperatures of metamorphism must have been in excess of 400°C.

Quartz is anhedral and occurs in lenticular masses, in discrete bands with plagioclase, or as disseminated grains. Plagioclase is always anhedral and is generally untwinned or weakly-twinned. Mildly zoned plagioclase is occasionally noted. Some analyses of both the core and rim of a zoned plagioclase in sample 117-1223 indicate that this zoning is from a core of An_{24-25} to a rim of An_{18-21}. In the quartz-muscovite schists, plagioclase compositions vary from An_3 to An_{26} with an average composition of An_{20}. A very few samples also show a pronounced helicitic texture suggesting some post-deformational growth of plagioclase (Spry, 1969).

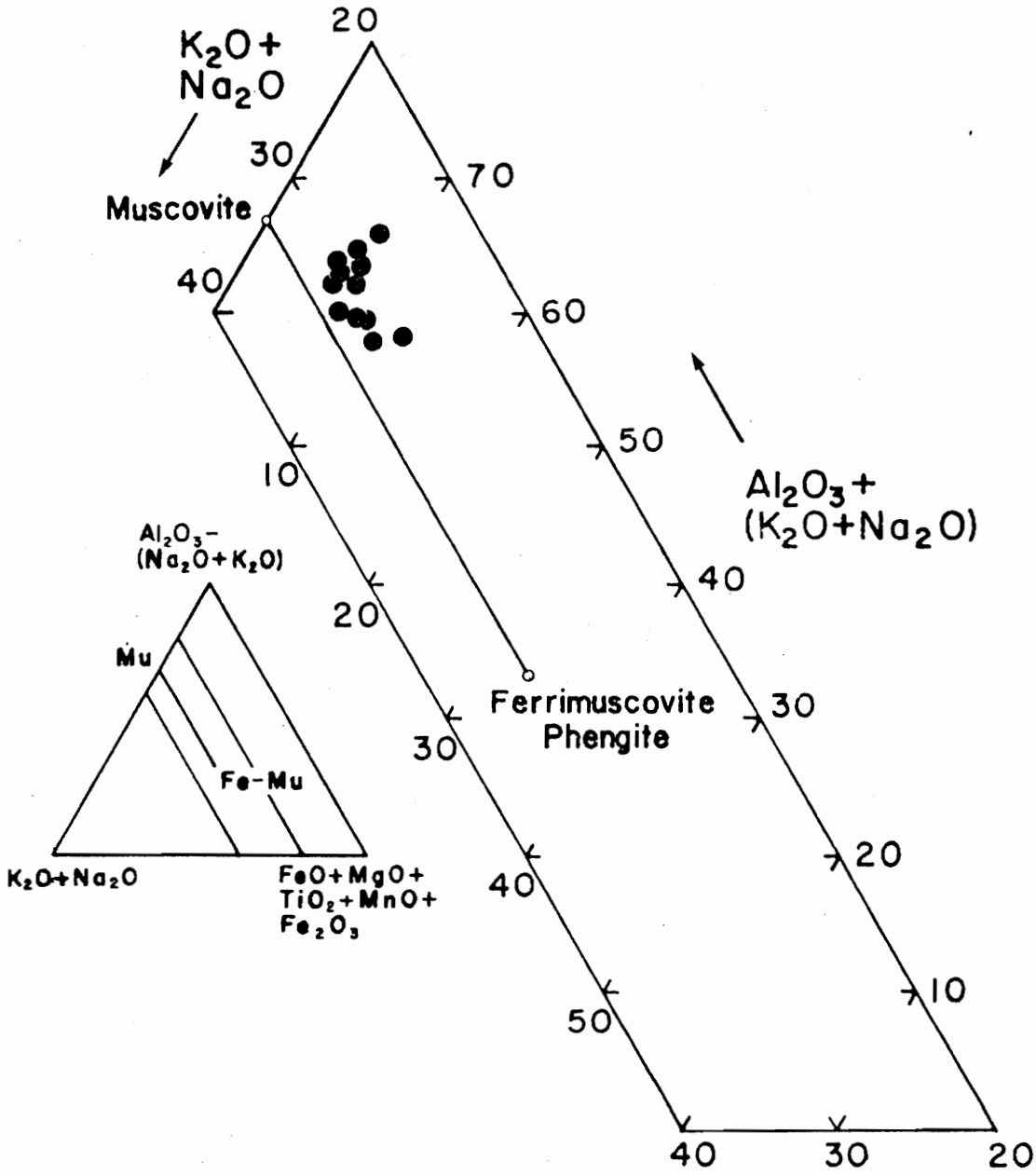

Figure 5. A modified AKF diagram showing the composition of muscovites from the Great Gossan Lead and surrounding schists.

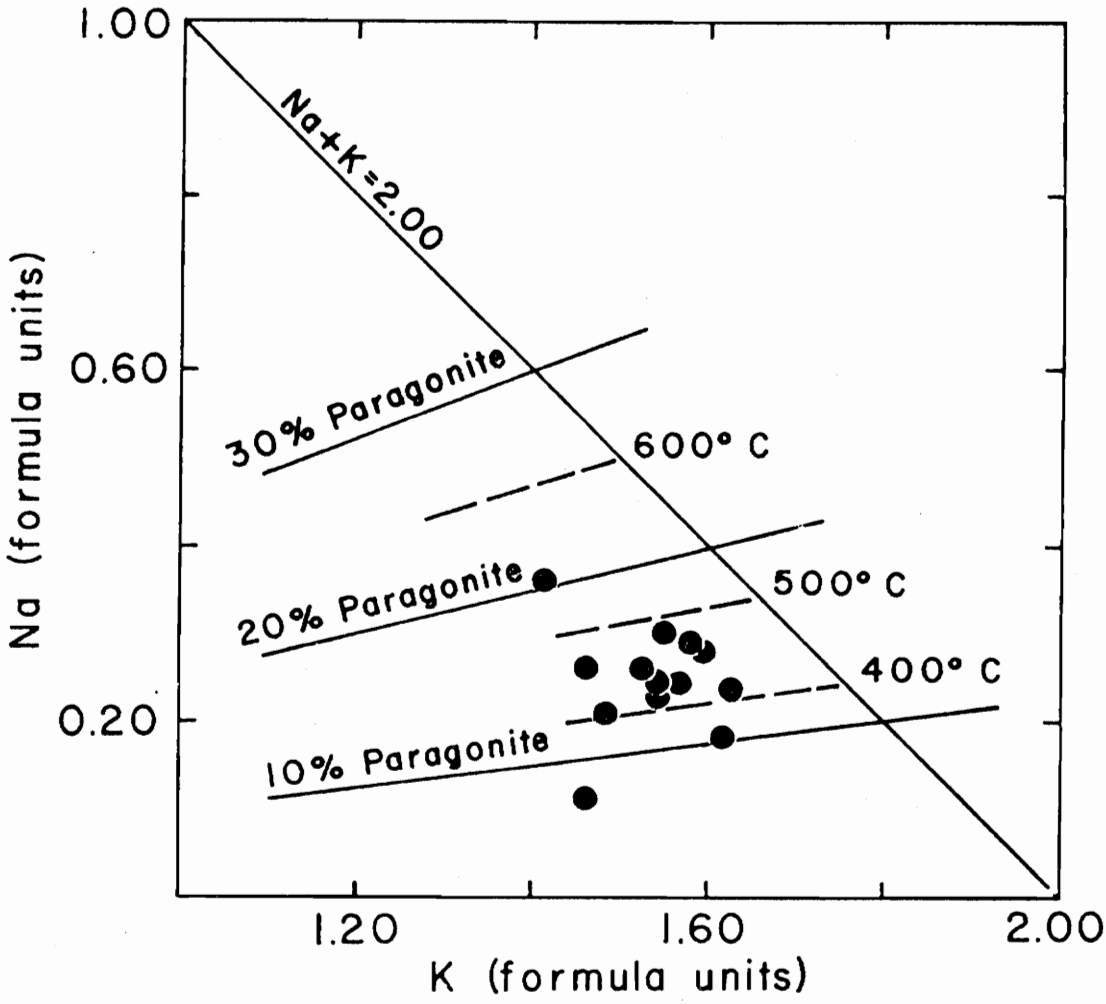

Figure 6. Paragonite content of muscovites in the Gossan Lead district. The temperatures of the solvus at 400°C, 500°C, and 600°C as determined by Eugster et al (1973) are also shown.

Chlorite is most frequently encountered as bent plates that appear to be primary, although some chlorite also occurs as an alteration of biotite and/or garnet. Chlorite greater than 2'-5' from the ore is generally moderately pleochroic green to clear. Chlorite in and near the ore or near apophyllite solution cavities is generally colorless in transmitted, plane-polarized light, and shows light, first-order grey interference colors. Figure 7 shows the variability in the composition of analyzed chlorites. While there is significant variation in the amount of Fe and Mg present, the Si content remains relatively constant. From this it is apparent that the chemical variation is due to simple Fe-Mg exchange reactions and not coupled with substitutions of other elements such as Al substituting for Si.

Garnets are nearly ubiquitous in the quartz muscovite schists throughout the length of both cores studied. They are occasionally euhedral, particularly in the more muscovite-rich samples. More frequently, however, the garnets are subhedral and occasionally anhedral. Quartz, chlorite, and clinozoisite are frequently poikiloblastically enclosed by garnet. Although most of the garnet is relatively fresh, some alteration to chlorite and/or clinozoisite has occurred. Garnet compositions are shown graphically on figure 8. The garnets show a relatively constant grossular component, but a significant variation in the almandine + pyrope and spessartine components. Each garnet has a relatively almandine-rich, spessartine-poor rim, and a spessartine-rich, almandine-poor core. Garnets from the country rock are relatively almandine-rich compared to the spessartine-rich garnets from the ore zone.

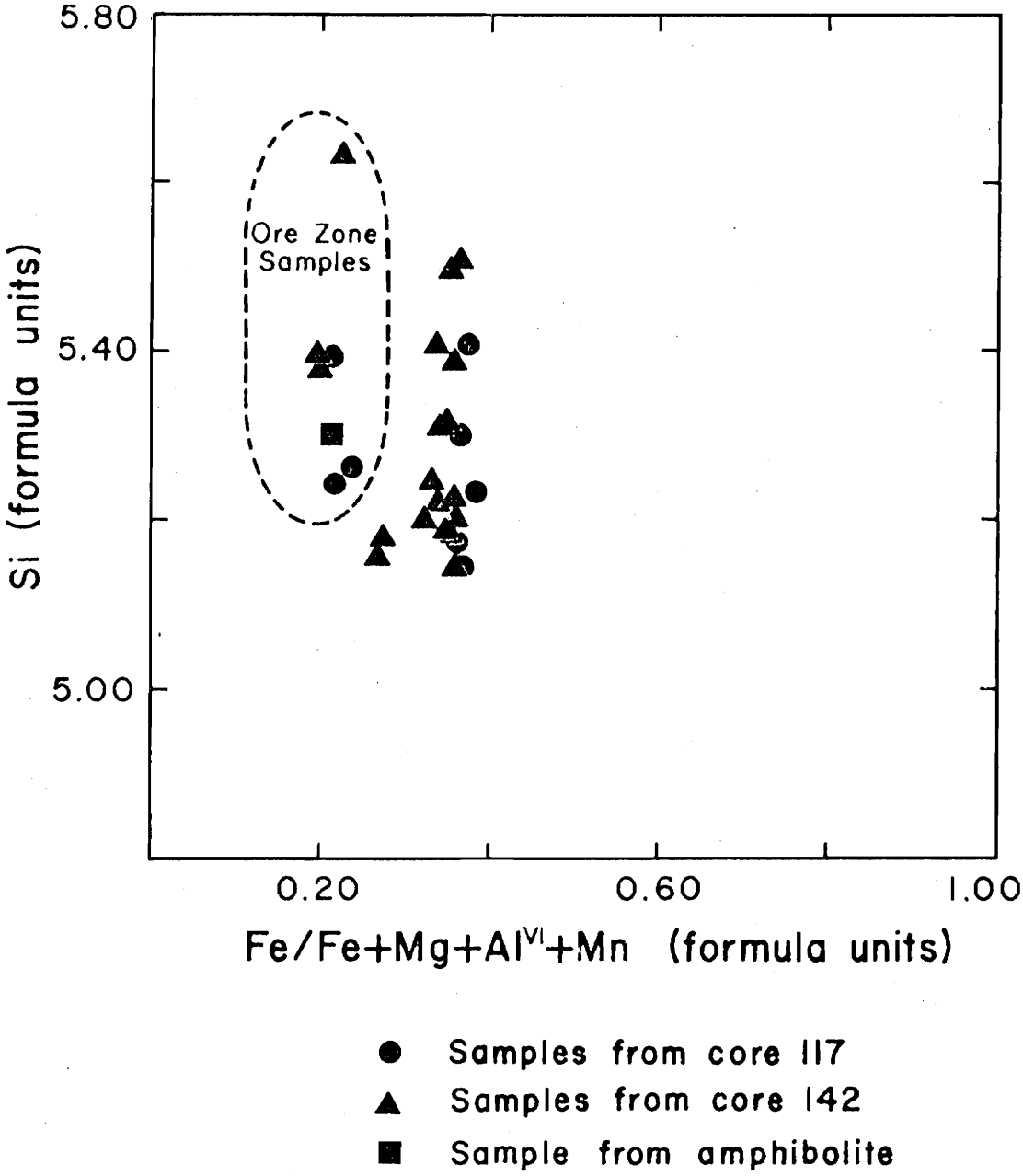

Figure 7. Compositions of chlorites from the ore zone and surrounding rocks of the Gossan Lead district and calculated on a 36 oxygen formula basis.

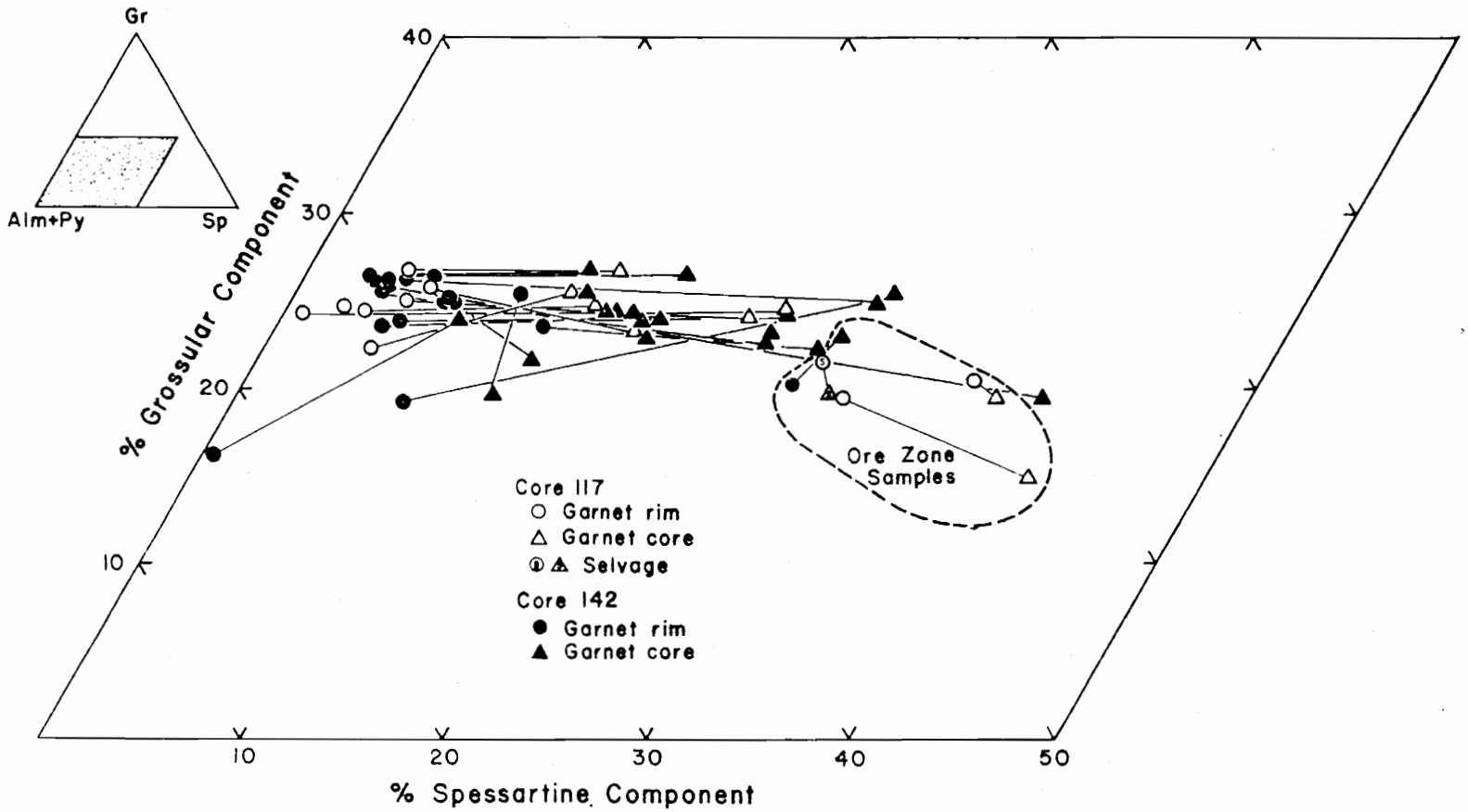

Figure 8. Core and rim compositions of garnets from the Gossan Lead district and calculated on a 12 oxygen formula basis

In many samples, from both ore zone and country rock, successive overgrowths are observed within the garnets. These overgrowths are parallel or subparallel to the crystal faces and are particularly well-developed in muscovite-rich samples. They have been observed to be separated by narrow zones of chloritic alteration. A traverse of one of these garnets (figure 9) shows that there are no compositional discontinuities across the overgrowths. The occurrence of overgrowths indicates that there have been successive intervals of garnet growth alternating with periods during which garnet growth ceased. absence of compositional discontinuities across the overgrowths indicates that the chemical system controlling the composition of garnet was not changing during the growth of the garnet. Since both ore zone garnets and garnets quite distant from the ore zone have overgrowths, the ore solutions cannot have caused the development of overgrowths. Therefore, the development of the garnet overgrowths must be due to some metamorphic process such as variations in fluid composition or fluid concentration, and not due to ore-forming processes.

The compositional zoning of the garnet shown in figure 9 is similar to the zoning described by Atherton (1968). As in the garnets investigated by Atherton (1968), the garnet becomes progressively less manganiferous with distance from the core; the zoning becoming more pronounced near the rim of the garnet. Manganese is preferentially concentrated in garnet. As the garnet continues to grow, it does not re-equilibrate with the surrounding rock. Therefore, as the garnet grows, manganese is progressively depleted and continued garnet growth produces a less manganiferous garnet.

Figure 9. Variation in the octahedral cation concentration along a traverse of a garnet showing distinct overgrowths.

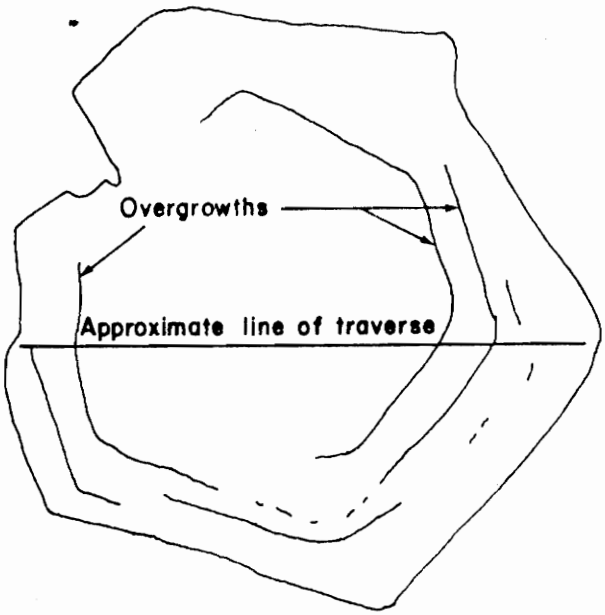
Overgrowths
Approximate line of traverse

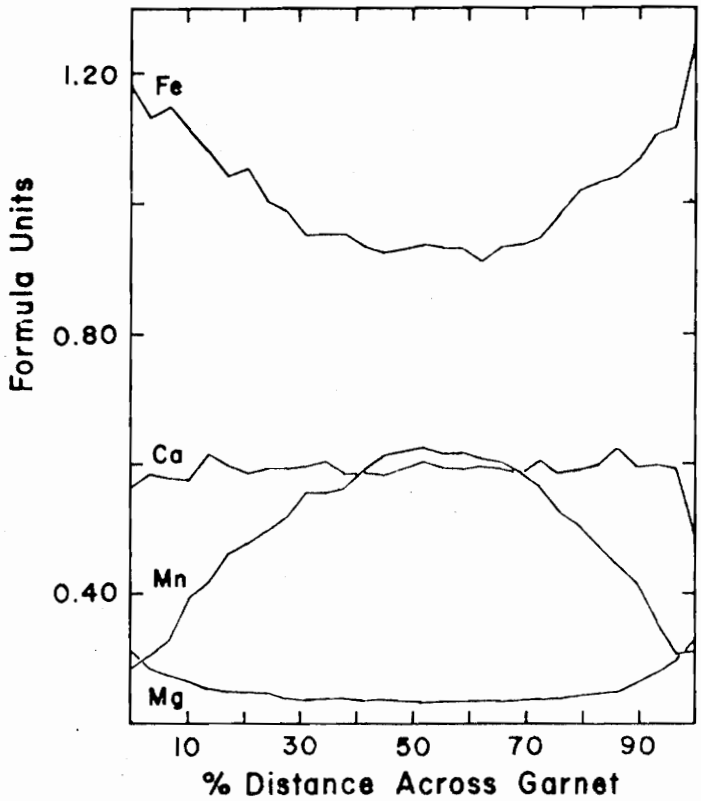
1.20
0.80
0.40
Formula Units
Fe
Ca
Mn
Mg
10
30
50
70
90
% Distance Across Garnet

Biotite occurs in nearly all samples and very frequently forms distinctively large porphyroblasts. Abundant inclusions of zircon, often submicroscopic, with distinct haloes are very common. Biotite varies in pleochroism between clear to brown and clear to pale-orange. Pleochroism is particularly weak in the more magnesian biotites from ore-zone samples. Analyzed biotite compositions are shown in figure 10. Note that these compositions are relatively aluminous.

Biotite compositions from samples with the limiting assemblage garnet-biotite-chlorite-muscovite-quartz plot on or near the phlogopite-siderophyllite join, suggesting that the simple substitutions (1) and (2) were not independent under the prevailing conditions.

$$Fe^{+2} \rightleftarrows Mg^{+2} \qquad (1)$$

$$Al^{VI} + Al^{IV} \rightleftarrows (Fe^{+2},Mg^{+2})^{VI} + Si^{IV} \qquad (2)$$

Those biotites from the ore-zone samples are more magnesian and slightly less aluminous than those from the country rocks.

Clinozoisite occurs commonly throughout both cores, but only occasionally, in plagioclase or calcite-rich samples do, crystals reach an appreciable size or quantity. Under crossed nichols, the normally anhedral clinozoisite is observed to have an anomalous blue and/or yellow interference colors. In figure 11, the compositions of three clinozoisites from schist samples, two from 142-1232 and one from 142-870, show that clinozoisites occurring in the schists have compositions with 0.34-0.45 formula units Fe^{3+} substituting for Al, corresponding to a pistacite content of Ps_{11-15}.

The development of sheet silicates in the quartz-muscovite schists and gneisses leads to several different textural varieties. In addition

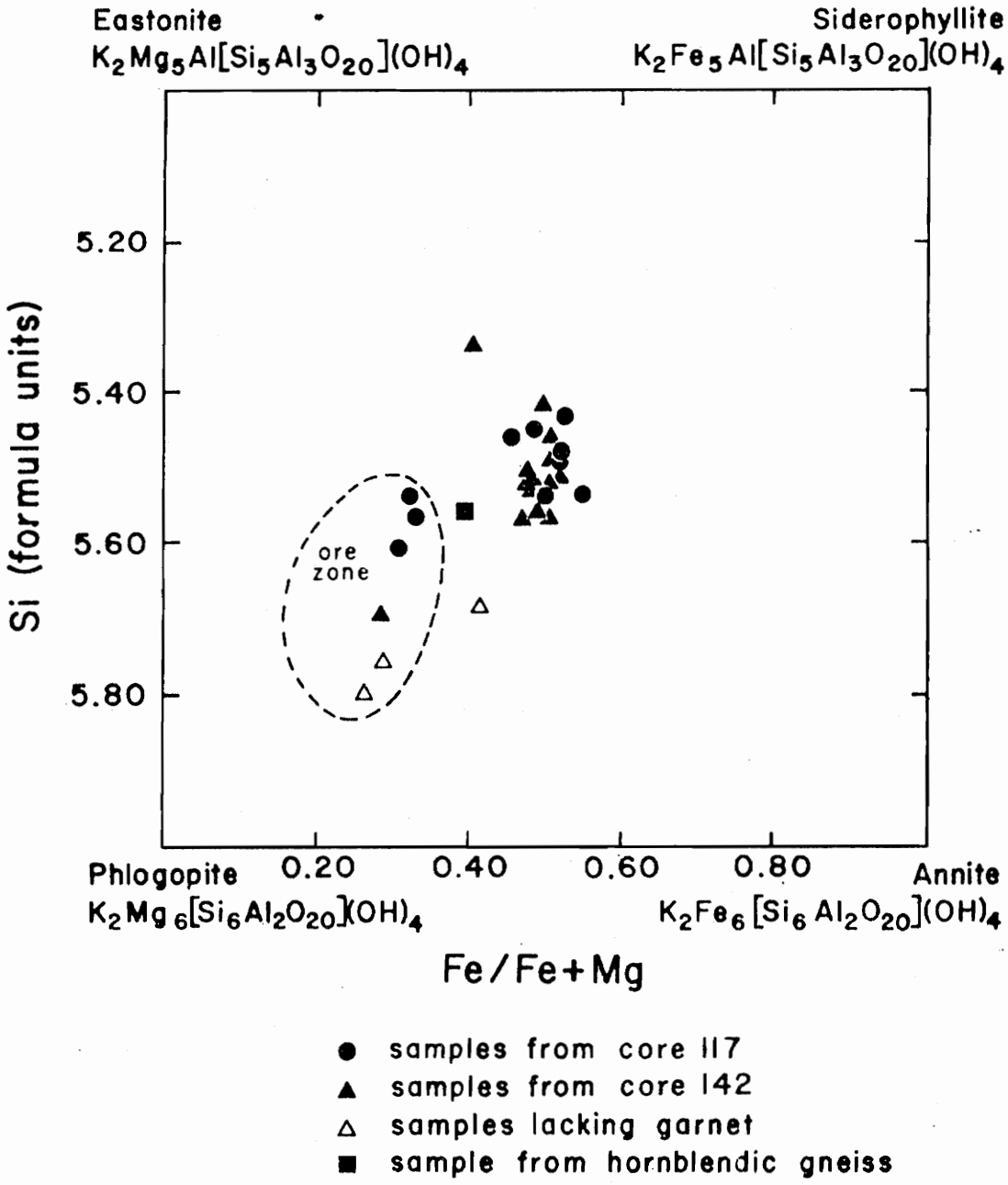

Figure 10. Compositions of biotites from the ore zone and surrounding rocks of the Gossan Lead district, calculated on a 24 oxygen formula basis.

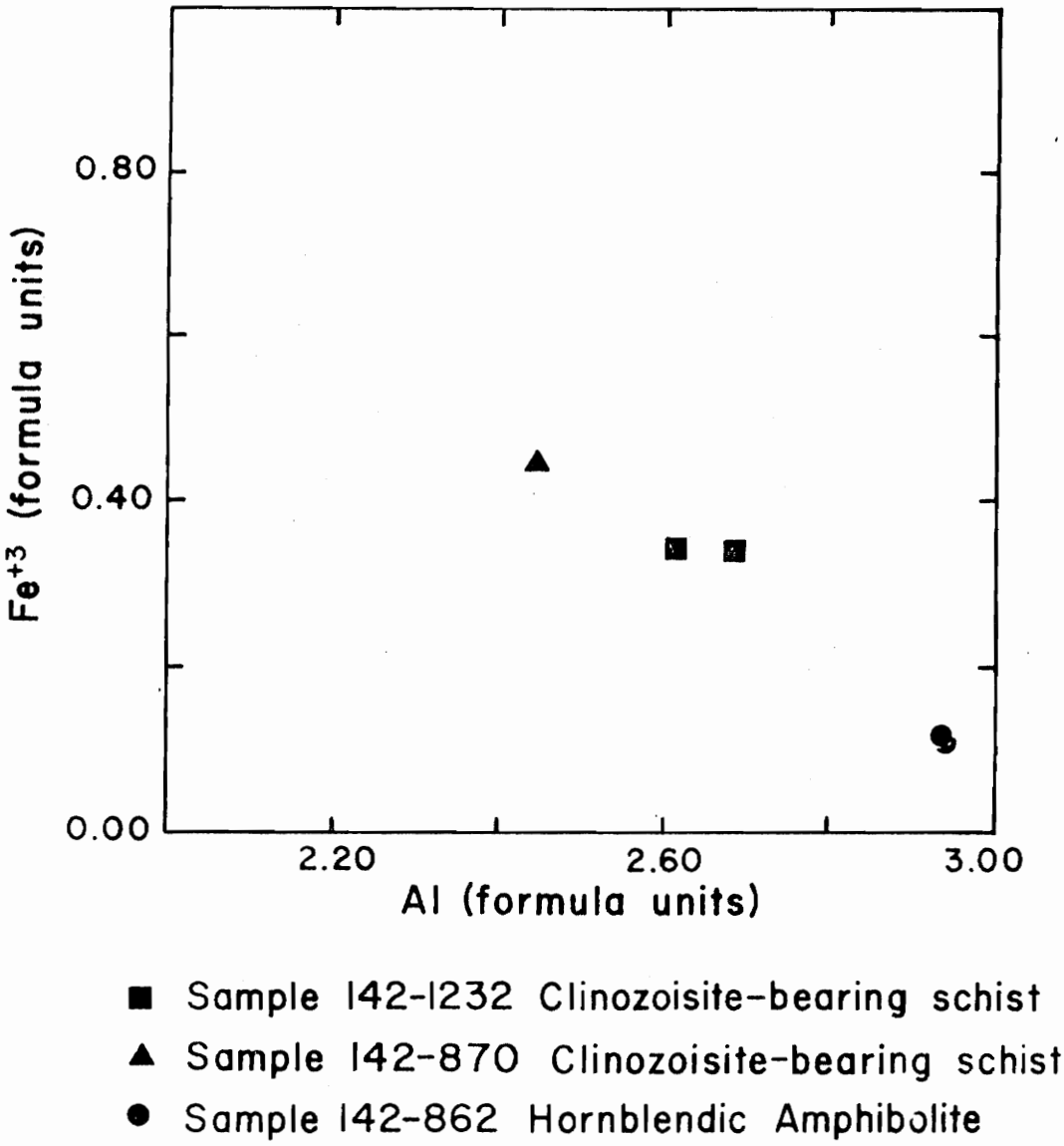

Figure 11. Compositions of epidote-group minerals from rocks of the Gossan Lead district, calculated on a 13 oxygen formula basis.

to the medium-grained texture already described, there are: 1) nearly pure layers of fine- to medium-grained biotite schists; 2) nearly pure layers of fine- to medium-grained chlorite schist; 3) medium- to coarse-grained biotite-chlorite gneiss with poorly-developed foliation; and 4) medium-grained, coarsely-banded biotite-chlorite schist. The last textural variety differs primarily in grain size and the extent of banding when compared to the more frequently-encountered fine- to medium-grained quartz-muscovite schist. Of the above-mentioned textural varieties 1, 2, and 3 are quite rare and are very rarely more than 5 cm thick.

Very rare secondary solution cavities, lined with clear, euhedral to subhedral aggregates of apophyllite, and in some cases weakly-pleochroic, coarse-grained chlorite, were observed in core 117 only. The apophyllite has a distinctive color-sector zoning showing interference colors ranging from anomalous deep blue to anomalous brown. As well as lining the cavities, apophyllite is also found disseminated throughout the schist for several centimeters away from the solution cavities.

Hornblende Gneiss

This unit is characterized by randomly oriented and slightly poikiloblastic hornblende prisms up to two centimeters long. Other phases include a significant quantity of biotite plates, anhedral quartz, and occasionally anhedral calcite. Minor phases include chlorite, plagioclase, garnet, and clinozoisite. There is only a weak foliation and no apparent lineation. Samples of hornblende gneiss from the sampled cores as well as other cores show that these layers range from 3-20 cm in thickness.

The composition of hornblende from this lithology as well as amphibolites from other lithologies observed in the cores are shown on figures 12 and 13. From both figures it can be seen that the amphibolites of the hornblende gneiss are distinctively aluminous and quite paragasitic. Analyzed plagioclase from the hornblende gneiss occurring at 977' in core 142 has a composition of An_{20}.

Hornblendic Amphibolite

The pale to medium green, medium-grained hornblendic amphibolite from core 142 (860-867) is largely subhedral to anhedral actinolitic hornblende and magnesiohornblende with relatively minor amounts of quartz, low-iron clinozoisite (see figure 11), magnesian chlorite (see figure 7), calcite, and trace quantities of sphene and plagioclase (An_{27}). Clinozoisite, frequently anhedral, also forms relatively long prisms. Chlorite occurs in aggregates of weakly-pleochroic plates. Opaque minerals are rather uncommon in the amphibolite, but bornite with chalcopyrite lamellae and irregular grains of chalcopyrite were observed. Examination of a number of other Freeport Sulfur Company cores revealed that the amphibolite layer(s) varied from 5 1/2' to 24' thick.

Ore Zone Lithologies

Silicate blocks occurring in the ore zone are lithologically very similar to those previously described. The major differences are in the mineral chemistry and textures. Aggregates of non-ore minerals were often observed to occur in rounded or nearly lenticular patches within the ore. Gangue minerals also occur as disseminated grains throughout the massive sulfide ore. Gangue minerals mixed with massive sulfide are frequently much coarser than their counterparts outside the

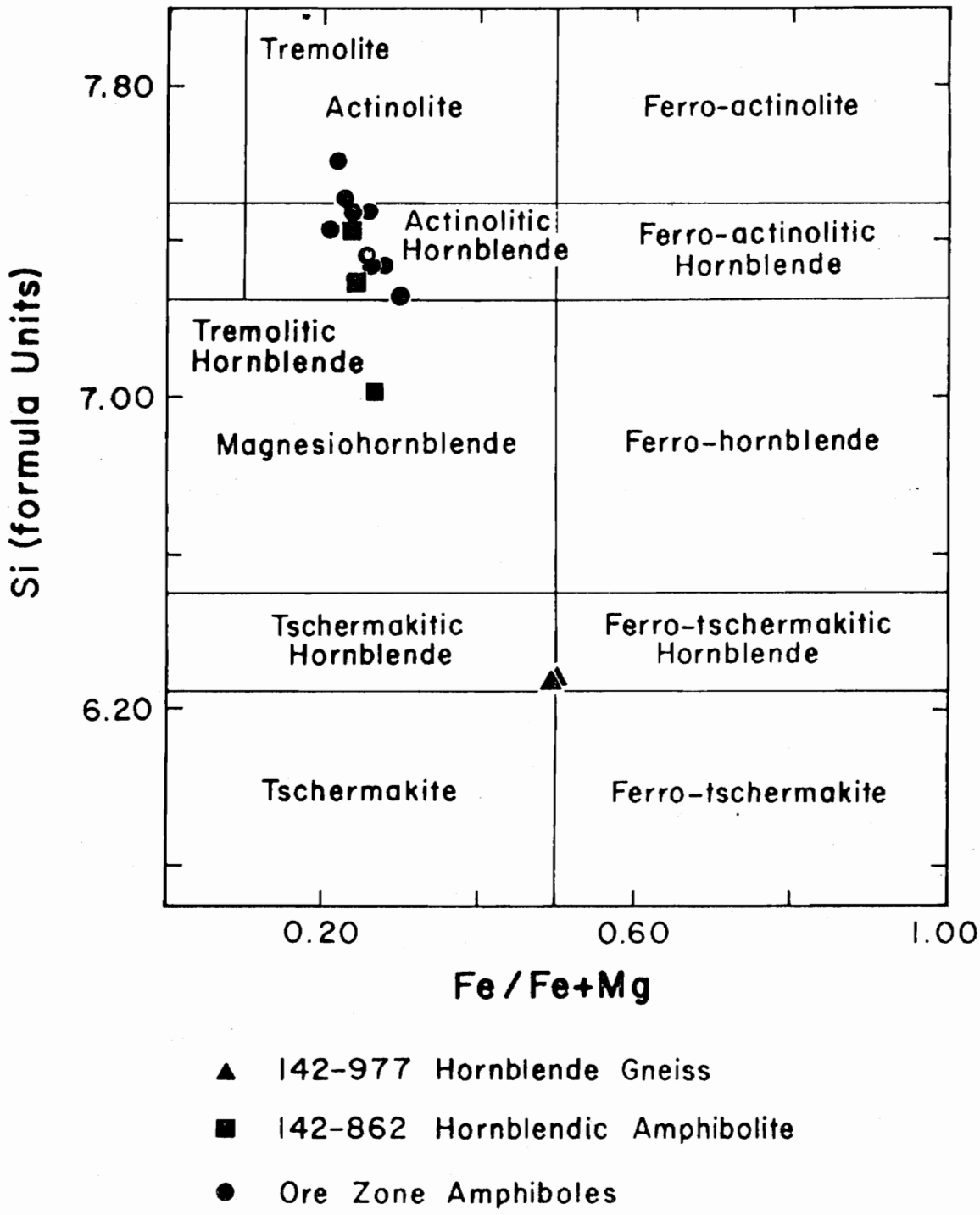

Figure 12. Compositions of amphiboles from the Gossan Lead district according to the terminology of Leake (1968) and calculated on a 24 oxygen formula basis.

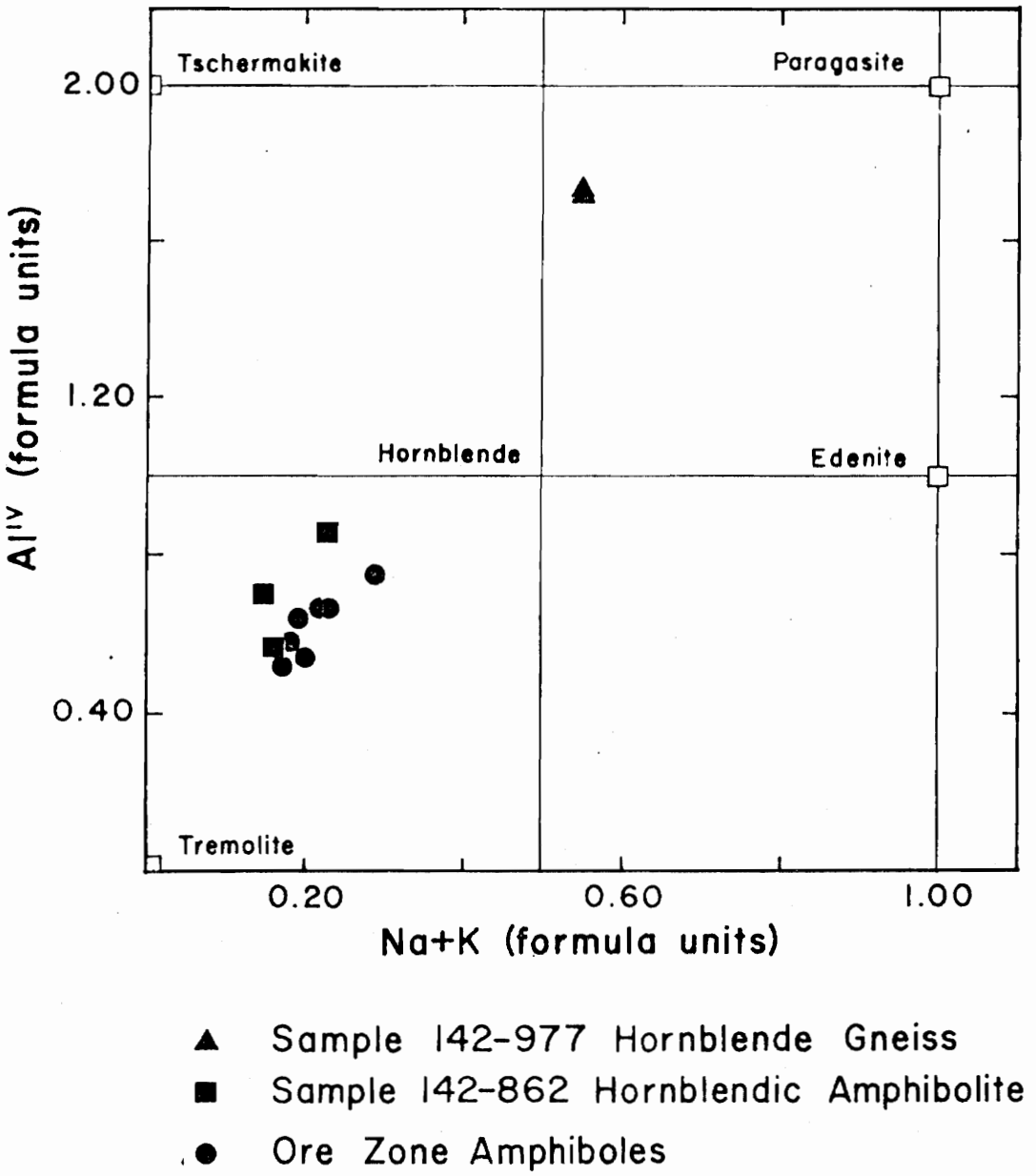

Figure 13. Alkali and tetrahedral aluminum of amphiboles from the Gossan Lead district.

ore zone. Chlorite, quartz, and calcite are more abundant in the ore zone, whereas biotite and muscovite are less abundant. All ferromagnesian minerals tend to be more magnesian in the ore zone than in the surrounding country rock.

Actinolitic hornblende and actinolite-tremolite occurring in the ore are occasionally found as large radiating bundles of zoned prisms several centimeters long with interstitial chlorite and biotite. Figure 14, adapted from Cameron (1975), shows the core and rim compositions of the same amphibole grain from the ore zone (1142-1144).

Nonpleochroic cummingtonite-composition rims were observed around actinolite-composition and/or actinolitic hornblende-composition cores. This feature was observed to occur in other ore zone samples but was not observed in any non-ore zone samples.

Selvages

Biotite-garnet and chlorite-garnet selvages were observed in both cores studies. Although selvages are observed to occur at the margins of silicate blocks within the ore zone, they do not occur at all such margins and it is not clear what parameters actually control the occurrence of selvages. However, the selvages only occur in the ore zone. Therefore, the selvages have developed during the formation of the ore. The selvages observed in the cores studied varied from 1-2 mm up to 10 cm.

The biotite-garnet selvage occurring at 1267' in core 117 has pale pink garnets up to 2 mm across with some very minor development of overgrowths parallel to the generally well-developed crystal faces. Biotite plates are often several millimeters across. Chlorite is also frequently present in relatively minor quantities. Chlorite, biotite, and garnet

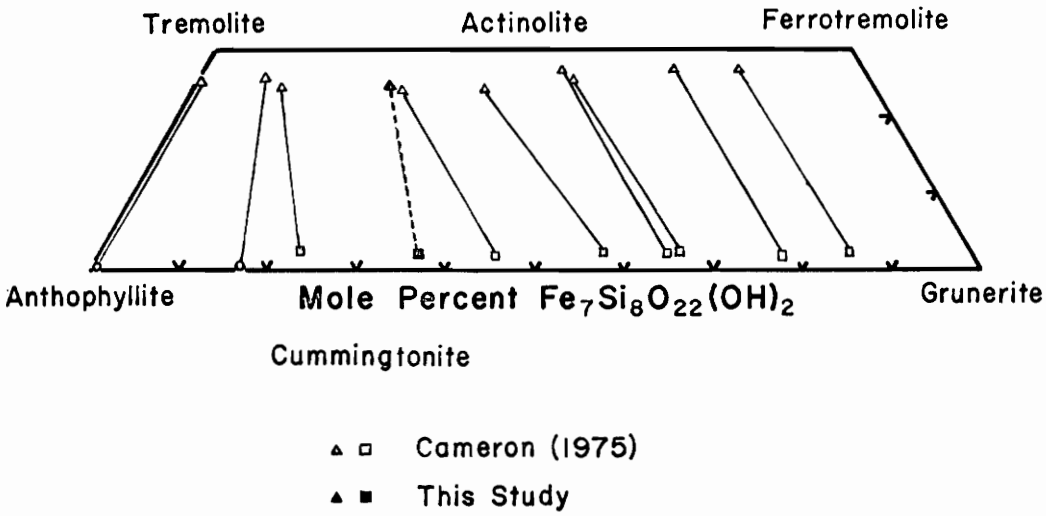

Figure 14. Compositions of actinolitic core and cummingtonite rim of a zoned amphibole from the ore zone of the Gossan Lead.

from sample 117-1267 were analyzed with the microprobe revealing mineral compositions similar to other ore zone samples although garnets are more manganiferous and not as strongly zoned in the selvage.

In addition to the biotite-garnet selvages, there are some very coarse-grained garnet-chlorite selvages (142-1133). The subhedral garnets in this particular lithology are up to 1 centimeter in diameter, but most frequently about 2-3 millimeters in diameter. Garnets in the chlorite-garnet selvages lack any development of overgrowths. Some zircon-riddled biotite books also occur in this lithology but are less common with sphalerite and pyrrhotite predominating.

Ore Mineralogy

The ore mineralogy has been recently studied by Craig et al (1971), and Henry et al (1976). According to their studies, the ore mineralogy is dominated by pyrrhotite, sphalerite, chalcopyrite, and galena.

Ore minerals coexisting with the silicate samples of this study are dominated by pyrrhotite ($Fe_{.912}S$, D. K. Henry, personal comm., 1976). A variety of textural features including kink bands and dihedral angles between intersecting pyrrhotite grains have been observed in polished section. As discussed by Stanton and Gorman (1968), the generation of dihedral angles between intersecting grains indicates recrystallization.

Brecciated intergrowths of sphalerite and pyrrhotite were observed. In these highly fragmented areas, the grain size of the opaque mineral grains is greatly diminished. It is in this type of area that the dihedral angles are best developed. This apparently indicates that some recrystallization has occurred after a period of minor brecciation.

Sphalerite also occurs fairly frequently with oriented exsolution lamellae of chalcopyrite and, less frequently, pyrrhotite. Sphalerite is frequently observed to have a complex intergrowth pattern with pyrrhotite.

Chalcopyrite, as well as occurring as exsolution lamellae in sphalerite, is often observed to concentrate along the grain boundaries between pyrrhotite, sphalerite, and silicates. Chalcopyrite has also been observed to occur oriented along the cleavage of silicate minerals.

Galena occurs in relatively minor quantities and is not present in all the ore samples. It most frequently occurs as small disseminated grains.

Pyrite occurs infrequently. Most of the pyrite grains are anhedral although nearly euhedral grains have been observed. Samples from cores with a sulfide zone near the surface were observed to have very large, often euhedral pyrite cubes in a matrix of pyrrhotite. This, however, is probably due to secondary alteration.

The opaque mineralogy of the enclosing schists is similar to the ore mineralogy. Pyrite, pyrrhotite, and less commonly sphalerite are all observed to occur as disseminated grains in non-ore samples. Pyrrhotite is also observed to occur in aggregates up to 1 cm across included within quartz veins. As indicated by the modes in Table 1, the opaque mineral content of non-ore samples does not vary appreciably, even adjacent to the ore zone.

Ilmenite, often occurring as euhedral grains and aggregates, appears to be more common in the non-ore samples while another titanium-rich phase, rutile, appears to occur more frequently in the ore zone. The

absence of ilmenite in the ore zone suggests the following reaction:

$$\text{Ilmenite} + S \rightleftarrows \text{Pyrrhotite} + \text{Rutile}$$

From this reaction and the data for biotite, chlorite, and garnet, it is apparent that iron-bearing phases are less stable in the presence of the sulfide ore than their less iron-rich counterparts.

Metamorphism in the Sylvatus Area

The Ashe Formation in the Sylvatus area has been metamorphosed to the epidote-amphibolite facies. As shown in figure 3 (Rankin et al, 1973), the staurolite and kyanite isograds are found farther to the southeast with metamorphic grade increasing in that direction. The assemblage hornblende-plagioclase (An_{27}, sample 142-862) in the amphibolite indicate that the metamorphic grade must be at or near the amphibolite facies boundary.

Applying the sphalerite geobarometer (Scott, 1976), a minimum pressure estimate of 4.1 kb is obtained from a sphalerite with 15.41% FeS (D. K. Henry, personal comm., 1976). This is a minimum pressure estimate since the presence of pyrite stably coexisting with pyrrhotite and sphalerite is somewhat questionable. As indicated by Scott (1976), if pyrite is absent the amount of FeS in the sphalerite will increase; this indicating a lower pressure determination.

The absence of staurolite in any of the schists of the Sylvatus area indicates that metamorphic temperatures were below 540-565°C (Hoschek, 1969). The assemblage muscovite-calcite-quartz-clinozoisite (Ps_{11-15})-plagioclase (An_{20},117-1356) further limits the possible metamorphic temperatures.

The equilibrium relations shown in figure 15 have been calculated from the experimental data of Hewitt (1973) and Johannes and Orville (1972)

Figure 15. The system muscovite-calcite-quartz calculated from the data of Hewitt (1973), and Johannes and Orville (1972) using the f_{H_2O} data of Burnham, Holloway, and Davis (1969), the f_{CO_2} data of Burnham and Wall (personal communication, NATO Conference on Volatiles in Metamorphism, 1974), and the data for the activity of plagioclase from Orville (1972).

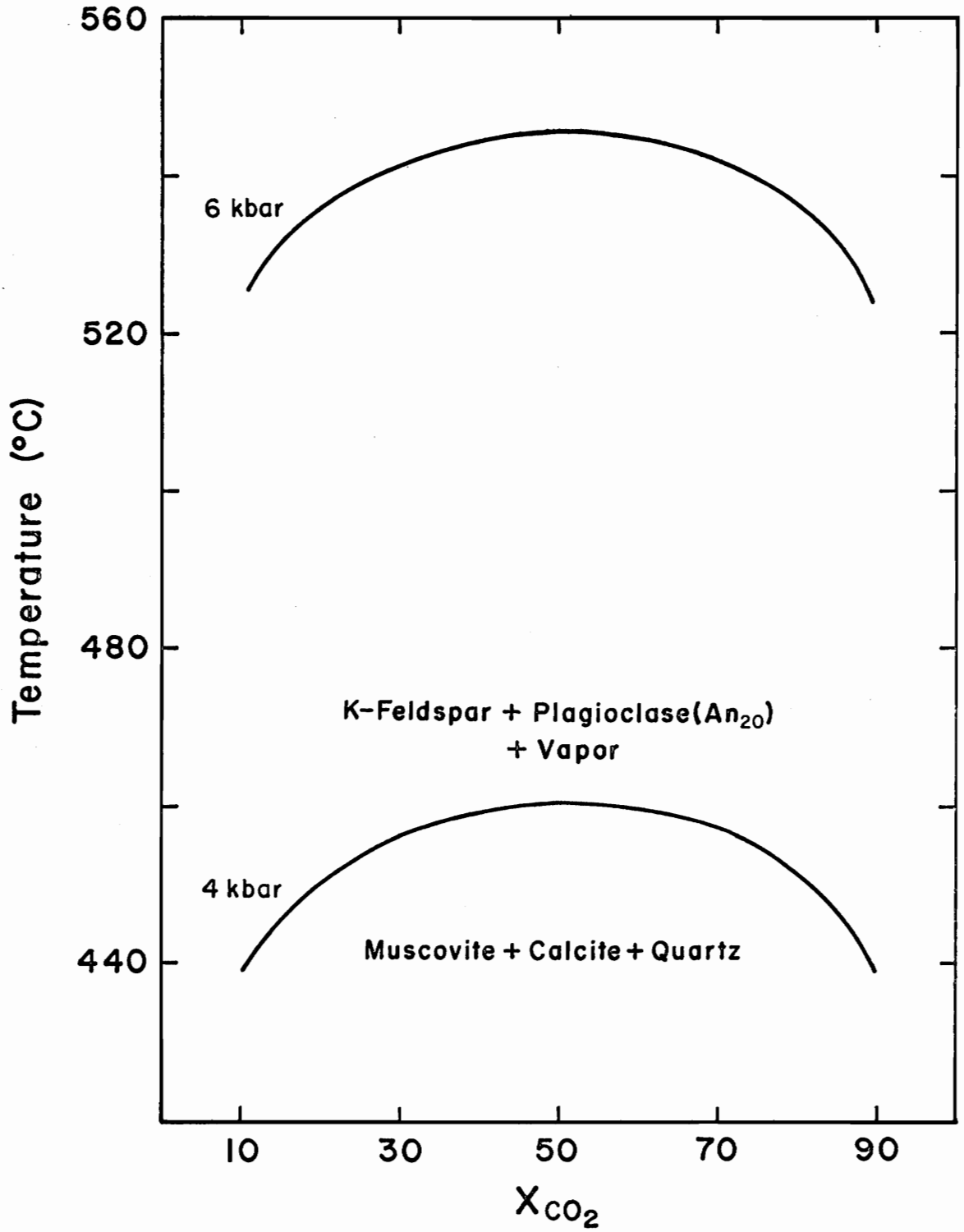
560
520
480
440
Temperature (°C)
6 kbar
K-Feldspar + Plagioclase(An20)
+ Vapor
4 kbar
Muscovite + Calcite + Quartz
10
30
50
70
90
XCO2

using the f_{H_2O} data of Burnham and Wall (personal communication, NATO Conference on Volatiles in Metamorphism, 1974), and the activities of plagioclase determined by Orville (1972). Due to the stability of the assemblages muscovite-calcite-quartz and plagioclase-clinozoisite-calcite, the maximum metamorphic temperature must have been 460°C for a pressure of 4 kbar and 546°C if the pressure was as high as 6 kbar.

Discussion

Figures 16 through 19 show the variations of the elements with significant changes of concentration in garnet rim, garnet core, biotite, and chlorite respectively. The elemental concentrations are plotted in terms of formula units, and are shown as they vary with depth in the two cores. In order to ensure that any variations reflect the effect of the presence of sulfur, and not due to a shift in bulk composition of the schists and gneisses, all samples shown in figures 15-18 contain the assemblage quartz-muscovite-biotite-chlorite-garnet-plagioclase$\pm$opaques$\pm$clinozoisite$\pm$rutile or ilmenite. Vertical lines through data points indicate the observed variation of the element as indicated by the analysis of two or more individual grains of that mineral in the same sample. Lines between samples are for the purposes of clarity only.

Garnet is distinctly zoned in virtually all samples. As shown on figures 16 and 17, both the rim and core compositions of garnets have been influenced by the presence of the ore; the considerably greater scatter of data points in figure 17 being due to the difficulty in determining the exact center of the garnet. Furthermore, the ore zone garnets are generally more manganiferous than non-ore zone garnets. This may further reflect the relative instability of the almandine component of the ore zone garnets. The fact that the core, as well as the rim compositions, are affected by the presence of the sulfide ore indicates that the ore was present prior to the major metamorphism of the area.

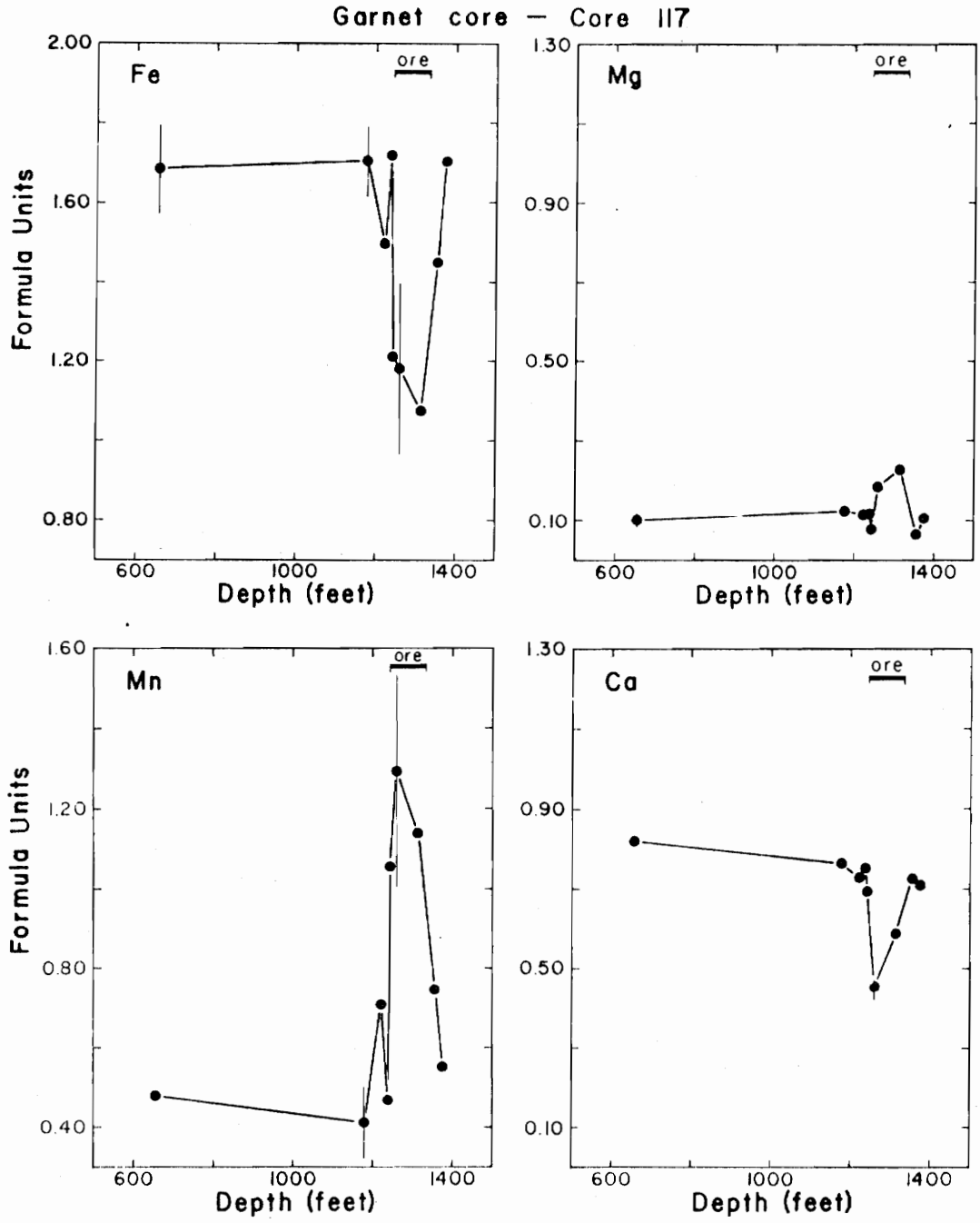

Figure 16A. Variations in the composition of garnet cores in core 117.

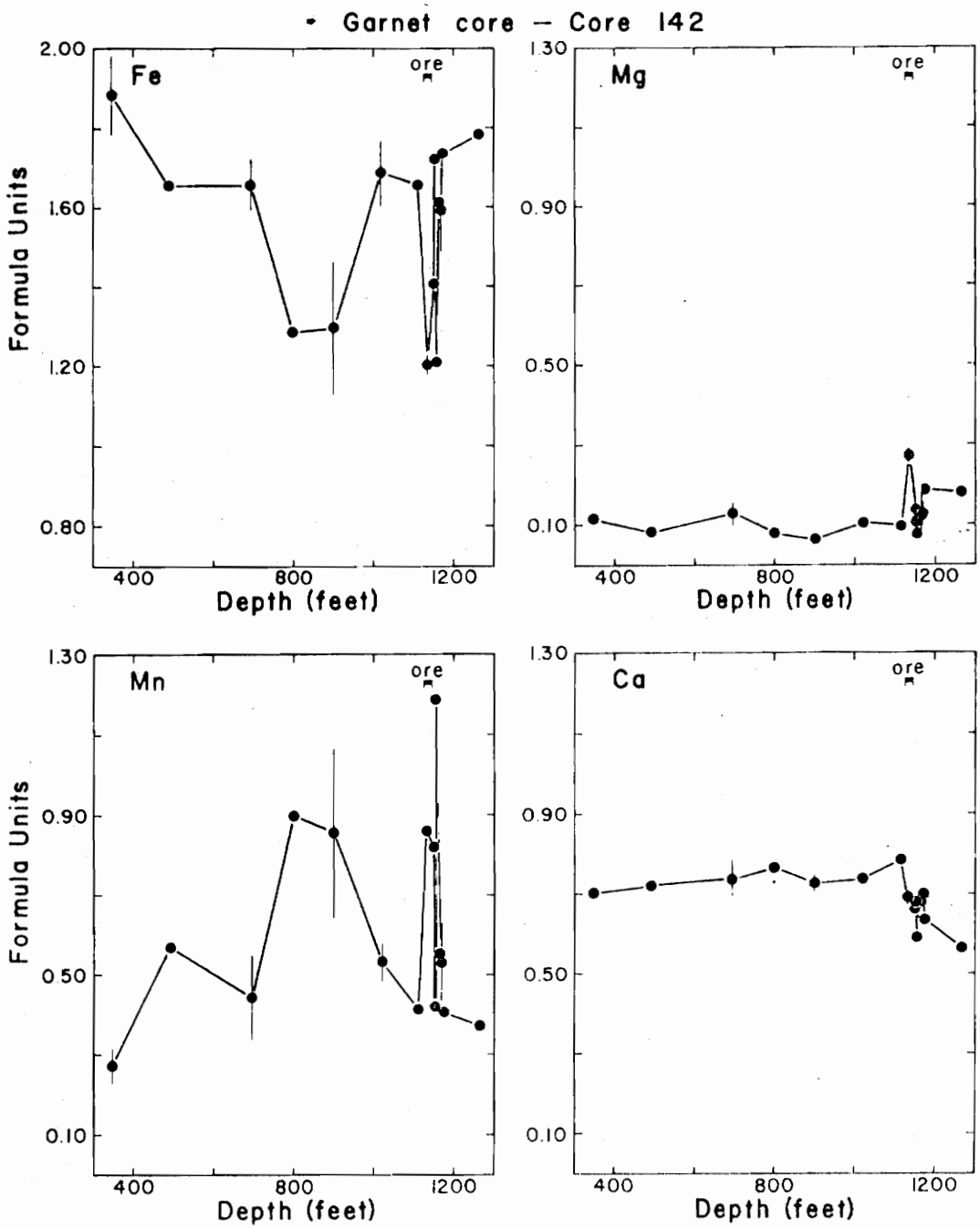

Figure 16B. Variations in the composition of garnet cores in core 142.

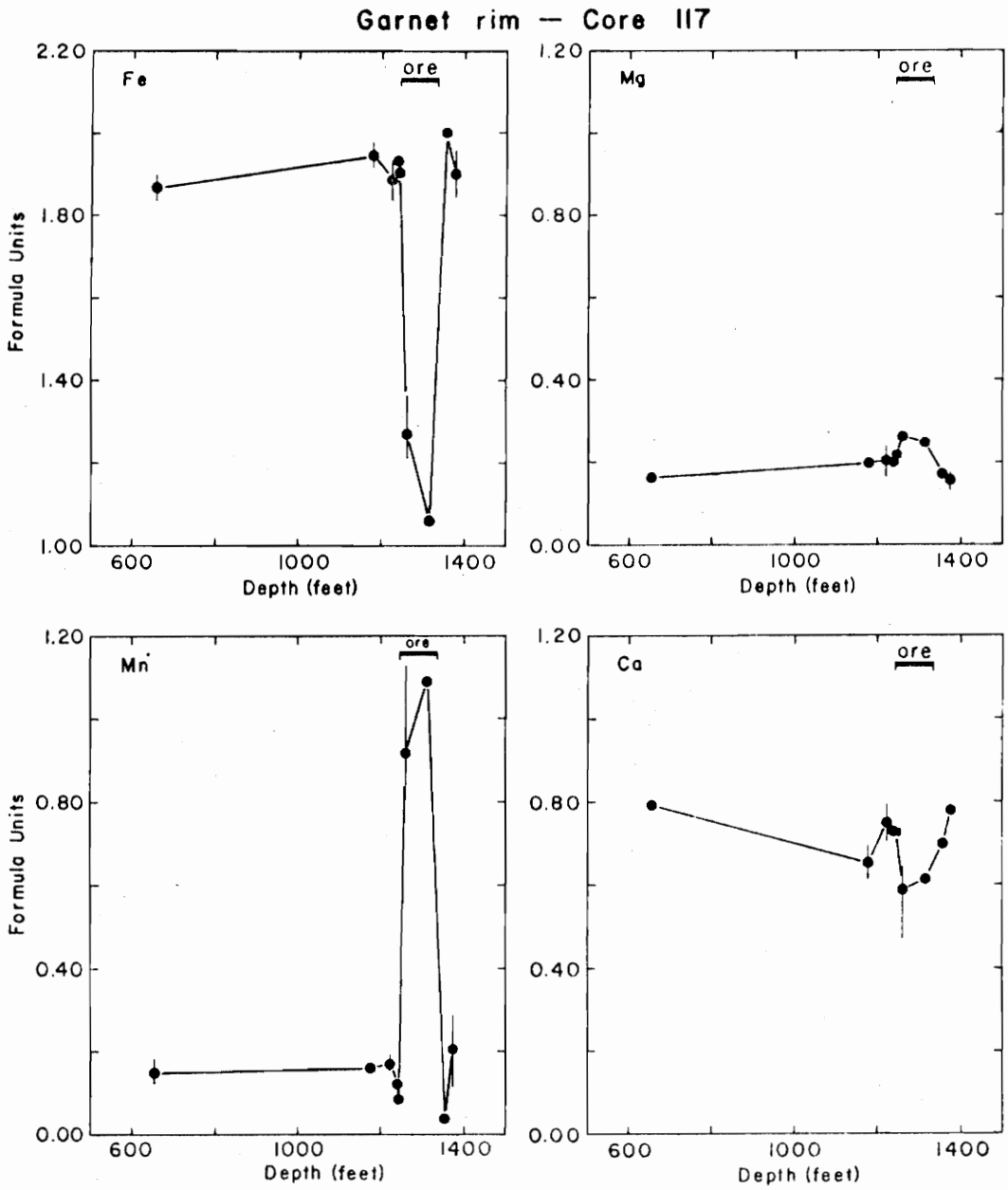

Figure 17A. Variations in the composition of garnet rims in core 117.

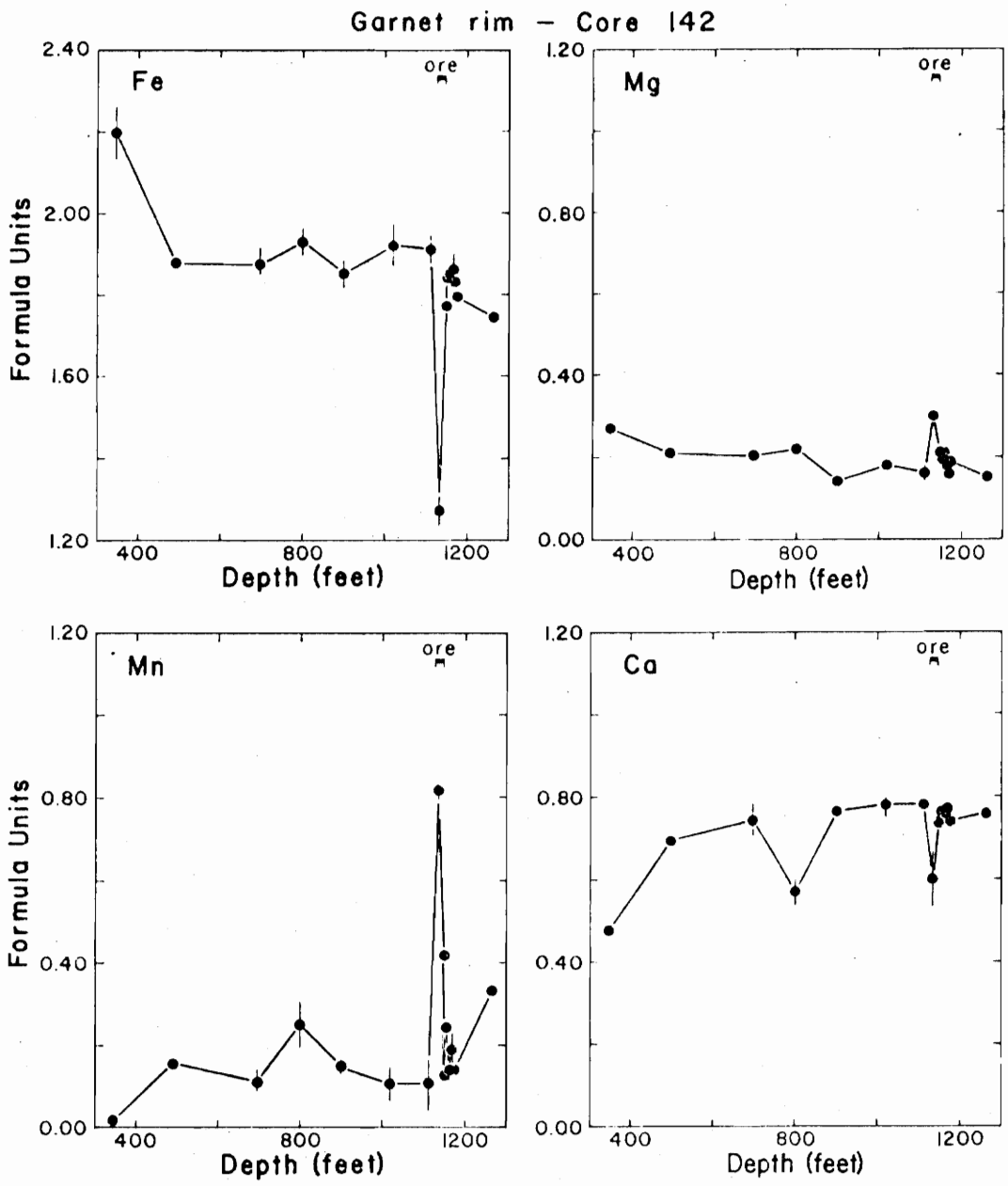

Figure 17B. Variations in the composition of garnet rims in core 142.

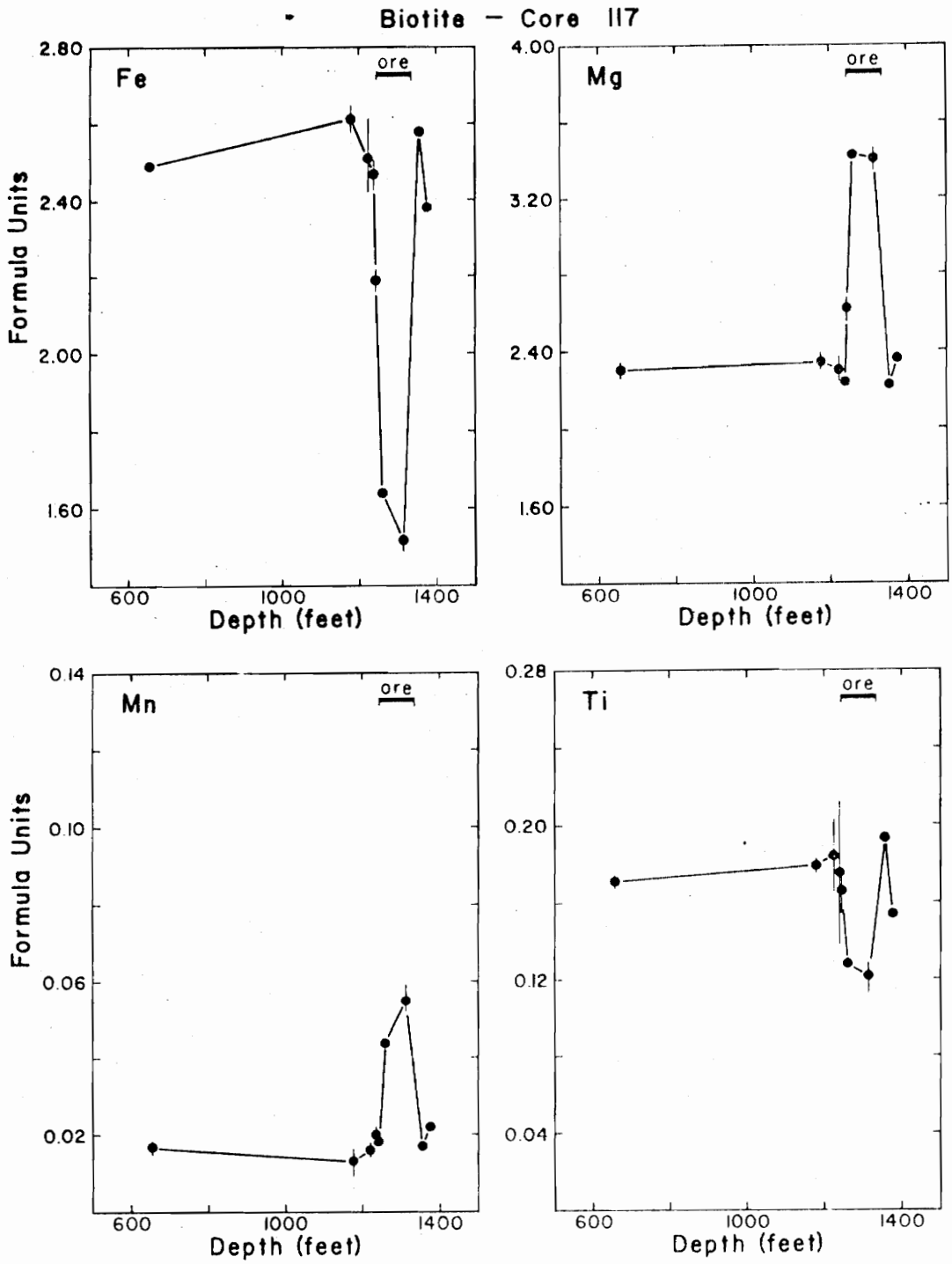

Figure 18A. Variations in the composition of biotite in core 117.

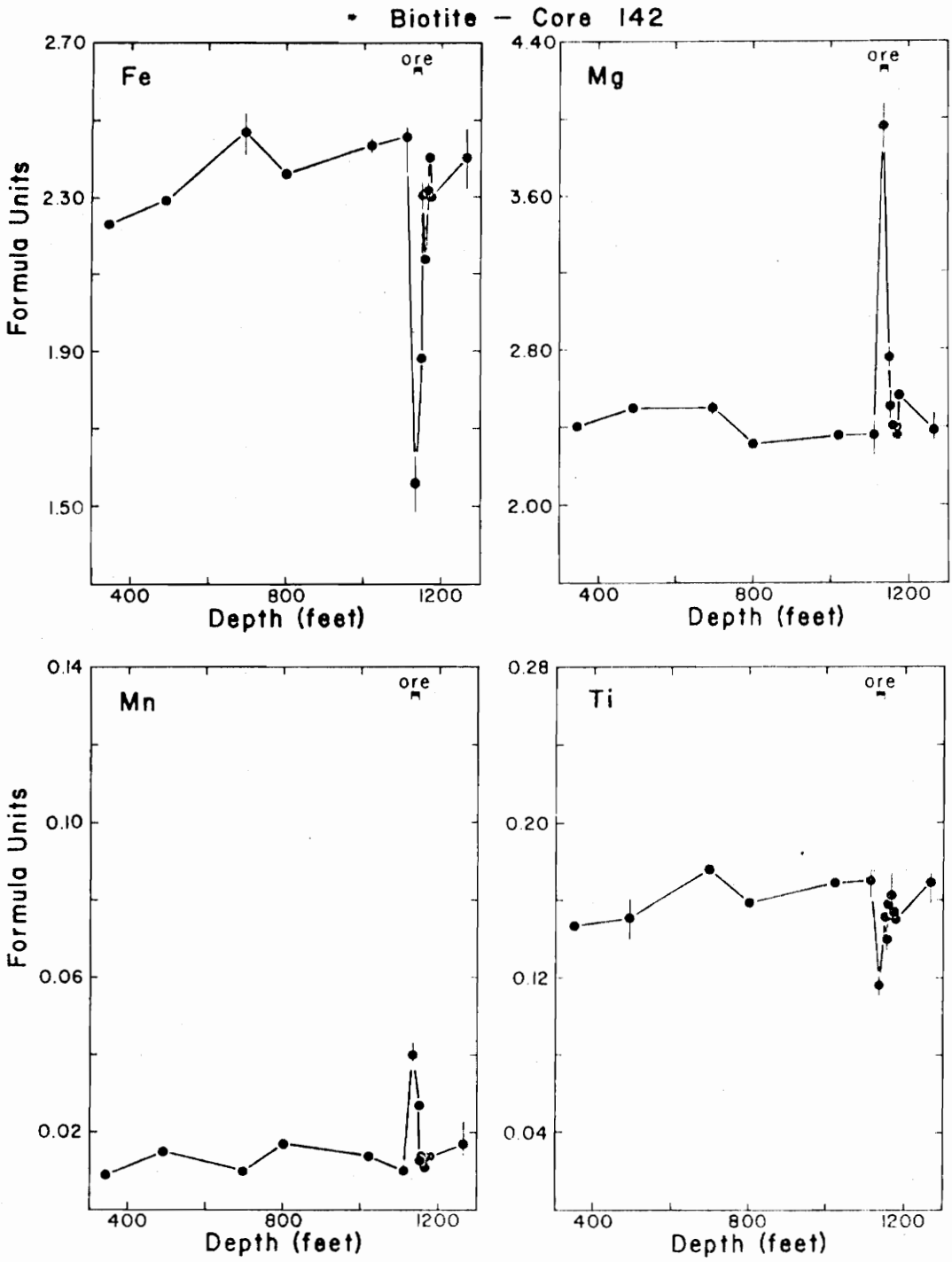

Figure 18B. Variations in the composition of biotite in core 142.

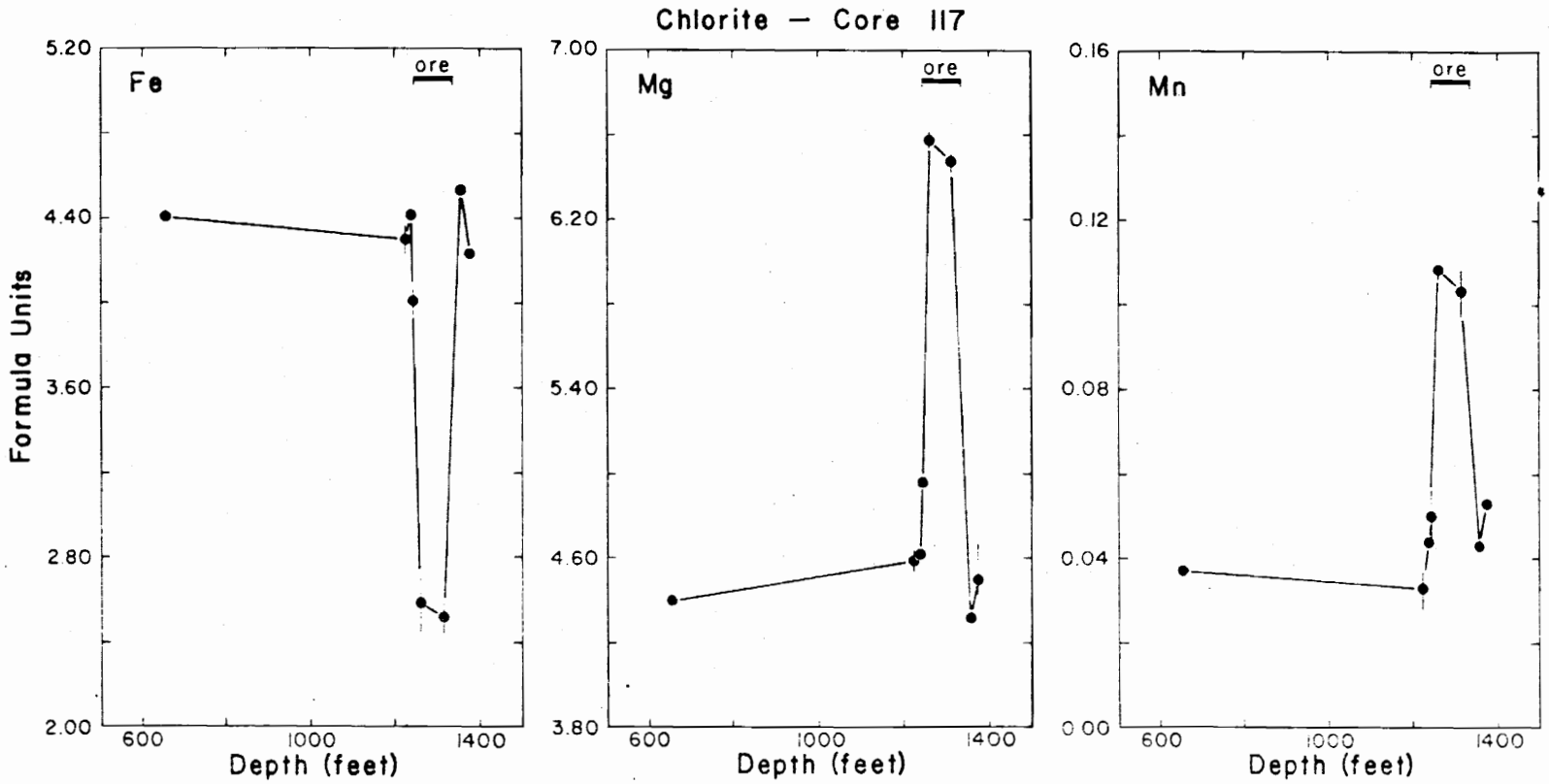

Figure 19A. Variations in the composition of chlorite in core 117.

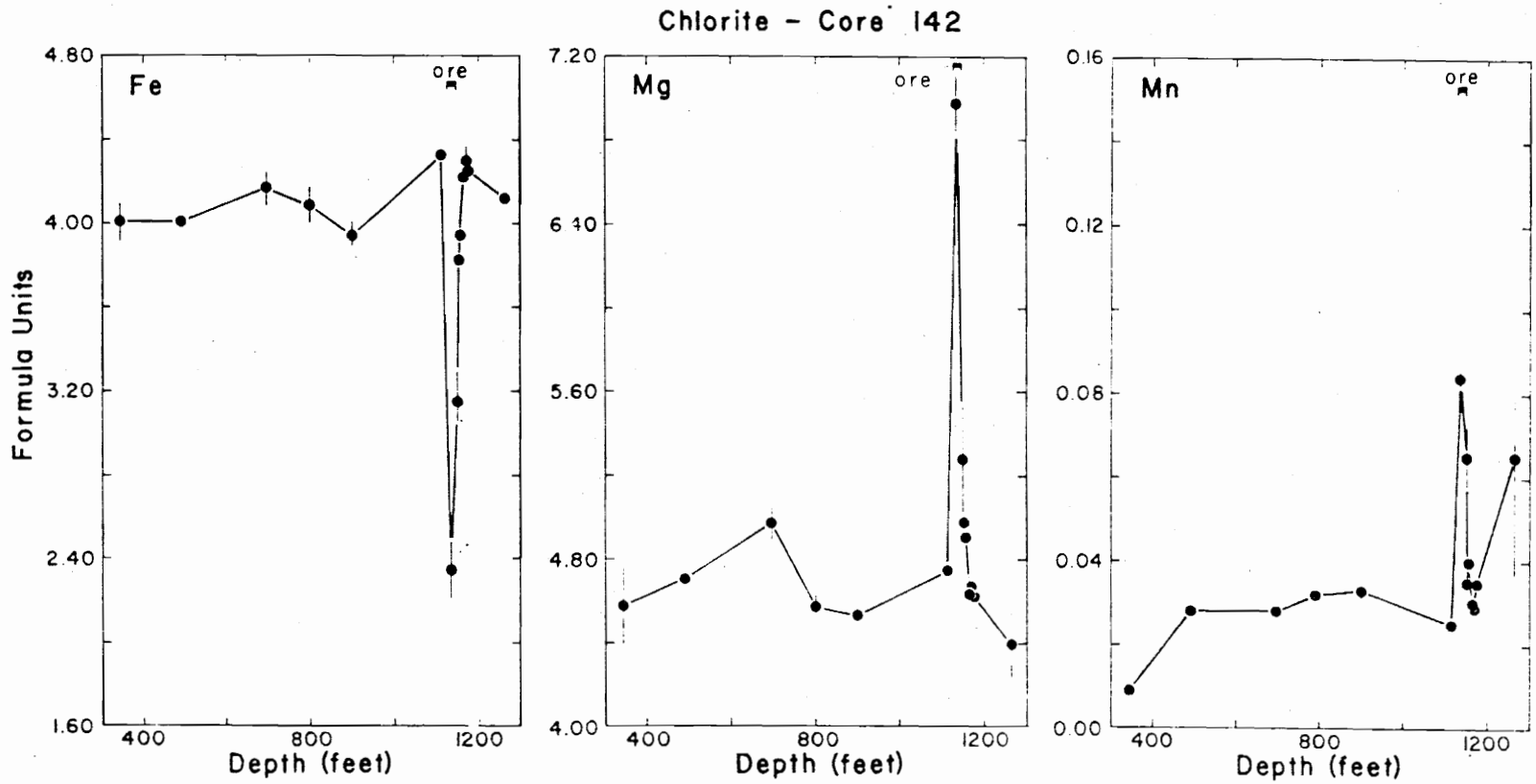

Figure 19B. Variations in the composition of chlorite in core 142

The variation diagrams indicate that the limits of the zone influenced by the ore is restricted to 2.5' beyond the ore in core 142 (∿20 foot ore thickness), and slightly over 5.5' beyond the ore in core 117 (∿47 foot ore thickness). The thicker ore zone of core 117 appears to have significantly increased of the volume of rock influenced by the sulfide ore. In contrast, the work of Fullagar et al (1967) on the Ore Knob, North Carolina, deposit show wallrock alteration extending several tens of feet away from the ore.

There is a greatly diminished iron content in ore zone garnet, biotite, and chlorite. In the sheet silicates, magnesium content in the ore zone is increased by nearly the same amount as the iron depletion. Manganese in the sheet silicates is also increased mildly, and there is a noticable decrease in the titanium content of the ore-zone biotites. Magnesium content of ore zone garnets is only slightly increased. However, the manganese content ore zone garnet rims is much higher than that recorded for the garnet rims of non-ore samples. The calcium content of the garnet decreases only slightly in the ore zone. These trends are consistent for both cores studies; no significant differences were observed when the chemical trends of each core were compared.

As indicated by the modes (samples 117-1249, 1253, 1271), the ore zone non-opaque mineralogy is dominated by chlorite, quartz, calcite, and biotite with only trace-1% garnet at best, compared with 1-5% garnet away from the ore. This suggests that the iron depletion of the silicates may be even more extreme than that indicated by the variation diagrams; the bulk composition of the non-opaques being shifted toward

more chlorite-rich, garnet-poor (or garnet-absent) assemblages as shown in figure 20. A shift of this type is consistent with what can be expected from a shift in the bulk composition of the nonsulfide portion of the rock to more magnesian, iron-poor compositions.

Experimental sulfidation of amphiboles conducted by Popp (1975) shows a significant depletion of iron in the amphiboles in the presence of sulfur. Amphiboles from the Gossan Lead are more aluminous and calcic than those examined by Popp. Therefore, the direct application of the experimental data is prohibited. However, qualitatively, the data in figures 12 and 13 do suggest that there is less Fe and more Si in amphiboles from the ore zone schists when compared to amphiboles from samples distant from the ore.

The distribution coefficient for Fe $\rightleftarrows$ Mg exchange reactions, as described by Kretz (1961), has been computed from the Fe/Fe + Mg ratios of biotite, garnet and chlorite for samples in both cores. The computed distribution coefficients are tabulated in Table 2, and shown on figures 21 and 22 for garnet-biotite pairs and garnet-chlorite pairs respectively. No clear trends were observed for the relative distribution of Mn in biotite, chlorite, and garnet except for the strong concentration of Mn in garnet. It is apparent that the distribution coefficients for the Fe-Mg exchange reaction for garnet-biotite and garnet-chlorite pairs are constant for both cores. Numerous authors (Albee, 1965; Kretz, 1961, 1964; Lyons and Morse, 1970; and many others) have shown that the distribution coefficient for Fe $\rightleftarrows$ Mg exchange reactions is particularly temperature sensitive. Finding the same K_D for both ore and non-ore samples indicates that the garnets and biotites

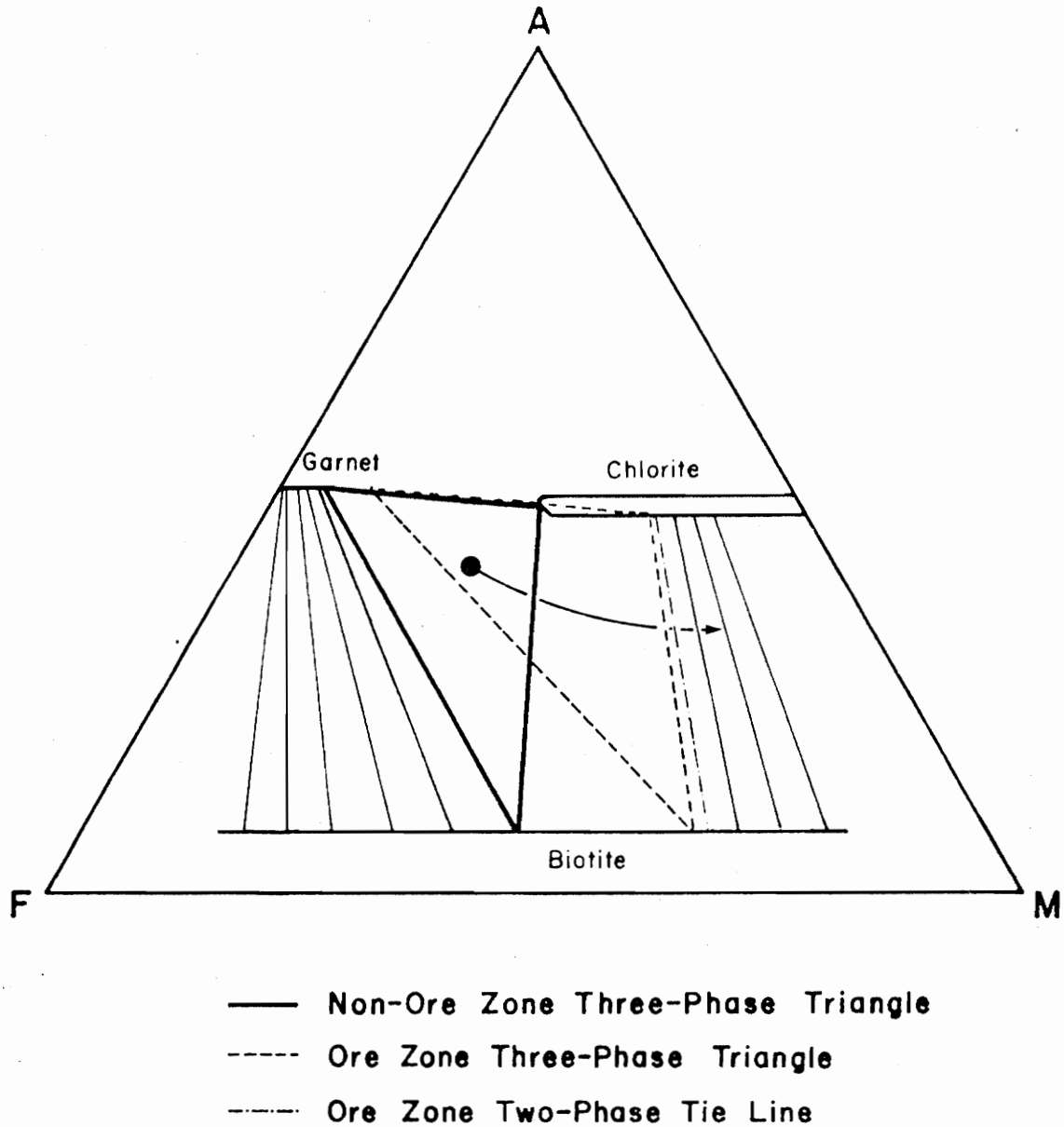

Figure 20. An AKFM plot of mineral assemblages of the Gossan Lead district. Sulfidation of the composition indicated could shift the composition of the remaining non-sulfide portion from the three-phase triangle into the biotite-chlorite two-phase field. The shift in the position of the three-phase field may be dur to the influence of calcium and/or manganese; species not considered by AKFM-type projections.

Table 2

Fe-Mg ratios and computed distribution coefficients for garnet-biotite and garnet-chlorite pairs

Core 117	Fe/Fe+Mg				
Depth	Biotite	Chlorite	Garnet	K_D*	K_D†
654	.520	.500	.918	11.22	10.40
1178	.527		.908		8.81
1223	.521	.484	.902	9.81	8.41
1238	.524	.489	.906	10.07	8.72
1243	.456	.447	.893	10.36	10.00
1260	.325	.283	.827	12.14	9.97
1267	.330		.830		9.87
1314	.309	.281	.810	10.91	9.53
1356	.549	.512	.920	10.89	9.38
1376	.502	.490	.924	12.58	12.00
Mean distribution coefficient for samples from core 117				11.00 ± 0.97	9.71 ± 1.93

*Distribution Coefficient, $K_D = \dfrac{X^{Fe}_{Gar}\ (1 - X^{Fe}_{Chl})}{X^{Fe}_{Chl}\ (1 - X^{Fe}_{Gar})}$

where $X^{Fe}_{Gar} = \dfrac{Fe}{Fe + Mg}$ in garnet

†Distribution coefficient, $K_D = \dfrac{X^{Fe}_{Gar}\ (1 - X^{Fe}_{Bio})}{X^{Fe}_{Bio}\ (1 - X^{Fe}_{Gar})}$

where $X^{Fe}_{Gar} = \dfrac{Fe}{Fe + Mg}$ in garnet

Table 2 (continued)

Core 142

Depth	Biotite	Fe/Fe+Mg Chlorite	Garnet	K_D*	K_D
345	.396	.467	.890	9.20	12.30
490	.478	.457	.899	10.56	9.68
696	.497	.456	.902	10.92	9.25
799	.505	.472	.897	9.75	8.54
899		.465	.928	14.95	
1020	.508		.914		10.28
1112	.509	.477	.922	13.07	11.45
1133	.283	.252	.809	12.58	10.76
1149	.406	.373	.893	13.97	12.19
1151	.479	.434	.897	11.35	9.47
1156	.470	.445	.904	11.78	10.66
1164	.491	.476	.913	11.57	10.92
1170	.504	.479	.921	12.71	11.49
1175	.474	.479	.906	10.44	10.66
1265	.502	.483	.920	12.29	11.40

Mean distribution coefficient for samples from core 142	11.80 ± 1.60	10.64 ± 1.11
Mean distribution coefficient for samples from both cores	11.51 ± 1.43	10.26 ± 1.15

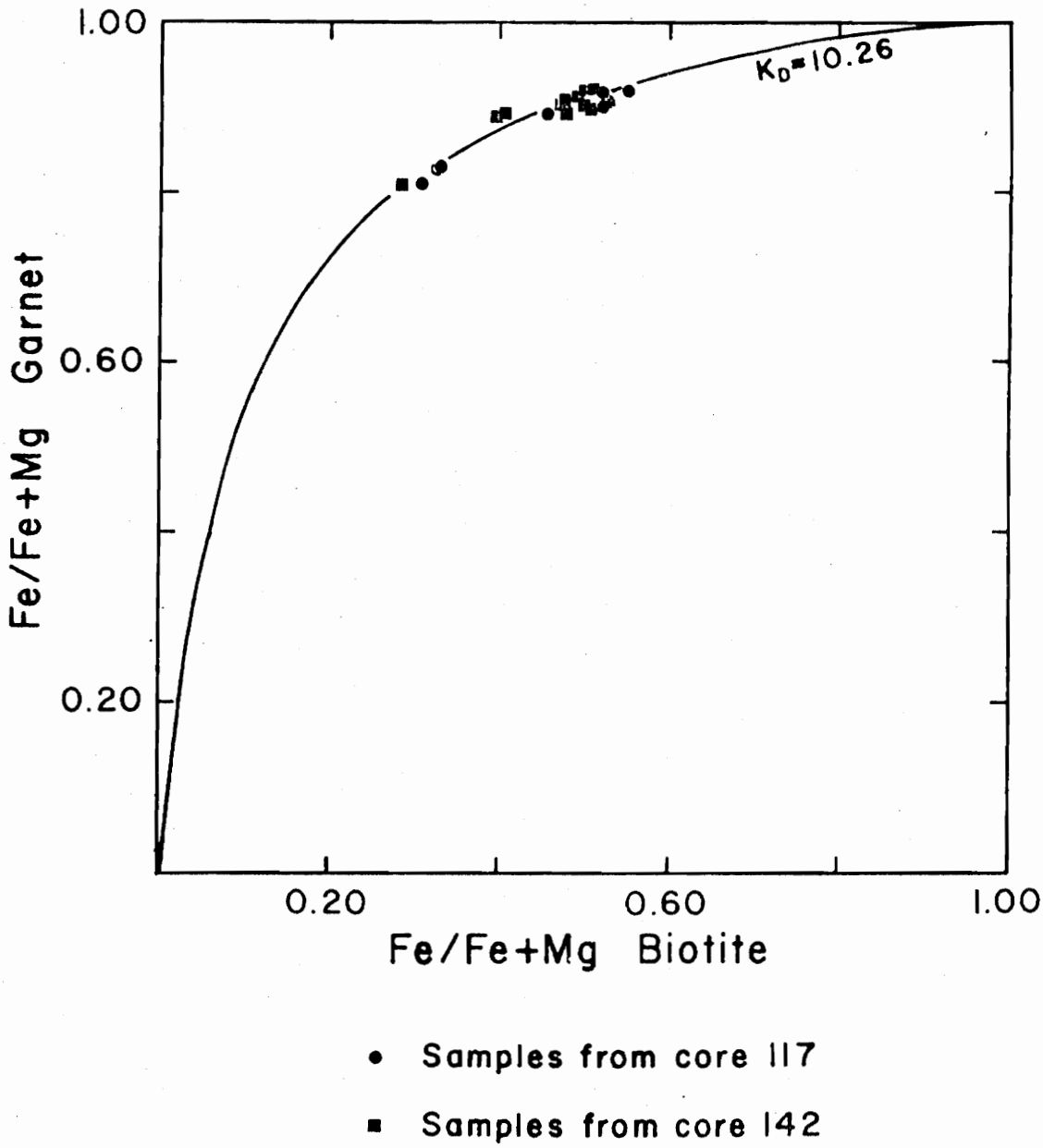

Figure 21. Fe/Fe+Mg ratios for garnet-biotite pairs in samples with the assemblage muscovite-quartz-plagioclase-garnet-biotite-chlorite and showing the line of constant distribution coefficient equal to the average of all the garnet-biotite pairs shown.

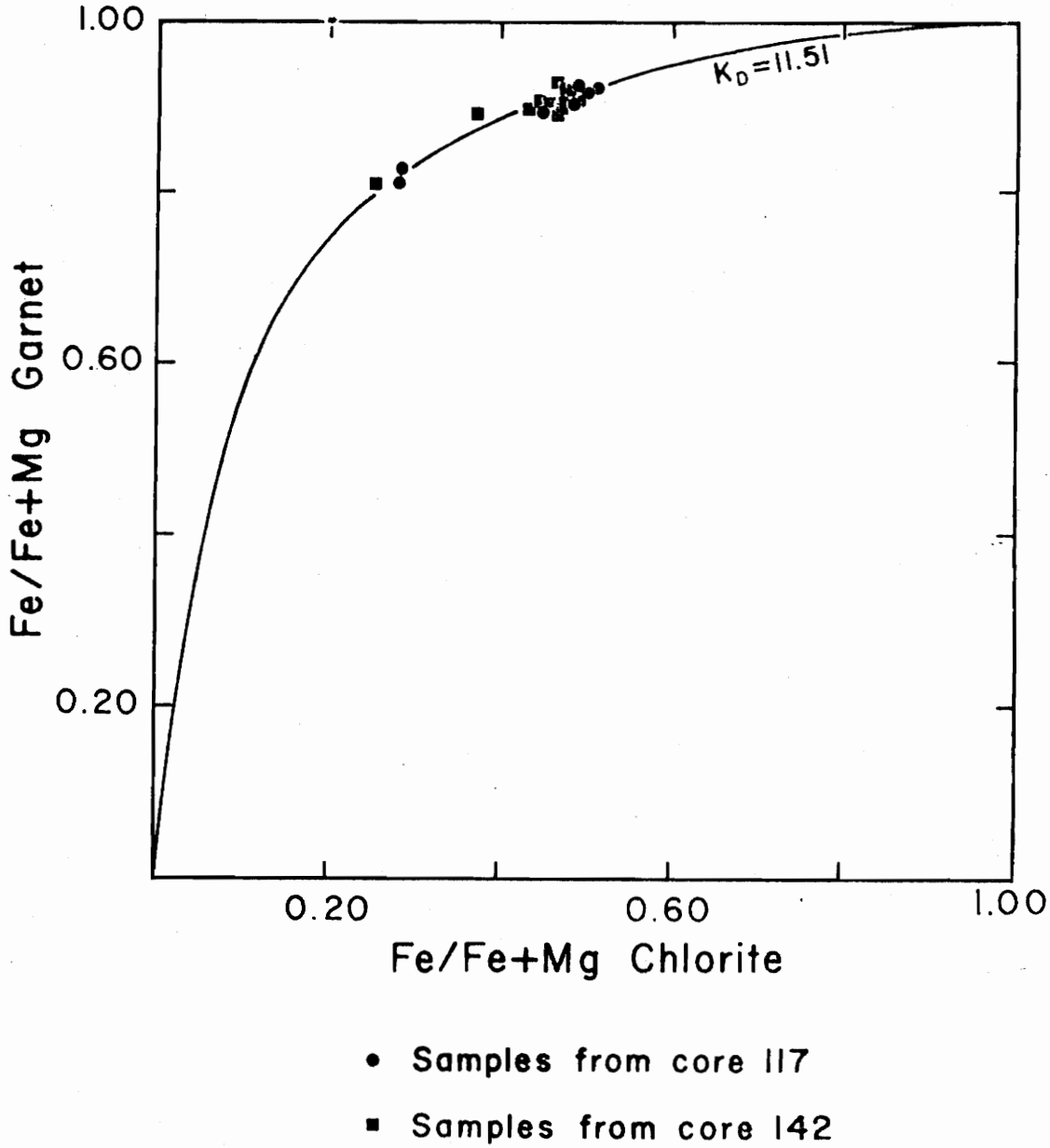

Figure 22. Fe/Fe+Mg ratios for garnet-chlorite pairs in samples with the assemblage muscovite-quartz-plagioclase-garnet-biotite-chlorite and showing the line of constant distribution coefficient equal to the average of all the garnet-chlorite pairs shown.

of both the ore zone and the surrounding rocks were formed under the same thermal conditions.

Saxena (1973) and Thompson (1976) have published possible geothermometers based on the garnet-biotite distribution coefficient. Saxena's (1973) geothermometer is for amphibolite and higher grades only. However, Thompson's (1976) geothermometer is extended to lower grades. Figure 23 shows the range of distribution coefficients from this study plotted on Thompson's geothermometer. From figure 21, metamorphic temperatures of 415-455°C are indicated, consistent with the 460°C (4 kbar)-546°C (6 kbar) maximum temperature determined from the system muscovite-calcite-quartz, and the 400°C minimum temperature indicated by the muscovite-paragonite data.

Stose and Stose (1957, p. 191), in discussing the origin of the Gossan Lead ore, conclude "that the hydrothermal solutions entered the country rock along foliation planes and migrated a long distance from their source. They were introduced after the major part of the deformation of the district was completed." This clearly conflicts with the distribution coefficient data shown in figures 21 and 22. The ore zone garnet-biotite pairs, clearly show the effects of the relatively high sulfur environment and have the same distribution coefficient as the non-ore zone garnet-biotite pairs. If, as Stose and Stose suggest, the ore entered after the major deformation was complete, another period of metamorphism of equal magnitude would be required to equilibrate the ferromagnesian minerals to the high sulfur environment. Evidence for another major period of metamorphism of equal magnitude is lacking in the southern Appalachians. Therefore, the data presented here

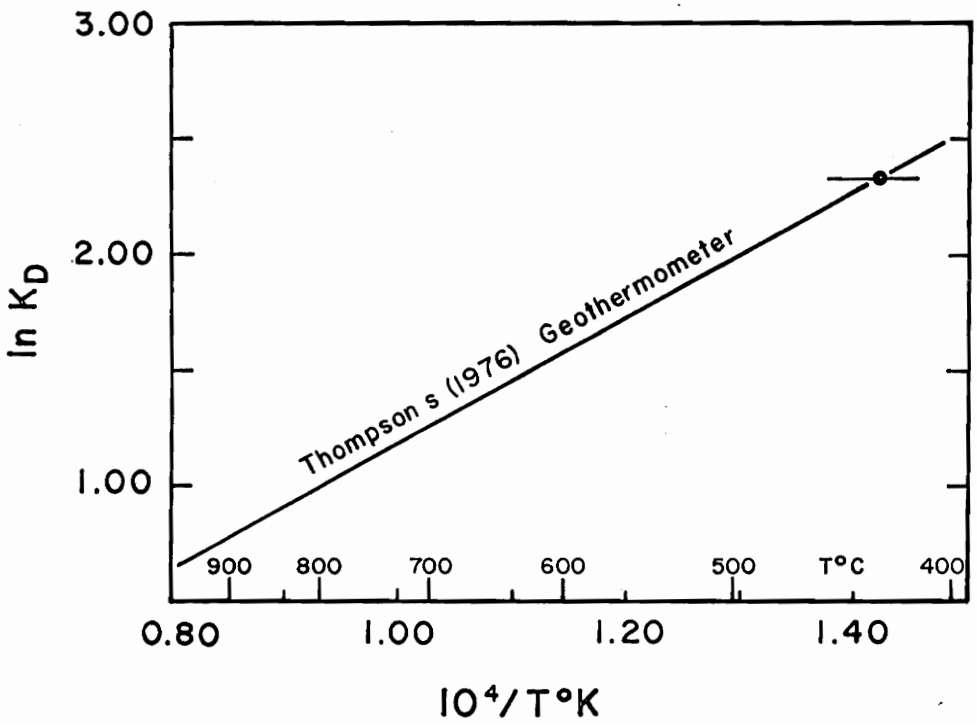

Figure 23. Distribution coefficient for garnet-biotite pairs of the Gossan Lead district plotted on Thompson's (1976) geothermometer.

clearly indicate that the ore must have been present at least at the peak of metamorphism if not before.

This study places some limits on the conditions of formation of the Great Gossan Lead ore. The data from the distribution coefficients as well as the data showing that the cores of the ore zone garnets were influenced by the presence of the ore indicate that the ore must have been present prior to the major metamorphism of the Ashe formation. In the paper by Fullagar and Bottino (1970), the ore zone Sr^{87}/Sr^{86} ratios are shown to be higher than those normally encountered in igneous rocks; leading them to conclude that some of the rock must have originated from pre-existing rock. Gilmour and Still (1968) proposed that the Iron King, massive sulfide deposit formed through volcanic hot springs on, or near, a submarine depositional surface. Based on the similarity of lithologies and the structural type of the enclosing host rocks, as well as the mineralogical composition of the ore, Gilmour and Still (1968) proposed that the Ducktown deposit and similar deposits of the Appalachians, such as the Gossan Lead, are of a similar origin. The data presented here is more consistent with the mode of origin proposed by Gilmour and Still (1968) than it is with the hydrothermal origin proposed by earlier investigators.

REFERENCES

Albee, A.L., (1965). Distribution of Fe, Mg, and Mn between garnet and biotite in natural mineral assemblages. Jour. Geol., v. 73, p. 155-164.

Bence, A.E., and Albee, A.L., (1968). Empirical correction factors for the electron microanalysis of silicates and exides. Jour. Geol., v. 76, p. 382-403.

Boyd, C.R., (1881). Resources of South-west Virginia: 3rd ed., p. 1-321, New York, John Wiley and Sons.

Brown, W.R., (1958). Geology and mineral resources of the Lynchburg Quadrangle, Virginia, Virginia Div. of Min. Res. Bulletin 74, 99 p.

Burnham, C.W., Holloway, J.R., and Davis, N.F., (1969). Thermodynamic properties of water to 1000°C and 10,000 bars, Geol. Soc. of Am. Special Paper 132, 96 p.

Butler, B.C.M., (1967). Chemical Study of minerals from the Moine Schists of the Ardnamurchan Area, Argyllshire, Scotland, Jour. Petrol., v. 8, p. 233-267.

Cameron, K.L., (1975). An experimental Study of actinolite-cummingtonite phase relations with notes on the synthesis of Fe-rich anthophyllite, Am. Min., v. 60, p. 375-390.

Craig, J.R., and Gilbert, M.C., (1974). Amphiboles in Appalachian Ores, (abstr.), Geol. Soc. of Am. Abstracts with Programs, v. 6, p. 346.

Craig, J.R., Sears, C.E., Gilbert, M.C., and Hewitt, D.A., The Gossan Lead District, VPI & SU Dept. of Geological Sciences, Geological Guidebook no. 5, p. 25-34.

Curry, R.O., (1880). The Copper and iron region of the Floyd-Carroll-Grayson plateau of the Blue Ridge in Virginia, etc.: The Virginias, v. 1, p. 62-64, 70-71, 74-77, 80-81, 95.

Eugster, H.P., Albee, A.L., Bence, A.E., Thompson, J.B. Jr., and Waldbaum, D.R., (1972). The two-phase region and excess mixing properties of paragonite-muscovite crystalline solutions, Jour. Petrol., v. 13, p. 147-179.

Fullagar, P.D., and Bottino, M.L., (1970). Sulfide Mineralization and Rubidium-Strontium Geochronology at Ore Knob, North Carolina, and Ducktown, Tennessee, Economic Geol., v. 65, p. 541-550.

Fullagar, P.D., Brown, H.S., and Hagner, A.F., (1967). Geochemistry of Wall Rock alteration and the role of sulfurization in the formation of the Ore Knob sulfide deposit, Jour. Geol. v. 62, p. 798-825.

Fullagar, P.D., and Dietrich, R.V., (1976). Rb-Sr Isotopic Study of the Lynchburg and probably correlative formations of the Blue Ridge and Western Piedmont of Virginia and North Carolina, Am. Jour. Sci., v. 276, p. 347-365.

Gilmour, P., and Still, A.R., (1968). The Geology of the Iron King Mine in Ore Deposits of the United States, 1933-1967 (The Graton-Sales volume), New York, v. 2, p. 1239-1257.

Hammerback, S., and Lindquist, B., (1972). The hydrothermal stability of annite in the presence of sulfur, Geologiska Forren.: Stockholm Forrhandl., v. 94, p. 549-564.

Henry, D.K., Craig, J.R., and Gilbert, M.C., (1976). Ore Mineralogy of a portion of the Gossan Lead district, Carroll and Grayson Counties, Virginia (abstr.) Geol. Soc. of Am. Abstracts with Programs, v. 8, p. 194.

Hewitt, D.A., (1973). Stability of the assemblage muscovite-calcite-quartz, Am. Min., v. 58, p. 785-791.

Hewitt, D.A., and Wones, D.R., (1975). Physical properties of some synthetic Fe-Mg-Al Trioctahedral biotites, Am. Min., v. 60, p. 854-862.

Hoschek, G., (1969). The stability of staurolite and chloritoid and their significance in metamorphism of pelitic rocks, Contr. Mineral. Petrol., v. 22, p. 208-232.

Johannes, W., and Orville, P.M., (1972). Zur Stabilitat der Mineral Paragenesen Muscovit + Calcit + Quarz, Zoisit + Muskovit + Quarz, Anorthit + F-Feldspar und Anorthit + Calcit. Fortschr. Mineral., v. 50, p. 46-47.

Jonas, A.I., (1927). Geologic reconnaissance in the piedmont of Virginia, Geol. Soc. of Am. Bulletin, v. 38, p. 837-846.

Keith, A., (1903). Description of the Cranberry Quadrangle (North Carolina-Tennessee): U.S. Geol. Survey Geol. Atlas of the U.S., Folio 90, 9

Kinkel, A.R., (1967). The Ore Knob Copper Deposit, North Carolina, and other massive sulfide deposits of the Appalachians, U.S. Geol. Survey prof. paper 558, 58 p.

Kinkel, A.R. Jr., Thomas, H.H., Marvin, R.F., and Walthall, F.G., (1965). Age and metamorphism of some massive sulfide deposits in Virginia, North Carolina, and Tennessee, Geochimica et Cosmochimica Acta, v. 29, p. 717-724.

Kretz, R., (1961). Some Applications of thermodynamics to coexisting minerals of variable composition. Examples: orthopyroxene-clinopyroxene, and orthopyroxene-garnet, Jour. Geol., v. 69, p. 361-387.

Kretz, R., (1963). Distribution of magnesium and iron between orthopyroxene and calcic pyroxene in natural assemblages, Jour. Geol., v. 71, p. 773-785.

Kullerud, G., and Yoder, H.S., (1963). Sulfide-silicate relations, Ann. Report to Director Geoph. Lab. 1962-63, p. 215-218.

Kullerud, G., and Yoder, H.S., (1964). Sulfide-silicate relations, Ann. Report to the Dir. of Geoph. Lab 1963-64, p. 218-222.

Leake, B.E., (1968). A catalog of analyzed calciferous and subcalciferous amphiboles together with their nomenclature and associated minerals, Geol. Soc. of Am. Special Paper 98, 210 p.

Lyons, J.B., and Morse, S.A., (1970). Mg/Fe partitioning in garnet and biotite from some granitic, pelitic, and calcic rocks, Am. Min., v. 55, p. 231-245.

Naldrett, A.J., (1966). The role of sulfurization in the genesis of iron-nickel sulfide deposits of the Porcupine District, Ontario, Canadian Mining and Metallur. Bulletin, v. 69, p. 147-155.

Naldrett, A.J., and Brown, G.M., (1968). Reaction between pyrrhotite and enstatite-ferrosilite solid solutions, Ann. Report to the Dir. of the Geoph. Lab 1966-67, p. 427-429.

Orville, P.M., (1972). Plagioclase cation exchange equilibria with aqueous chlorite solution; results at 700°C and 2000 bars in the presence of quartz. Am. Jour. Sci., v. 272, p. 234-272.

Popp, R.K., (1975). Iron-Magnesium Amphiboles: Synthesis and stability with respect to temperature, pressure, oxygen fugacity, and sulfur fugacity, unpubl. Ph.D. Dissertation, VPI & SU, 122 p.

Popp, R.K., and Gilbert, M.C., (1974). Sulfurization of intermediate Fe-Mg amphiboles (abstr.), Geol. Soc. of Am. Abstracts with Programs, v. 6, p. 1058.

Rankin, D.W., (1970). Stratigraphy and structure of Precambrian rocks in northwestern North Carolina, in Fisher, G.W., Pettijohn, F.J., Reed, J.C., Weaver, K.N., eds., Studies of Appalachian Geology: Central and Southern, Interscience, New York, p. 227-245.

Rankin, D.W., Espenshade, G.H., and Shaw, K.W., (1973). Stratigraphy and Structure of the metamorphic belt in northwestern North Carolina and southwestern Virginia: A study from the Blue Ridge across the Brevard fault zone to the Saurtown Mountains Anticlinorium. Am. Jour. Sci., Cooper Vol., p. 1-40.

Ross, C.S., (1935). Origin of the Copper deposits of the Ducktown type in the southern Appalachian region, U.S. Geop. Survey Prof. Paper 179, 165 p.

Rucklidge, J.C., (1971). Specifications of Fortran Program SUPERRECAL., Dept. of Geology, Univ. of Toronto.

Saxena, S.K., (1973). Thermodynamics of Rock-forming Crystalline Solutions, Springer-Verlag, New York, 186 p.

Scott, S.D., (1976). Application of the sphalerite geobarometer to regionally metamorphosed terrains, Am. Min., v. 61, p. 661-670.

Spry, A., (1969). Metamorphic Textures, Pergamon Press, New York, 350 p.

Stanton, R.L., and Gorman, H., (1968). A phenomenological Study of grain boundary migration in some common sulfides, Economic Geol., v. 63, p. 907-923.

Staten, W.T., and Hewitt, D.A., (1976). Silicate petrology of the Great Gossan Lead and the surrounding rocks in southwest Virginia (abstr.) Geol. Soc. of Am. Abstracts with Programs, v. 8, p. 276.

Stose, A.J., and Stose, G.W., (1957). Geology and Mineral Resources of the Gossan Lead District and Adjacent Areas in Virginia, Virginia Div. of Min. Res. Bulletin 72, 233 p.

Thompson, A.B., (1976). Mineral Reactions in pelitic rocks: II. Calculation of some P-T-X (Fe-Mg) phase relations, Am. Jour. Sci., v. 276, p. 425-454.

Tso, J., and Gilbert, M.C., Craig, J.R., (1976). Sulfurization of synthetic biotites (abstr.) Geol. Soc. of Am. Abstracts with Programs, v. 8, p. 289-290.

Velde, B., (1965). Phengite micas-synthesis, stability, and natural occurrence, Am. Jour. Sci., v. 263, p. 886-913.

Watson, T.L., (1907). Mineral resources of Virginia, Virginia-Jamestown Exposition Comm., Lynchburg, Va., 618 p.

APPENDIX A

Log of Core 117

Depth (feet)	Lithology
0-80	not preserved
80-88.3	fine- to medium-grained quartz-muscovite schist
88.3-88.4	coarse-grained, weakly-foliated, biotite-chlorite schist
88.4-99.9	fine- to medium-grained quartz-muscovite schist
99.9-100.4	quartz vein
100.5-104.8	fine- to medium-grained quartz-muscovite schist
104.8-106	95% quartz vein, 5% quartz-muscovite schist
106-106.3	fine- to medium-grained quartz-muscovite schist
106.3-106.4	medium-grained biotite schist
106.4-110.5	fine- to medium-grained quartz-muscovite schist
110.5-110.6	medium-grained biotite schist
110.6-160	fine- to medium-grained quartz-muscovite schist
160-161	90% quartz, 6% pale-green chlorite, 4% marble
161-181.4	fine- to medium-grained quartz-muscovite schist
181.4-181.6	medium-grained biotite schist
181.6-195.1	fine- to medium-grained quartz-muscovite schist
195.1-195.3	medium-grained chlorite schist
195.3-219	fine- to medium-grained quartz-muscovite schist
219-233.6	graphitic fine-grained quartz-muscovite schist
233.6-235.2	fine- to medium-grained quartz-muscovite schist
235.2-237	graphitic fine-grained quartz-muscovite schist
237-238	coarse-grained well-foliated biotite-chlorite-quartz-muscovite schist
238-246.5	fine- to medium-grained quartz-muscovite schist
246.5-246.7	medium-grained chlorite schist
246.7-251	fine- to medium-grained quartz-muscovite schist
251-251.2	coarse-grained chlorite-biotite schist
251.2-270.3	fine- to medium-grained quartz-muscovite schist
270.3-271.3	quartz vein with minor chlorite inclusions
271.3-382	fine- to medium-grained quartz-muscovite schist
382-386.5	fine- to medium-grained muscovite-quartz gneiss
386.5-482	fine- to medium-grained quartz-muscovite schist
482-483	coarse-grained, well-foliated biotite-chlorite-quartz-muscovite schist
483-488.4	fine- to medium-grained quartz-muscovite schist
488.4-491	slightly graphitic fine-medium-grained quartz-muscovite schist
491-510	fine- to medium-grained muscovite-quartz gneiss
510-518.2	medium-grained quartz-muscovite schist
518.2-539	slightly hornblendic quartz-muscovite gneiss
539-541.7	fine- to medium-grained quartz-muscovite schist
541.7-542	hornblendic gneiss
542-546.3	fine- to medium-grained quartz-muscovite schist
546.3-546.4	hornblendic gneiss
546.4-552.3	fine- to medium-grained quartz-muscovite schist

Log of Core 117, continued

552.3-562	medium-grained quartz-muscovite schist
562-591.2	fine- to medium-grained quartz-muscovite schist
591.2-591.8	quartz vein
591.8-608	medium-grained quartz-muscovite schist with biotite-rich layers
608-619.5	fine- to medium-grained quartz-muscovite schist
619.5-638	fine- to medium-grained muscovite-quartz gneiss
638-638.8	medium-grained, quartz-muscovite schist
638.8-644.8	fine- to medium-grained muscovite-quartz gneiss
644.8-645.7	medium-grained, quartz-muscovite schist
645.7-647.3	fine- to medium-grained muscovite-quartz gneiss
647.3-653.6	medium-grained quartz-muscovite schist
653.6-654.6	5% pyrrhotite, 95% medium-grained quartz-muscovite schist
654.6-659.1	medium-grained quartz-muscovite schist
659.1-664.1	fine- to medium-grained muscovite-quartz gneiss
664.1-664.8	medium-grained quartz-muscovite schist
664.8-667.8	fine- to medium-grained muscovite-quartz gneiss
667.8-668.3	medium-grained, well-foliated biotite-chlorite-quartz-muscovite schist
668.3-669.3	fine- to medium-grained muscovite-quartz gneiss
669.3-669.9	medium-grained quartz-muscovite schist
669.9-673.6	fine- to medium-grained muscovite-quartz gneiss
673.6-678	medium-grained quartz-muscovite schist
678-833.5	interlayered fine- to medium-grained muscovite-quartz gneiss and coarse- to medium-grained biotite-chlorite-quartz-muscovite schist
833.5-833.9	quartz vein
833.9-835.8	fine- to medium-grained muscovite-quartz gneiss
835.8-836.3	quartz vein
836.3-836.5	fine- to medium-grained muscovite-quartz gneiss
836.5-882	fine- to medium-grained quartz-muscovite schist
882-882.1	hornblendic gneiss
882.1-884.1	fine- to medium-grained muscovite-quartz gneiss
884.1-884.2	hornblendic gneiss
884.2-886.8	fine- to medium-grained muscovite-quartz gneiss
886.8-887	fine- to medium-grained quartz-muscovite schist
887-890.8	fine- to medium-grained muscovite-quartz gneiss
890.8-891.3	80% quartz vein, 20% muscovite-quartz schist with minor fractures across core at ∿40°
891.3-896.3	fine- to medium-grained muscovite-quartz gneiss
896.3-896.8	60% quartz, 40% chlorite schist
896.8-902.8	fine- to medium-grained muscovite-quartz gneiss
902.8-903	5% pyrrhotite, 70% quartz, 25% quartz-muscovite schist
903-903.9	fine- to medium-grained muscovite-quartz gneiss
903.9-904.5	5% pyrrhotite, 95% quartz-muscovite schist
904.5-906.1	fine- to medium-grained muscovite-quartz gneiss

Log of Core 117, continued

906.1-906.8	3-5% pyrrhotite, 95-97% quartz-muscovite schist
906.8-944.2	fine- to medium-grained quartz-muscovite schist
944.2-944.3	hornblendic gneiss
944.3-947.7	fine- to medium-grained quartz-muscovite schist
944.7-944.9	hornblendic gneiss
944.9-967	fine- to medium-grained quartz-muscovite schist
967-967.6	98% quartz, 2% pyrrhotite
967.6-976.7	fine- to medium-grained quartz-muscovite schist
976.7-977.3	hornblendic gneiss
977.3-978.7	fine- to medium-grained quartz-muscovite schist
978.7-979.2	hornblendic gneiss (hornblende prisms not well-developed)
979.2-1046.3	fine- to medium-grained quartz-muscovite schist
1046.3-1046.5	medium-grained well-foliated biotite-chlorite schist
1046.5-1048.6	fine- to medium-grained muscovite-quartz gneiss
1048.6-1049	medium-grained, well-foliated biotite-chlorite schist
1049-1049.6	medium-grained, poorly-foliated biotite-chlorite schist
1049.6-1051.8	fine- to medium-grained quartz-muscovite schist
1051.8-1051.9	biotite schist
1051.9-1054.1	medium-grained quartz-muscovite schist
1054.1-1054.8	medium-grained, well-foliated biotite-chlorite schist
1054.8-1057	fine- to medium-grained quartz-muscovite schist
1057-1057.8	medium-grained, well-foliated biotite-chlorite schist
1057.8-1183	fine- to medium-grained quartz-muscovite schist
1183-1183.3	fine- to medium-grained muscovite-quartz gneiss
1183.3-1183.4	hornblendic gneiss
1183.4-1183.8	fine- to medium-grained muscovite quartz gneiss
1183.8-1207.8	interlayered fine- to medium-grained quartz-muscovite schist and medium-grained, well-foliated biotite-chlorite-quartz-muscovite schist
1207.8-1207.9	apophyllite solution cavities in quartz-muscovite schist
1207.9-1212	fine- to medium-grained quartz-muscovite schist
1212-1212.2	apophyllite solution cavities in quartz-muscovite schist
1212.2-1217.2	fine- to medium-grained quartz-muscovite schist
1217.2-1217.3	apophyllite solution cavities in quartz-muscovite schist
1217.3-1246.1	fine- to medium-grained quartz-muscovite schist
1246.1-1249.4	5% sulfide, 95% chlorite-muscovite schist
1249.4-1250.8	25% sulfide, 75% chlorite schist
1250.8-1251	5% sulfide, 95% chlorite schist

Log of Core 117, continued

1251-1251.6	25% sulfide, 75% chlorite schist
1251.6-1251.8	5% sulfide, 95% chlorite schist
1251.8-1252.8	30-40% sulfide, 60-70% chlorite schist
1252.8-1258.7	fine- to medium-grained muscovite schist
1258.7-1261.8	40% sulfide, 60% chlorite schist
1261.8-1263.3	10% sulfide, 90% chlorite schist
1263.3-1264.9	chlorite schist
1264.9-1265.3	15-20% sulfide, 80-85% chlorite schist
1265.3-1265.5	chlorite-garnet selvage
1265.5-1265.7	biotite-garnet selvage
1265.7-1268.5	chlorite-biotite schist
1268.5-1269.2	quartz vein
1269.2-1270.1	15% sulfide, 85% chlorite schist
1270.1-1275.8	fine- to medium-grained, chlorite-rich quartz-muscovite schist
1275.8-1277.6	90% quartz, 10% pyrrhotite
1277.6-1297.1	interlayered 2-4 inch quartz veins and fine- to medium-grained quartz-muscovite schist
1297.1-1298.1	25% sulfide, 75% chlorite schist
1298.1-1302.1	fine- to medium-grained chlorite-quartz-muscovite schist
1302.1-1302.3	5% pyrrhotite and chalcopyrite, 95% quartz-muscovite schist
1302.3-1305.7	fine- to medium-grained quartz-muscovite schist
1305.7-1313.2	10% sulfide, 90% chlorite-quartz-muscovite schist
1313.2-1314	20% sulfide, 80% chlorite schist
1314-1314.7	fine- to medium-grained chlorite-quartz-muscovite schist
1314.7-1315.2	10-15% sulfide, 85-90% chlorite schist
1315.2-1317.1	25% sulfide, 75% chlorite schist
1317.1-1331.3	fine- to medium-grained chlorite-quartz-muscovite schist
1331.3-1331.4	30% sulfide, 70% chlorite schist
1331.4-1331.5	fine- to medium-grained chlorite-quartz-muscovite schist
1331.5-1332.2	30% sulfide, 70% chlorite schist
1332.2-1332.6	5% sulfide, 95% chlorite-quartz-muscovite schist
1332.6-1333.1	40% sulfide, 60% chlorite schist
1333.1-1334	20% sulfide, 80% chlorite schist
1334-1334.9	30-40% sulfide, 60-70% chlorite schist
1334.9-1342.4	fine- to medium-grained quartz-muscovite schist
1342.4-1342.6	hornblendic gneiss
1342.6-1343.8	fine- to medium-grained muscovite-quartz gneiss
1343.8-1351.1	fine- to medium-grained quartz-muscovite schist
1351.1-1351.2	hornblendic gneiss
1351.2-1368.7	fine- to medium-grained quartz-muscovite schist
1368.7-1369.7	quartz vein
1369.7-1370.3	medium-grained quartz-muscovite schist
1370.3-1371.9	quartz vein

Log of Core 117, continued

1371.9-1372.8	fine- to medium-grained quartz-muscovite schist
1372.8-1372.9	50% sulfide, 50% chlorite schist
1372.9-1396.9	fine- to medium-grained quartz-muscovite schist
1396.9-1397.2	biotite-chlorite schist
1397.2-1397.8	50% sulfide, 50% chlorite schist
1397.8-1397.9	chlorite schist
1397.9-1398	50% sulfide, 50% chlorite schist
1398-1398.3	chlorite schist
1398.3-1398.4	50% sulfide, 50% chlorite schist
1398.4-1398.5	chlorite schist
1398.5-1398.7	50% sulfide, 50% chlorite schist
1398.7-1405.3	medium-grained quartz-muscovite schist
1405.3-1405.6	quartz vein
1405.6-1428.3	fine- to medium-grained quartz-muscovite schist
1428.3-1428.7	25% pyrrhotite, 75% quartz-chlorite schist
1428.7-1455.5	fine- to medium-grained quartz-muscovite schist
1455.5-1456.3	10-15% sulfide, 85-90% chlorite-quartz-muscovite schist
1456.3-1469.4	fine- to medium-grained quartz-muscovite schist
1469.4-1470	quartz vein
1470-1544.3	fine- to medium-grained quartz-muscovite schist
1544.3-1545.6	quartz vein
1545.6-1570.5	fine- to medium-grained quartz-muscovite schist
1570.5-1572.1	medium-grained, well-foliated garnet-biotite-chlorite schist
1572.1-1598.5	fine- to medium-grained quartz-muscovite schist
1598.5-1598.8	quartz vein
1598.8-1636.3	fine- to medium-grained quartz-muscovite schist
1636.3-1639.4	medium-grained, well-foliated biotite-chlorite schist
1639.4-1639.8	quartz vein
1639.8-1644.7	medium-grained, well-foliated biotite-chlorite schist
1644.7-1644.8	50% marble, 50% quartz-muscovite schist
1644.8-1645.8	medium-grained, well-foliated biotite-chlorite schist
1645.8-1646.3	80% marble, 20% biotite-chlorite schist
1646.3-1647.2	medium-grained, well-foliated biotite-chlorite schist
1647.2-1647.7	25% marble, 25% quartz, 50% quartz-muscovite schist
1647.7-1842.8	fine- to medium-grained quartz-muscovite schist
1842.8-1842.9	hornblendic gneiss
1842.9-1846	fine- to medium-grained muscovite-quartz gneiss
1846-1846.2	hornblendic gneiss
1846.2-1852	fine- to medium-grained muscovite-quartz gneiss
1852-1852.7	medium-grained quartz-muscovite schist
1852.7-1853.3	chlorite schist
1853.3-1854.1	fine- to medium-grained quartz-muscovite schist
1854.1-1854.9	quartz vein

Log of Core 117, continued

1854.9-1927.8	fine- to medium-grained quartz-muscovite schist
1927.8-1928.3	quartz vein
1928.3-1934.8	fine- to medium-grained quartz-muscovite schist
1934.8-1954	medium-grained, slightly graphitic quartz-muscovite schist
1954-1962	fine- to medium-grained quartz-muscovite schist
1962-1964.1	fine- to medium-grained muscovite-quartz gneiss
1964.1-1964.3	hornblendic gneiss
1964.3-1966.7	fine- to medium-grained muscovite-quartz gneiss
1966.7-1966.9	hornblendic gneiss
1966.9-1969	fine- to medium-grained muscovite-quartz gneiss
1969-1970.3	hornblendic gneiss
1970.3-1972.5	fine- to medium-grained muscovite-quartz gneiss
1972.5-1997.4	fine- to medium-grained quartz-muscovite schist
1997.4-1997.6	quartz and marble
1997.6-1997.9	fine- to medium-grained quartz-muscovite schist
1997.9-1998.2	marble
1998.2-2000.2	fine- to medium-grained quartz-muscovite schist
2000.2-2000.4	50% marble, 50% quartz-muscovite schist
2000.4-2003.2	fine- to medium-grained quartz-muscovite schist
2003.2-2003.3	biotite schist
2003.3-2052	fine- to medium-grained quartz-muscovite schist

Log of Core 142

Depth (feet)	Lithology
0-53	not preserved
53-118	fine- to medium-grained quartz-muscovite schist
118-129.5	fine- to medium-grained muscovite-quartz gneiss
129.5-135.7	medium-grained quartz-muscovite schist
135.7-137.7	fine- to medium-grained muscovite-quartz gneiss
137.7-148	medium-grained quartz-muscovite schist
148-165	fine- to medium-grained muscovite-quartz gneiss
165-175.8	fine- to medium-grained quartz-muscovite schist
175.8-176.3	quartz vein
176.3-217	fine- to medium-grained, slightly graphitic quartz-muscovite schist
217-217.8	quartz vein
217.8-228.8	fine- to medium-grained quartz-muscovite schist
228.8-229.3	quartz vein
229.3-230.3	fine- to medium-grained quartz-muscovite schist
230.3-230.8	fine- to medium-grained muscovite-quartz gneiss
230.8-230.9	hornblendic gneiss
230.9-235	fine- to medium-grained muscovite-quartz gneiss
235-259	fine- to medium-grained quartz-muscovite schist
259-259.2	medium-grained, poorly-foliated, biotite-chlorite schist
259.2-266	medium-grained quartz-muscovite schist
266-267.1	quartz vein
267.1-301.6	medium-grained, occassionally graphitic quartz-muscovite schist
301.6-335.5	fine- to medium-grained muscovite-quartz gneiss with minor interlayers of quartz-muscovite schist
335.5-335.6	hornblendic gneiss
335.6-336.1	medium-grained quartz-muscovite schist
336.1-336.5	fine- to medium-grained muscovite-quartz gneiss
336.5-336.6	hornblendic gneiss
336.6-337	fine- to medium-grained quartz-muscovite schist
337-337.3	hornblendic gneiss
337.3-345.8	fine- to medium-grained quartz-muscovite schist
345.8-345.9	hornblendic gneiss
345.9-363.7	medium-grained quartz-muscovite schist
363.7-364.3	fine- to medium-grained muscovite-quartz gneiss
364.3-364.4	medium-grained, well-foliated biotite-chlorite schist
364.4-364.5	fine- to medium-grained muscovite-quartz gneiss
364.5-364.6	hornblendic gneiss
364.6-376	fine- to medium-grained muscovite-quartz gneiss
376-473.8	fine- to medium-grained, occassionally slightly graphitic quartz-muscovite schist
473.8-474.1	50% quartz, 50% chlorite-biotite schist
474.1-474.4	fine- to medium-grained quartz-muscovite schist

Log of Core 142, continued

474.4-474.8	quartz vein
474.8-513.9	fine- to medium-grained, graphitic, quartz-muscovite schist
513.9-514.3	70% marble, 30% quartz-muscovite schist
514.3-515.3	medium-grained, graphitic, quartz-muscovite schist
515.3-515.7	50% marble, 50% quartz-muscovite schist
515.7-516.5	medium-grained, slightly graphitic quartz-muscovite schist
516.5-518.1	50% marble, 50% quartz-muscovite schist
518.1-542.2	medium-grained, slightly graphitic quartz-muscovite schist
542.2-542.8	quartz vein
542.8-567.5	medium-grained, graphitic quartz-muscovite schist
567.5-567.9	quartz vein
567.9-572	fine- to medium-grained, occassionally graphitic quartz-muscovite schist
572-572.3	quartz vein
572.3-573.7	medium-grained quartz-muscovite schist
573.7-573.8	biotite schist
573.8-574.3	medium-grained quartz-muscovite schist
574.3-574.4	chlorite schist
574.4-574.6	quartz vein
574.6-574.8	medium-grained, chlorite-rich quartz-muscovite schist
574.8-575.5	quartz vein
575.5-608.9	fine- to medium-grained, occassionally graphitic quartz-muscovite schist
608.9-614	fine- to medium-grained muscovite-quartz gneiss
614-620.5	fine- to medium-grained, graphitic quartz-muscovite schist
620.5-635	fine- to medium-grained muscovite-quartz gneiss with some biotite-rich layers
635-683.5	fine- to medium-grained graphitic quartz-muscovite-schist
683.5-683.9	quartz vein
683.9-733.3	fine- to medium-grained, slightly graphitic quartz-muscovite schist
733.3-733.7	medium-grained, weakly-foliated, biotite-chlorite schist
733.7-733.9	medium-grained, graphitic, quartz-muscovite schist
733.9-734.7	quartz vein
734.7-734.8	biotite schist
734.8-735.1	medium-grained, graphitic quartz-muscovite schist
735.1-735.5	quartz vein
735.6-757.4	fine- to medium-grained quartz-muscovite schist
757.4-757.6	quartz vein
757.6-757.8	marble
757.8-757.9	medium-grained quartz-muscovite schist
757.9-758.2	biotite schist

Log of Core 142, continued

758.2-758.3	quartz vein
758.3-758.4	biotite schist
758.4-842.1	fine- to medium-grained quartz-muscovite schist
842.1-842.3	fine- to medium-grained muscovite-quartz gneiss
842.3-842.4	hornblendic gneiss
842.4-846.8	fine- to medium-grained muscovite-quartz gneiss
846.8-847.7	medium-grained, chlorite-rich quartz-muscovite schist
847.7-860.2	fine- to medium-grained muscovite-quartz gneiss with minor layers of quartz-muscovite schist
860.2-870.3	hornblende amphibolite
870.3-920.3	interlayered fine- to medium-grained quartz-muscovite schist and gneiss
920.3-921.2	quartz vein
921.2-921.3	biotite schist
921.3-921.8	quartz vein
921.8-964.9	interlayered fine- to medium-grained quartz-muscovite schist and gneiss
964.9-965.9	hornblendic gneiss
965.9-972.3	fine- to medium-grained muscovite-quartz gneiss
972.3-974.1	fine- to medium-grained quartz-muscovite schist
974.1-974.6	fine- to medium-grained muscovite-quartz gneiss
974.6-977.2	hornblendic gneiss
977.2-977.7	fine- to medium-grained muscovite-quartz gneiss
977.7-1010.4	fine- to medium-grained quartz-muscovite schist
1010.4-1011.2	quartz vein
1011.2-1011.4	fine- to medium-grained quartz-muscovite schist
1011.4-1011.6	quartz vein
1011.6-1022.8	fine- to medium-grained quartz-muscovite schist
1022.8-1023.6	quartz vein
1023.6-1041	fine- to medium-grained, occassionally graphitic quartz-muscovite schist
1041-1041.8	quartz vein
1041.8-1045	medium-grained quartz-muscovite schist
1045-1045.5	quartz vein
1045.5-1053.8	medium-grained quartz muscovite schist
1053.8-1054.6	quartz vein
1054.6-1055	fine- to medium-grained quartz-muscovite schist
1055-1056.2	quartz vein
1056.2-1080.6	interlayered fine- to medium-grained quartz-muscovite schist and gneiss
1080.6-1081	quartz vein
1081-1120.8	interlayered fine- to medium-grained muscovite quartz gneiss and schist
1120.8-1121.3	quartz vein
1121.3-1128.3	fine- to medium-grained chlorite-muscovite schist
1128.3-1129.8	40% sulfide, 60% chlorite schist
1129.8-1132.2	50% sulfide, 50% chlorite schist
1132.2-1132.5	chlorite-garnet selvage

Log of Core 142, continued

1132.5-1133.3	60% sulfide, 40% chlorite schist
1133.3-1133.5	chlorite-garnet selvage
1133.6-1135	40% sulfide, 60% chlorite schist
1135-1137.1	30% sulfide, 70% chlorite schist
1137.1-1137.2	chlorite schist
1137.2-1137.3	quartz
1137.3-1139.2	25-30% sulfide, 70-75% chlorite schist
1139.2-1142.8	15-20% sulfide, 80-85% chlorite-garnet schist
1142.8-1148.5	5-10% sulfide, 90-95% chlorite-garnet schist
1148.5-1149.5	fine- to medium-grained quartz-muscovite schist
1149.5-1151	fine- to medium-grained muscovite-quartz gneiss
1151-1220	interlayered fine- to medium-grained, occassionally graphitic quartz-muscovite schist and gneiss
1120-1220.2	hornblendic gneiss
1220.2-1221	fine- to medium-grained muscovite-quartz gneiss
1221-1275.6	fine- to medium-grained, graphitic, quartz-muscovite schist
1275.6-1275.8	marble
1275.8-1305	fine- to medium-grained, graphitic quartz-muscovite schist

APPENDIX B

Table 1A

Core 117

Garnet Rim

Depth	654		1178	1178		1223	1223	1238	1243
CaO	9.27	9.56	8.21	7.20	8.96	8.36	9.27	8.45	8.42
TiO_2	0.04	0.03	0.02	0.02	0.13	0.05	0.04	0.02	0.06
MnO	2.71	1.84	2.52	2.26	7.42	2.30	2.86	1.80	1.41
FeO	27.84	28.76	28.87	29.61	24.20	29.29	27.52	28.89	28.50
Al_2O_3	22.04	21.77	22.04	22.08	22.03	21.55	21.94	21.72	21.82
SiO_2	37.81	37.82	37.51	37.19	36.86	37.84	36.96	37.20	37.64
MgO	1.45	1.38	1.59	1.74	0.96	2.06	1.41	1.69	1.94
Sum	101.16	101.16	100.76	100.10	100.56	101.45	100.00	99.77	99.79
Si	2.979	2.984	2.972	2.967	2.941	2.981	2.952	2.974	2.993
Al^{IV}	0.021	0.016	0.028	0.033	0.059	0.019	0.048	0.026	0.007
Al^{VI}	2.025	2.008	2.029	2.042	2.011	1.981	2.017	2.020	2.038
Ti	0.002	0.002	0.001	0.001	0.008	0.003	0.002	0.001	0.004
Mn	0.181	0.123	0.169	0.153	0.501	0.153	0.193	0.122	0.095
Fe	1.834	1.898	1.913	1.975	1.615	1.930	1.838	1.932	1.895
Mg	0.170	0.162	0.188	0.207	0.114	0.242	0.168	0.201	0.230
Ca	0.782	0.808	0.697	0.615	0.766	0.706	0.793	0.724	0.717
O	12.000	12.000	12.000	12.000	12.000	12.000	12.000	12.000	12.000
Fe/Fe+Mg	0.922	0.926	0.917	0.911	0.949	0.896	0.924	0.911	0.896

Table 1A (continued)

Core 117

Garnet Rim

Depth	1243	1260	1260	1260	1267	1267	1314	1356	1376	1376
CaO	8.61	7.42	7.50	5.50	7.44	8.06	7.20	8.19	9.02	9.05
TiO_2	0.02	0.13	0.08	0.10	0.02	0.03	0.07	0.03	0.04	0.05
MnO	1.13	11.80	11.92	16.53	13.79	11.96	16.11	0.50	1.70	4.26
FeO	28.85	18.55	20.20	18.03	19.20	19.80	15.96	29.93	28.95	27.54
Al_2O_3	22.17	21.39	22.14	20.86	20.33	21.15	21.38	21.90	21.11	21.03
SiO_2	37.63	37.28	35.59	37.01	37.94	38.26	37.46	37.46	36.81	37.27
MgO	1.89	2.31	2.17	2.18	2.14	2.35	2.11	1.47	1.48	1.14
Sum	100.30	98.88	99.60	100.21	100.86	101.61	100.29	99.48	99.11	100.34
Si	2.978	2.993	2.872	2.975	3.020	3.005	2.983	2.995	2.974	2.985
Al^{IV}	0.022	0.007	0.128	0.025	0.000	0.000	0.017	0.005	0.026	0.015
Al^{VI}	2.046	2.016	1.977	1.951	1.907	1.957	1.990	2.058	1.984	1.970
Ti	0.001	0.008	0.005	0.006	0.001	0.002	0.004	0.002	0.002	0.003
Mn	0.076	0.802	0.815	1.126	0.930	0.796	1.087	0.034	0.116	0.289
Fe	1.910	1.245	1.363	1.212	1.278	1.300	1.063	2.001	1.956	1.845
Mg	0.223	0.276	0.261	0.261	0.254	0.275	0.250	0.175	0.178	0.136
Ca	0.730	0.638	0.648	0.474	0.635	0.678	0.614	0.701	0.781	0.777
O	12.000	12.000	12.000	12.000	12.000	12.000	12.000	12.000	12.000	12.000
Fe/Fe+Mg	0.899	0.881	0.893	0.899	0.897	0.884	0.896	0.921	0.921	0.940

Table 1B

Core 142

Garnet Rim

Depth	345	345	490	490	696	696	696	799	799
CaO	5.53	5.58	8.30	8.07	8.37	9.22	8.67	6.95	6.28
TiO_2	0.17	0.04	0.03	0.01	0.02	0.02	0.02	0.02	0.00
MnO	0.35	0.18	2.42	2.23	2.17	1.46	1.35	2.89	4.54
FeO	33.55	31.97	28.38	28.51	29.05	27.84	27.92	29.07	28.30
Al_2O_3	20.74	21.88	21.74	22.39	21.89	21.32	21.62	20.87	21.04
SiO_2	37.14	37.67	37.63	37.93	37.71	38.13	38.12	37.19	37.77
MgO	2.28	2.28	1.79	1.81	1.77	1.62	1.81	1.93	1.76
Sum	99.76	99.60	100.29	100.95	100.98	99.61	99.51	98.92	99.69
Si	2.993	3.007	2.989	2.984	2.979	3.034	3.030	3.007	3.030
Al^{IV}	0.007	0.000	0.011	0.016	0.021	0.000	0.000	0.000	0.000
Al^{VI}	1.963	2.058	2.023	2.059	2.017	1.999	2.025	1.989	1.989
Ti	0.010	0.002	0.002	0.001	0.001	0.001	0.001	0.001	0.000
Mn	0.024	0.012	0.163	0.149	0.145	0.098	0.091	0.198	0.308
Fe	2.261	2.134	1.885	1.876	1.919	1.853	1.856	1.966	1.898
Mg	0.274	0.271	0.212	0.212	0.208	0.192	0.214	0.233	0.210
Ca	0.478	0.477	0.706	0.680	0.708	0.786	0.738	0.602	0.540
O	12.000	12.000	12.000	12.000	12.000	12.000	12.000	12.000	12.000
Fe/Fe+Mg	0.893	0.888	0.906	0.905	0.908	0.910	0.901	0.903	0.913

Table 1B (continued)

Core 142

Garnet Rim

Depth	870	870	899	899	977	1020	1020	1112	1112
CaO	9.38	10.03	9.08	9.04	8.69	9.39	8.92	9.03	9.11
TiO_2	0.06	0.02	0.06	0.04	0.03	0.10	0.04	0.02	0.07
MnO	1.70	1.24	2.51	2.00	3.46	2.16	1.01	0.65	2.47
FeO	29.44	29.07	27.92	28.32	26.57	27.91	29.97	29.07	27.99
Al_2O_3	19.96	21.13	22.15	22.00	21.54	21.45	21.84	21.22	21.21
SiO_2	36.91	38.03	38.90	37.38	37.07	37.14	37.89	37.72	37.45
MgO	1.58	1.27	1.12	1.31	2.08	1.39	1.67	1.52	1.18
Sum	99.03	100.79	101.74	100.09	99.44	99.54	101.34	99.23	99.48
Si	2.999	3.013	3.033	2.976	2.969	2.978	2.983	3.022	3.005
Al^{IV}	0.001	0.000	0.000	0.024	0.031	0.022	0.017	0.000	0.000
Al^{VI}	1.911	1.973	2.035	2.040	2.002	2.005	2.009	2.003	2.006
Ti	0.004	0.001	0.004	0.002	0.002	0.006	0.002	0.001	0.004
Mn	0.117	0.083	0.166	0.135	0.235	0.147	0.067	0.044	0.168
Fe	2.001	1.926	1.820	1.885	1.780	1.871	1.973	1.948	1.879
Mg	0.191	0.150	0.130	0.155	0.248	0.166	0.196	0.181	0.141
Ca	0.817	0.851	0.758	0.771	0.746	0.807	0.752	0.775	0.783
O	12.000	12.000	12.000	12.000	12.000	12.000	12.000	12.000	12.000
Fe/Fe+Mg	0.917	0.931	0.939	0.929	0.890	0.924	0.912	0.916	0.935

Table 1B (continued)

Core 142

Garnet Rim

Depth	1133	1133	1149	1151	1156	1164	1164	1164	1170
CaO	7.91	6.33	8.51	8.82	8.89	9.11	8.76	8.39	9.14
TiO_2	0.09	0.06	0.04	0.06	0.04	0.00	0.04	0.03	0.10
MnO	11.97	12.49	6.09	1.94	3.58	2.20	2.10	1.63	3.42
FeO	18.86	19.84	26.21	27.96	27.64	27.50	28.05	28.59	27.32
Al_2O_3	22.29	22.54	19.50	21.82	21.00	21.79	21.91	21.44	22.06
SiO_2	37.36	37.15	37.50	38.11	37.21	38.09	37.75	37.99	36.84
MgO	2.57	2.55	1.77	1.80	1.64	1.50	1.50	1.57	1.26
Sum	101.05	100.96	99.62	100.51	100.00	100.19	100.11	99.64	100.14
Si	2.940	2.933	3.033	3.008	2.982	3.016	2.997	3.028	2.942
Al^{IV}	0.060	0.067	0.000	0.000	0.018	0.000	0.003	0.000	0.058
Al^{VI}	2.007	2.030	1.858	2.029	1.965	2.033	2.046	2.014	2.018
Ti	0.005	0.004	0.002	0.004	0.002	0.000	0.002	0.002	0.006
Mn	0.798	0.835	0.417	0.130	0.243	0.148	0.141	0.110	0.231
Fe	1.241	1.310	1.773	1.845	1.853	1.821	1.862	1.906	1.825
Mg	0.301	0.300	0.213	0.212	0.196	0.177	0.177	0.187	0.150
Ca	0.667	0.535	0.737	0.746	0.763	0.773	0.745	0.716	0.782
O	12.000	12.000	12.000	12.000	12.000	12.000	12.000	12.000	12.000
Fe/Fe+Mg	0.871	0.877	0.911	0.903	0.915	0.917	0.919	0.915	0.932

Table 1B (continued)

Core 142

Garnet Rim

Depth	1170	1175	1203	1203	1265
CaO	8.80	86.0	8.24	8.29	8.78
TiO_2	0.06	0.04	0.03	0.06	0.06
MnO	2.30	3.57	2.53	2.80	4.91
FeO	27.41	26.82	27.96	28.27	25.94
Al_2O_3	21.50	22.10	21.30	20.99	21.50
SiO_2	37.55	36.93	37.93	37.99	36.91
MgO	1.36	1.57	1.71	1.86	1.27
Sum	98.98	99.63	99.70	100.26	99.37
Si	3.013	2.954	3.025	3.022	2.971
Al^{IV}	0.000	0.046	0.000	0.000	0.029
Al^{VI}	2.033	2.038	2.002	1.968	2.010
Ti	0.004	0.002	0.002	0.004	0.004
Mn	0.156	0.242	0.171	0.189	0.335
Fe	1.840	1.794	1.865	1.881	1.746
Mg	0.163	0.187	0.203	0.221	0.152
Ca	0.757	0.737	0.704	0.707	0.757
O	12.000	12.000	12.000	12.000	12.000
Fe/Fe+Mg	0.925	0.916	0.909	0.904	0.932

Table 2A

Core 117

Garnet Core

Depth	654	654	1178	1223	1238	1243	1260	1260	1267
CaO	9.72	9.53	8.78	8.54	8.66	8.14	5.64	4.84	7.13
TiO_2	0.12	0.09	0.06	0.15	0.03	0.13	0.22	0.14	0.10
MnO	8.98	5.24	4.72	10.51	6.82	15.65	15.41	22.23	13.71
FeO	23.57	27.10	26.55	22.44	25.34	18.19	20.74	14.14	20.15
Al_2O_3	21.08	21.63	21.11	21.29	21.29	21.67	21.42	20.00	21.07
SiO_2	37.16	37.21	37.13	37.24	36.35	37.09	35.97	36.91	37.59
MgO	0.69	1.01	1.07	0.98	0.94	0.66	1.61	1.43	1.51
Sum	101.32	101.81	99.42	101.15	99.43	101.53	101.01	99.69	101.26
Si	2.962	2.945	2.993	2.967	2.947	2.950	2.897	3.006	2.988
Al^{IV}	0.038	0.055	0.007	0.033	0.053	0.050	0.103	0.000	0.012
Al^{VI}	1.942	1.962	1.998	1.965	1.980	1.981	1.930	1.919	1.962
Ti	0.007	0.005	0.004	0.009	0.002	0.008	0.013	0.009	0.006
Mn	0.606	0.351	0.322	0.709	0.468	1.054	1.051	1.533	0.923
Fe	1.571	1.794	1.790	1.495	1.718	1.210	1.397	0.963	1.340
Mg	0.082	0.119	0.129	0.116	0.114	0.078	0.193	0.174	0.179
Ca	0.830	0.808	0.758	0.729	0.752	0.694	0.487	0.422	0.607
O	12.000	12.000	12.000	12.000	12.000	12.000	12.000	12.000	12.000
Fe/Fe+Mg	0.964	0.947	0.943	0.950	0.951	0.967	0.927	0.935	0.927

Table 2A (continued)

Core 117

Garnet Core

Depth	1267	1267	1314	1356	1376
CaO	6.71	6.97	6.77	8.40	8.24
TiO_2	0.20	0.04	0.09	0.14	0.06
MnO	14.23	11.76	16.61	10.91	8.11
FeO	19.83	21.90	15.86	21.49	25.30
Al_2O_3	21.16	20.71	20.46	21.39	20.75
SiO_2	37.02	36.84	37.22	37.00	37.13
MgO	1.21	1.79	1.90	0.53	0.88
Sum	100.36	100.01	98.91	99.86	100.47
Si	2.974	2.972	3.014	2.979	2.986
Al^{IV}	0.026	0.028	0.000	0.021	0.014
Al^{VI}	1.977	1.940	1.953	2.009	1.953
Ti	0.012	0.002	0.005	0.008	0.004
Mn	0.968	0.803	1.139	0.744	0.552
Fe	1.332	1.477	1.074	1.447	1.702
Mg	0.145	0.215	0.229	0.064	0.105
Ca	0.578	0.602	0.587	0.725	0.710
O	12.000	12.000	12.000	12.000	12.000
Fe/Fe+Mg	0.941	0.914	0.906	0.972	0.955

Table 2B

Core 142

Garnet Core

Depth	345	345	490	696	696	799	870	870	899
CaO	7.90	8.37	8.43	8.09	9.11	8.87	9.18	9.45	8.32
TiO_2	0.04	0.05	0.08	0.08	0.07	0.14	0.15	0.14	0.10
MnO	3.36	4.65	8.43	8.16	4.99	13.11	8.52	8.43	15.97
FeO	29.30	26.61	24.84	23.83	25.66	18.98	23.70	23.65	17.09
Al_2O_3	21.33	21.59	21.39	20.74	21.82	20.37	20.27	20.44	22.02
SiO_2	36.66	37.44	37.22	37.98	37.15	37.38	37.32	36.88	37.73
MgO	0.94	0.96	0.70	1.30	0.82	0.66	0.71	0.55	0.45
Sum	99.53	99.67	101.09	100.18	99.62	99.51	99.85	99.54	101.68
Si	2.966	3.001	2.970	3.034	2.979	3.022	3.013	2.991	2.980
Al^{IV}	0.034	0.000	0.030	0.000	0.021	0.000	0.000	0.009	0.020
Al^{VI}	2.000	2.039	1.982	1.953	2.041	1.940	1.928	1.944	2.029
Ti	0.002	0.003	0.005	0.005	0.004	0.009	0.009	0.009	0.006
Mn	0.230	0.316	0.570	0.552	0.339	0.898	0.583	0.579	1.068
Fe	1.983	1.784	1.658	1.592	1.721	1.283	1.600	1.604	1.129
Mg	0.113	0.115	0.083	0.155	0.098	0.080	0.085	0.066	0.053
Ca	0.685	0.719	0.721	0.693	0.783	0.768	0.794	0.821	0.704
O	12.000	12.000	12.000	12.000	12.000	12.000	12.000	12.000	12.000
Fe/Fe+Mg	0.951	0.948	0.964	0.933	0.955	0.965	0.962	0.970	0.976

Table 2B (continued)

Core 142

Garnet Core

Depth	899	977	1020	1020	1112	1133	1133	1149	1151
CaO	8.63	8.62	8.79	8.40	9.15	8.44	7.98	7.79	7.92
TiO_2	0.10	0.11	0.22	0.10	0.12	0.06	0.09	0.43	0.02
MnO	9.38	7.16	8.64	7.03	6.04	12.90	13.00	12.22	6.20
FeO	21.51	24.36	24.16	26.02	24.56	17.98	18.71	21.21	25.68
Al_2O_3	22.25	21.34	21.40	21.07	21.29	22.31	22.65	22.13	21.23
SiO_2	36.13	36.54	37.61	36.20	37.38	37.50	37.17	36.98	37.73
MgO	0.64	1.55	0.78	0.94	0.80	2.48	2.17	0.88	1.16
Sum	98.64	99.68	101.60	99.76	99.34	101.67	101.77	101.64	99.94
Si_{IV}	2.932	2.944	2.979	2.937	3.006	2.937	2.916	2.929	3.019
Al^{IV}	0.068	0.056	0.021	0.063	0.000	0.062	0.084	0.071	0.000
Al^{VI}	2.059	1.969	1.977	1.951	2.017	1.995	2.010	1.995	2.002
Ti	0.006	0.007	0.013	0.006	0.007	0.004	0.005	0.026	0.001
Mn	0.645	0.489	0.580	0.483	0.411	0.856	0.864	0.820	0.420
Fe	1.460	1.641	1.600	1.765	1.652	1.177	1.227	1.405	1.718
Mg	0.077	0.186	0.092	0.114	0.096	0.289	0.254	0.104	0.138
Ca	0.750	0.744	0.746	0.730	0.788	0.708	0.671	0.661	0.679
O	12.000	12.000	12.000	12.000	12.000	12.000	12.000	12.000	12.000
Fe/Fe+Mg	0.965	0.920	0.959	0.952	0.956	0.875	0.892	0.955	0.939

Table 2B (continued)

Core 142

Garnet Core

Depth	1156	1164	1164	1164	1170	1170	1175	1203	1265
CaO	6.77	7.74	8.05	7.99	7.94	8.22	7.38	8.51	6.54
TiO_2	0.13	0.17	0.13	0.14	0.10	0.10	0.07	0.13	0.09
MnO	17.30	12.66	1.63	10.32	6.38	9.26	5.95	11.17	5.45
FeO	17.80	21.33	28.59	22.64	25.29	22.09	25.82	21.70	26.40
Al_2O_3	20.73	21.55	21.44	21.38	22.10	21.57	21.92	21.26	21.53
SiO_2	36.73	37.46	37.99	37.59	36.70	37.26	36.91	37.44	37.32
MgO	0.61	0.71	1.57	0.77	1.30	0.81	1.55	0.78	1.49
Sum	100.07	101.62	99.40	100.83	99.81	99.31	99.60	100.99	98.82
Si	2.978	2.973	3.032	2.996	2.943	2.998	2.962	2.984	3.010
Al^{IV}	0.022	0.027	0.000	0.004	0.057	0.002	0.038	0.016	0.000
Al^{VI}	1.958	1.989	2.017	2.003	2.032	2.043	2.035	1.981	2.046
Ti	0.008	0.010	0.008	0.008	0.006	0.006	0.004	0.008	0.005
Mn	1.188	0.851	0.110	0.697	0.433	0.631	0.404	0.754	0.372
Fe	1.207	1.416	1.908	1.509	1.696	1.486	1.733	1.446	1.781
Mg	0.074	0.084	0.187	0.091	0.155	0.098	0.185	0.093	0.179
Ca	0.588	0.658	0.688	0.682	0.682	0.709	0.635	0.727	0.565
O	12.000	12.000	12.000	12.000	12.000	12.000	12.000	12.000	12.000
Fe/Fe+Mg	0.970	0.964	0.915	0.960	0.932	0.956	0.920	0.960	0.923

Table 3A

Core 117

Biotite

Depth	654	654	1178	1178	1223	1223	1238	1238	1243
CaO	0.00	0.00	0.00	0.00	0.00	0.00	0.05	0.03	0.00
TiO_2	1.52	1.46	1.57	1.51	1.80	1.44	1.86	1.21	1.57
MnO	0.12	0.14	0.07	0.12	0.14	0.11	0.14	0.16	0.14
FeO	19.55	19.65	20.46	19.99	20.82	18.88	19.19	19.75	17.69
Al_2O_3	18.27	18.86	17.64	17.43	19.02	18.78	18.88	19.97	19.16
SiO_2	36.20	36.03	35.54	35.87	36.24	36.21	36.32	35.44	36.40
K O	9.02	8.98	8.33	8.38	7.99	8.20	8.49	8.58	8.42
N O	0.14	0.17	0.20	0.17	0.13	0.14	0.24	0.20	0.18
MgO	10.35	10.00	9.97	10.38	10.02	10.45	9.93	9.89	11.39
H_2O	3.94	3.95	3.87	3.88	3.99	3.94	3.96	3.95	3.99
Sum	99.11	99.24	97.65	97.73	100.15	98.15	99.06	99.18	98.94
Si	5.501	5.468	5.500	5.533	5.442	5.508	5.492	5.373	5.467
Al^{IV}	2.499	2.532	2.500	2.467	2.558	2.492	2.508	2.627	2.533
Al^{VI}	0.773	0.841	0.716	0.701	0.807	0.875	0.856	0.941	0.858
Ti	0.174	0.167	0.183	0.175	0.203	0.165	0.212	0.138	0.177
Mn	0.015	0.018	0.009	0.016	0.018	0.014	0.018	0.021	0.018
Fe	2.485	2.494	2.648	2.579	2.615	2.402	2.427	2.504	2.222
Mg	2.344	2.262	2.300	2.386	2.243	2.369	2.238	2.234	2.550
Ca	0.000	0.000	0.000	0.000	0.000	0.000	0.008	0.005	0.000
Na	0.041	0.050	0.060	0.051	0.038	0.041	0.070	0.059	0.052
K	1.748	1.738	1.644	1.649	1.530	1.591	1.637	1.659	1.613
H	4.000	4.000	4.000	4.000	4.000	4.000	4.000	4.000	4.000
O	24.000	24.000	24.000	24.000	24.000	24.000	24.000	24.000	24.000
w	1.790	1.788	1.704	1.699	1.568	1.632	1.716	1.723	1.665
x	5.792	5.782	5.855	5.856	5.886	5.825	5.750	5.839	5.825
Fe/Fe+Mg	0.516	0.526	0.536	0.521	0.540	0.505	0.522	0.530	0.468

Table 3A (continued)

Core 117

Biotite

Depth	1243	1260	1267	1267	1314	1314	1314	1356	1356
CaO	0.00	0.00	0.00	0.00	0.00	0.00	0.00	0.00	0.00
TiO_2	1.37	1.18	1.14	1.12	1.17	1.12	1.03	1.67	1.35
MnO	0.14	0.36	0.46	0.45	0.47	0.43	0.42	0.13	0.17
FeO	17.25	13.64	13.32	13.08	12.43	12.21	12.51	20.09	18.73
Al_2O_3	19.17	18.82	18.18	18.14	18.14	18.56	18.39	18.53	18.57
SiO_2	36.41	38.49	37.33	37.68	38.04	38.41	38.51	36.07	36.42
K_2O	8.49	8.29	8.52	8.69	8.88	8.27	8.64	7.98	8.52
Na_2O	0.18	0.14	0.08	0.08	0.05	0.09	0.15	0.08	0.19
MgO	12.00	15.93	15.55	14.50	15.48	15.95	15.30	9.25	10.41
H_2O	4.00	4.16	4.05	4.02	4.07	4.11	4.09	3.90	3.94
Sum	99.01	101.01	98.63	97.76	98.73	99.15	99.04	97.70	98.30
Si	5.457	5.538	5.521	5.613	5.598	5.595	5.634	5.538	5.539
Al^{IV}	2.543	2.462	2.479	2.387	2.402	2.405	2.366	2.462	2.461
Al^{VI}	0.842	0.728	0.690	0.798	0.744	0.781	0.805	0.891	0.867
Ti	0.154	0.128	0.127	0.125	0.129	0.123	0.113	0.193	0.154
Mn	0.018	0.044	0.058	0.057	0.059	0.053	0.052	0.017	0.022
Fe	2.162	1.641	1.648	1.630	1.530	1.487	1.531	2.580	2.382
Mg	2.680	3.416	3.428	3.220	3.395	3.463	3.337	2.117	2.360
Ca	0.000	0.000	0.000	0.000	0.000	0.000	0.000	0.000	0.000
Na	0.052	0.039	0.023	0.023	0.014	0.025	0.043	0.024	0.056
K	1.623	1.521	1.607	1.651	1.667	1.536	1.612	1.563	1.653
H	4.000	4.000	4.000	4.000	4.000	4.000	4.000	4.000	4.000
O	24.000	24.000	24.000	24.000	24.000	24.000	24.000	24.000	24.000
w	1.675	1.560	1.630	1.674	1.681	1.562	1.655	1.587	1.709
x	5.856	5.957	5.950	5.829	5.857	5.906	5.837	5.797	5.786
Fe/Fe+Mg	0.448	0.330	0.332	0.344	0.319	0.308	0.322	0.551	0.505

Table 3B

Core 142

Biotite

Depth	345	490	490	696	696	799	977	977	1020
CaO	0.00	0.04	0.00	0.00	0.00	0.00	0.00	0.02	0.00
TiO_2	1.28	1.44	1.24	1.54	1.53	1.40	1.35	1.14	1.47
MnO	0.07	0.11	0.12	0.07	0.08	0.13	0.12	0.14	0.10
FeO	17.51	18.49	18.15	19.65	19.30	18.65	16.87	14.85	19.10
Al_2O_3	19.29	19.24	19.46	18.72	18.78	19.19	18.25	18.16	19.12
SiO_2	36.23	37.24	36.32	35.23	35.98	36.51	37.74	36.54	36.40
K_2O	8.28	7.45	7.48	7.84	7.86	8.11	7.96	8.34	8.06
Na_2O	0.21	0.21	0.21	0.13	0.13	0.16	0.14	0.14	0.00
MgO	10.56	11.17	11.34	10.84	11.17	10.27	12.88	13.85	10.45
H_2O	3.93	4.03	3.98	3.9	3.96	3.96	4.04	3.96	3.96
Sum	97.36	99.42	98.30	97.93	98.79	98.38	99.35	97.14	98.66
Si	5.519	5.540	5.470	5.395	5.442	5.524	5.595	5.522	5.500
Al^{IV}	2.481	2.460	2.530	2.605	2.558	2.476	2.405	2.478	2.500
Al^{VI}	0.981	0.914	0.924	0.774	0.788	0.946	0.783	0.757	0.905
Ti	0.147	0.161	0.140	0.177	0.174	0.159	0.151	0.130	0.167
Mn	0.009	0.014	0.015	0.009	0.101	0.017	0.015	0.018	0.013
Fe	2.231	2.301	2.286	2.517	2.441	2.360	2.091	1.877	2.414
Mg	2.398	2.477	2.546	2.474	2.518	2.316	2.846	3.123	2.354
Ca	0.000	0.006	0.000	0.000	0.000	0.000	0.000	0.003	0.000
Na	0.062	0.061	0.061	0.039	0.038	0.047	0.040	0.041	0.000
K	1.609	1.414	1.437	1.531	1.516	1.565	1.505	1.508	1.553
H	4.000	4.000	4.000	4.000	4.000	4.000	4.000	4.000	4.000
O	24.000	24.000	24.000	24.000	24.000	24.000	24.000	24.000	24.000
w	1.671	1.481	1.498	1.570	1.554	1.612	1.545	1.652	1.553
x	5.765	5.866	5.911	5.951	5.932	5.797	5.886	5.901	5.852
Fe/Fe+Mg	0.483	0.483	0.475	0.505	0.493	0.506	0.425	0.378	0.508

Table 3B (continued)

Core 142

Biotite

Depth	1020	1112	1112	1112	1133	1133	1135	1135	1144
CaO	0.00	0.01	0.00	0.00	0.02	0.07	0.00	0.00	0.00
TiO_2	1.49	1.42	1.51	1.54	1.11	1.01	1.07	1.19	1.03
MnO	0.11	0.08	0.08	0.09	0.35	0.30	0.26	0.32	0.21
FeO	19.36	19.35	19.35	19.58	12.28	13.39	12.44	12.73	11.93
Al_2O_3	19.05	19.45	19.22	18.80	15.78	15.77	15.86	15.82	15.72
SiO_2	36.22	36.11	36.26	36.00	39.92	38.51	39.57	39.41	40.42
K_2O	7.99	7.75	8.27	8.12	7.94	7.30	7.60	8.29	7.36
Na_2O	0.00	0.00	0.14	0.14	0.34	0.42	0.29	0.27	0.18
MgO	10.45	10.85	10.01	10.63	17.77	18.81	18.55	16.59	18.99
H_2O	3.96	3.98	3.96	3.95	4.14	4.11	4.14	4.08	4.18
Sum	98.63	99.00	98.80	98.85	99.65	99.69	99.78	98.70	100.01
Si	5.483	5.437	5.488	5.456	5.782	5.609	5.720	5.789	5.793
Al^{IV}	2.517	2.563	2.512	2.544	2.218	2.391	2.280	2.211	2.207
Al^{VI}	0.882	0.887	0.916	0.813	0.476	0.315	0.421	0.527	0.447
Ti	0.170	0.161	0.172	0.176	0.121	0.111	0.116	0.131	0.111
Mn	0.014	0.010	0.010	0.012	0.043	0.037	0.032	0.040	0.025
Fe	2.451	2.436	2.449	2.481	1.488	1.631	1.504	1.564	1.430
Mg	2.358	2.435	2.258	2.401	3.837	4.083	3.997	3.632	4.056
Ca	0.000	0.002	0.000	0.000	0.003	0.011	0.000	0.000	0.000
Na	0.000	0.000	0.041	0.041	0.095	0.119	0.081	0.077	0.050
K	1.543	1.488	1.596	1.570	1.467	1.356	1.401	1.553	1.344
H	4.000	4.000	4.000	4.000	4.000	4.000	4.000	4.000	4.000
O	24.000	24.000	24.000	24.000	24.000	24.000	24.000	24.000	24.000
w	1.543	1.490	1.638	1.611	1.566	1.486	1.482	1.630	1.394
x	5.874	5.929	5.805	5.883	5.964	6.177	6.070	5.894	6.070
Fe/Fe+Mg	0.511	0.501	0.521	0.509	0.285	0.290	0.278	0.306	0.264

Table 3B (continued)

Core 142

Biotite

Depth	1144	1149	1149	1151	1151	1156	1164	1164	1164
CaO	0.00	0.01	0.07	0.00	0.00	0.02	0.00	0.00	0.00
TiO_2	1.00	1.33	1.37	1.18	1.26	1.41	1.35	1.42	1.54
MnO	0.17	0.21	0.22	0.11	0.09	0.11	0.10	0.05	0.11
FeO	12.03	15.14	15.13	18.59	17.89	17.11	18.75	18.52	18.05
Al_2O_3	15.49	20.94	21.81	18.87	19.02	19.63	19.01	18.92	18.93
SiO_2	40.35	36.71	35.13	36.64	36.59	37.30	37.09	37.01	37.11
K_2O	7.20	6.77	8.19	7.74	8.05	7.99	8.32	8.02	8.18
Na_2O	0.18	0.17	0.12	0.07	0.16	0.23	0.17	0.17	0.16
MgO	19.10	12.73	12.17	11.50	10.78	10.83	10.71	10.77	10.73
H_2O	4.17	4.05	4.01	3.98	3.95	4.01	4.00	3.99	3.99
Sum	99.69	98.06	98.22	98.68	97.79	98.64	99.50	98.87	98.80
Si	5.801	5.429	5.248	5.513	5.548	5.570	5.550	5.559	5.570
Al^{IV}	2.199	2.571	2.752	2.487	2.452	2.430	2.450	2.441	2.430
Al^{VI}	0.425	1.078	1.086	0.859	0.946	1.025	0.902	0.907	0.919
Ti	0.108	0.148	0.154	0.134	0.144	0.158	0.152	0.160	0.174
Mn	0.021	0.026	0.028	0.014	0.012	0.014	0.013	0.006	0.014
Fe	1.446	1.873	1.890	2.339	2.268	2.137	2.346	2.326	2.266
Mg	4.093	2.806	2.710	2.579	2.436	2.411	2.389	2.411	2.401
Ca	0.000	0.002	0.011	0.000	0.000	0.003	0.000	0.000	0.000
Na	0.050	0.049	0.035	0.020	0.047	0.067	0.049	0.050	0.047
K	1.320	1.277	1.560	1.485	1.557	1.522	1.588	1.536	1.566
H	4.000	4.000	4.000	4.000	4.000	4.000	4.000	4.000	4.000
O	24.000	24.000	24.000	24.000	24.000	24.000	24.000	24.000	24.000
w	1.370	1.327	1.606	1.506	1.604	1.592	1.637	1.586	1.613
x	6.092	5.931	5.868	5.925	5.805	5.744	5.801	5.811	5.773
Fe/Fe+Mg	0.264	0.404	0.414	0.477	0.483	0.472	0.497	0.492	0.487

Table 3B (continued)

Core 142

Biotite

Depth	1170	1175	1232	1265	1265	1265	1265
CaO	0.00	0.00	0.02	0.00	0.00	0.00	0.00
TiO_2	1.34	1.32	1.34	1.53	1.39	1.53	1.50
MnO	0.11	0.11	0.09	0.11	0.18	0.11	0.12
FeO	18.96	18.21	16.33	19.37	19.52	18.78	18.40
Al_2O_3	18.55	18.64	17.80	18.81	18.98	18.63	18.63
SiO_2	36.80	36.57	38.03	36.74	35.68	36.80	37.06
K_2O	8.05	8.04	7.21	8.69	8.18	8.39	8.51
Na_2O	0.16	0.21	0.00	0.09	0.08	0.14	0.18
MgO	10.47	11.35	12.92	10.60	10.95	10.46	10.38
H_2O	3.96	3.97	4.01	4.00	3.95	3.97	3.97
Sum	98.40	98.42	97.75	99.94	98.91	98.81	98.75
Si	5.573	5.523	5.685	5.507	5.410	5.556	5.589
Al^{IV}	2.427	2.477	2.315	2.493	2.590	2.444	2.411
Al^{VI}	0.884	0.841	0.821	0.830	0.800	0.870	0.899
Ti	0.153	0.150	0.151	0.172	0.158	0.174	0.170
Mn	0.014	0.014	0.011	0.014	0.023	0.014	0.015
Fe	2.401	2.300	2.042	2.428	2.475	2.371	2.321
Mg	2.363	2.555	2.879	2.368	2.474	2.354	2.333
Ca	0.000	0.000	0.003	0.000	0.000	0.000	0.000
Na	0.047	0.061	0.000	0.026	0.024	0.041	0.053
K	1.555	1.549	1.375	1.661	1.582	1.616	1.637
H	4.000	4.000	4.000	4.000	4.000	4.000	4.000
O	24.000	24.000	24.000	24.000	24.000	24.000	24.000
w	1.602	1.610	1.378	1.688	1.605	1.657	1.690
x	5.815	5.860	5.903	5.813	5.932	5.783	5.739
Fe/Fe+Mg	0.505	0.475	0.416	.508	0.502	0.503	0.500

Table 4A

Core 117

Chlorite

Depth	654	1232	1232	1238	1243	1243	1260	1260	1267
CaO	0.00	0.00	0.00	0.15	0.00	0.00	0.00	0.00	0.00
TiO_2	0.09	0.05	0.06	0.02	0.05	0.02	0.05	0.02	0.03
MnO	0.21	0.21	0.16	0.25	0.24	0.32	0.65	0.63	0.66
FeO	25.25	25.05	24.11	25.41	23.15	22.73	14.86	16.47	16.76
Al_2O_3	22.58	23.52	23.64	23.43	22.51	23.41	23.02	22.89	22.53
SiO_2	25.93	24.89	24.56	24.77	25.01	25.01	27.24	26.73	26.02
K_2O	0.01	0.00	0.04	0.00	0.01	0.00	0.00	0.00	0.01
Na_2O	0.00	0.00	0.00	0.00	0.00	0.00	0.00	0.00	0.00
MgO	14.15	14.61	14.82	14.93	15.76	16.06	22.42	22.14	21.46
H_2O	11.50	11.50	11.42	11.54	11.38	11.53	12.12	12.09	11.85
Sum	99.72	99.83	98.81	100.50	98.11	99.08	100.36	100.97	99.32
Si	5.406	5.187	5.154	5.142	5.267	5.200	5.384	5.298	5.261
Al^{IV}	2.594	2.813	2.846	2.858	2.733	2.800	2.616	2.702	2.739
Al^{VI}	2.952	2.964	3.000	2.874	2.853	2.936	2.746	2.644	2.628
Ca	0.000	0.000	0.000	0.033	0.000	0.000	0.000	0.000	0.000
Ti	0.014	0.008	0.009	0.003	0.008	0.003	0.007	0.003	0.005
Mn	0.037	0.037	0.028	0.044	0.043	0.056	0.109	0.106	0.113
Fe	4.402	4.366	4.231	4.412	4.077	3.953	2.456	2.730	2.834
K	0.003	0.000	0.011	0.000	0.003	0.000	0.000	0.000	0.003
Na	0.000	0.000	0.000	0.000	0.000	0.000	0.000	0.000	0.000
Mg	4.397	4.539	4.636	4.620	4.947	4.977	6.605	6.541	6.467
H	16.000	16.000	16.000	16.000	16.000	16.000	16.000	16.000	16.000
O	36.000	36.000	36.000	36.000	36.000	36.000	36.000	36.000	36.000
x	11.805	11.913	11.916	11.986	11.930	11.926	11.924	12.023	12.049
Fe/Fe+Mg	0.502	0.492	0.479	0.491	0.454	0.446	0.280	0.302	0.313

Table 4A (continued)

Core 117

Chlorite

Depth	1314	1314	1356	1376	1376
CaO	0.00	0.00	0.02	0.00	0.00
TiO_2	0.02	0.04	0.02	0.02	0.02
MnO	0.63	0.57	0.24	0.29	0.30
FeO	15.37	14.64	25.39	24.66	24.69
Al_2O_3	22.78	22.93	22.91	23.37	22.50
SiO_2	26.70	26.96	24.53	25.26	25.24
K_2O	0.00	0.00	0.00	0.01	0.00
Na_2O	0.00	0.00	0.00	0.02	0.01
MgO	21.36	21.82	13.57	13.85	14.94
H_2O	11.89	11.96	11.24	11.42	11.42
Sum	98.75	98.92	97.92	98.90	99.12
Si	5.381	5.401	5.232	5.302	5.295
Al^{IV}	2.619	2.599	2.768	2.698	2.705
Al^{VI}	2.791	2.813	2.990	3.081	2.857
Ca	0.000	0.000	0.005	0.000	0.000
Ti	0.003	0.006	0.003	0.003	0.003
Mn	0.108	0.097	0.043	0.052	0.053
Fe	2.590	2.453	4.529	4.328	4.331
K	0.000	0.000	0.000	0.003	0.000
Na	0.000	0.000	0.000	0.008	0.004
Mg	6.416	6.515	4.314	4.333	4.671
H	16.000	16.000	16.000	16.000	16.000
O	36.000	36.000	36.000	36.000	36.000
x	11.908	11.884	11.883	11.808	11.920
Fe/Fe+Mg	0.296	0.281	0.515	0.503	0.484

Table 4B

Core 142

Chlorite

Depth	345	345	490	696	696	799	799	862	870
CaO	0.04	0.01	0.02	0.00	0.00	0.00	0.00	0.03	0.00
TiO_2	0.06	0.19	0.03	0.06	0.10	0.20	0.11	0.01	0.03
MnO	0.05	0.05	0.16	0.16	0.16	0.18	0.18	0.19	0.18
FeO	24.15	22.47	22.98	23.58	24.25	23.07	23.94	15.98	23.59
Al_2O_3	24.91	23.16	23.85	23.15	22.62	23.04	23.39	22.87	22.16
SiO_2	25.98	25.64	25.04	24.80	24.95	25.83	25.30	27.09	26.18
K_2O	0.00	0.00	0.02	0.00	0.06	0.86	0.46	0.00	0.00
Na_2O	0.00	0.00	0.00	0.00	0.00	0.02	0.00	0.00	0.00
MgO	14.55	15.32	15.16	16.34	15.68	14.98	14.57	23.45	15.05
H_2O	11.82	11.49	11.49	11.54	11.46	11.56	11.50	12.25	11.46
Sum	101.56	98.33	98.75	99.64	99.28	99.74	99.45	101.87	98.65
Si	5.269	5.350	5.221	5.149	5.218	5.356	5.274	5.299	5.475
Al^{IV}	2.731	2.650	2.779	2.851	2.782	2.644	2.726	2.701	2.525
Al^{VI}	3.222	3.044	3.082	2.816	2.793	2.985	3.021	2.571	2.935
Ca	0.009	0.002	0.004	0.000	0.000	0.000	0.000	0.006	0.000
Ti	0.009	0.030	0.005	0.009	0.016	0.031	0.017	0.001	0.005
Mn	0.009	0.009	0.028	0.028	0.028	0.032	0.032	0.031	0.032
Fe	4.096	3.921	4.007	4.095	4.242	4.000	4.174	2.614	4.125
K	0.000	0.000	0.005	0.000	0.016	0.227	0.122	0.000	0.000
Na	0.000	0.000	0.000	0.000	0.000	0.008	0.000	0.000	0.000
Mg	4.398	4.764	4.712	5.057	4.888	4.630	4.527	6.837	4.691
H	16.000	16.000	16.000	16.000	16.000	16.000	16.000	16.000	16.000
O	36.000	36.000	36.000	36.000	36.000	36.000	36.000	36.000	36.000
x	11.742	11.770	11.843	12.005	11.983	11.913	11.893	12.061	11.788
Fe/Fe+Mg	0.483	0.452	0.461	0.449	0.466	0.466	0.482	0.279	0.470

Table 4B (continued)

Core 142

Chlorite

Depth	870	899	899	899	977	1112	1112	1133	1133
CaO	0.04	0.02	0.01	0.00	0.06	0.00	0.00	0.02	0.04
TiO_2	0.02	0.08	0.08	0.08	0.05	0.04	0.03	0.10	0.07
MnO	0.20	0.20	0.19	0.18	0.21	0.57	0.14	0.51	0.49
FeO	23.73	22.67	23.14	22.59	19.54	14.64	24.90	14.95	13.39
Al_2O_3	22.58	23.70	23.59	23.74	22.60	22.93	23.41	21.88	22.46
SiO_2	26.70	26.30	26.01	26.18	25.56	26.96	24.75	27.31	27.09
K_2O	0.00	0.00	0.00	0.01	0.00	0.00	0.01	0.00	0.00
Na_2O	0.00	0.05	0.02	0.04	0.00	0.00	0.00	0.00	0.00
MgO	14.84	14.83	14.57	14.84	20.40	21.82	15.36	23.11	24.10
H_2O	11.60	11.63	11.56	11.61	11.82	11.96	11.54	12.06	12.12
Sum	99.71	99.48	99.17	99.27	100.24	98.92	100.14	99.94	99.76
Si	5.516	5.418	5.390	5.403	5.181	5.401	5.142	5.429	5.358
Al^{IV}	2.484	2.582	2.610	2.597	2.819	2.599	2.858	2.571	2.642
Al^{VI}	3.013	3.170	3.151	3.177	2.578	2.813	2.872	2.554	2.592
Ca	0.009	0.004	0.002	0.000	0.013	0.000	0.000	0.004	0.008
Ti	0.003	0.012	0.012	0.012	0.008	0.006	0.005	0.015	0.010
Mn	0.035	0.035	0.033	0.031	0.036	0.097	0.025	0.086	0.082
Fe	4.100	3.905	4.010	3.899	3.312	2.453	4.326	2.485	2.215
K	0.000	0.000	0.000	0.003	0.000	0.000	0.003	0.000	0.000
Na	0.000	0.020	0.008	0.016	0.000	0.000	0.000	0.000	0.000
Mg	4.570	4.553	4.501	4.565	6.163	6.515	4.756	6.847	7.104
H	16.000	16.000	16.000	16.000	16.000	16.000	16.000	16.000	16.000
O	36.000	36.000	36.000	36.000	36.000	36.000	36.000	36.000	36.000
x	11.729	11.701	11.718	11.704	12.110	11.884	11.987	11.991	12.012
Fe/Fe+Mg	0.475	0.464	0.473	0.463	0.352	0.281	0.478	0.273	0.244

Table 4B (continued)

Core 142

Chlorite

Depth	1135	1144	1144	1149	1149	1149	1151	1156	1164
CaO	0.04	0.00	0.02	0.00	0.02	0.05	0.01	0.01	0.00
TiO	0.09	0.06	0.03	0.09	0.06	0.06	0.05	0.05	0.03
MnO	0.44	0.36	0.28	0.43	0.34	0.38	0.20	0.23	0.17
FeO	15.61	14.47	14.83	19.09	19.45	17.73	22.16	22.71	23.96
Al_2O_3	21.71	21.76	22.23	25.10	23.89	28.48	24.00	23.45	22.48
SiO_2	27.80	27.38	27.63	26.33	26.02	24.69	25.26	25.27	25.29
K_2O	0.00	0.00	0.01	0.00	0.00	0.00	0.00	0.00	0.00
Na_2O	0.00	0.00	0.00	0.00	0.00	0.00	0.00	0.00	0.00
MgO	20.55	24.13	25.09	17.72	18.37	16.91	16.23	15.88	15.08
H_2O	11.83	12.13	12.38	11.98	11.84	12.00	11.63	11.55	11.39
Sum	98.07	100.29	102.50	100.74	99.99	100.30	99.54	99.15	98.40
Si	5.631	5.410	5.347	5.269	5.267	4.930	5.203	5.243	5.323
Al^{IV}	2.369	2.590	2.653	2.731	2.733	3.070	2.797	2.757	2.677
Al^{VI}	2.814	2.477	2.417	4.188	2.965	3.630	3.028	2.977	2.898
Ca	0.009	0.000	0.004	0.000	0.004	0.011	0.002	0.002	0.000
Ti	0.014	0.009	0.004	0.014	0.009	0.009	0.008	0.008	0.005
Mn	0.075	0.060	0.046	0.073	0.058	0.064	0.035	0.040	0.030
Fe	2.644	2.391	2.400	3.195	3.292	2.960	3.817	3.941	4.217
K	0.000	0.000	0.002	0.000	0.000	0.000	0.000	0.000	0.000
Na	0.000	0.000	0.000	0.000	0.000	0.000	0.000	0.000	0.000
Mg	6.205	7.107	7.238	5.285	5.542	5.032	4.983	4.911	4.731
H	16.000	16.000	16.000	16.000	16.000	16.000	16.000	16.000	16.000
O	36.000	36.000	36.000	36.000	36.000	36.000	36.000	36.000	36.000
x	11.761	12.045	12.112	11.755	11.872	11.707	11.873	11.879	11.882
Fe/Fe+Mg	0.305	0.256	0.253	0.382	0.377	0.375	0.436	0.448	0.473

Table 4B (continued)

Core 142

Chlorite

Depth	1164	1164	1170	1170	1175	1203	1265	1265
CaO	0.00	0.00	0.00	0.00	0.00	0.00	0.00	0.00
TiO_2	0.06	0.07	0.06	0.09	0.04	0.04	0.10	0.06
MnO	0.16	0.18	0.16	0.17	0.20	0.23	0.52	0.21
FeO	24.00	23.88	24.83	24.48	24.37	24.07	23.33	23.54
Al_2O_3	22.59	21.95	23.13	23.39	23.39	22.65	22.31	22.64
SiO_2	25.36	26.05	24.56	25.31	25.06	24.81	26.59	25.82
K_2O	0.15	0.00	0.01	0.00	0.05	0.00	0.45	0.37
Na_2O	0.00	0.00	0.00	0.00	0.00	0.00	0.00	0.00
MgO	14.65	14.61	14.90	15.20	14.88	16.09	13.55	14.58
H_2O	11.37	11.38	11.40	11.59	11.49	11.47	11.40	11.43
Sum	98.34	98.12	99.05	100.23	99.48	99.36	98.25	98.65
Si	5.343	5.488	5.162	5.235	5.225	5.183	5.589	5.412
Al^{IV}	2.657	2.512	2.838	2.765	2.775	2.817	2.411	2.588
Al^{VI}	2.952	2.936	2.890	2.935	2.971	2.758	3.115	3.003
Ca	0.000	0.000	0.000	0.000	0.000	0.000	0.000	0.000
Ti	0.010	0.011	0.009	0.014	0.006	0.006	0.016	0.009
Mn	0.029	0.032	0.028	0.030	0.035	0.041	0.093	0.037
Fe	4.229	4.207	4.364	4.234	4.249	4.205	4.101	4.126
K	0.040	0.000	0.003	0.000	0.013	0.000	0.121	0.099
Na	0.000	0.000	0.000	0.000	0.000	0.000	0.000	0.000
Mg	4.601	4.587	4.668	4.686	4.624	5.010	4.246	4.555
H	16.000	16.000	16.000	16.000	16.000	16.000	16.000	16.000
O	36.000	36.000	36.000	36.000	36.000	36.000	36.000	36.000
x	11.860	11.774	11.963	11.898	11.899	12.020	11.690	11.830
Fe/Fe+Mg	0.481	0.480	0.485	0.476	0.481	0.459	0.497	0.478

Table 5A

Core 117

Muscovite

Depth	1238	1243	1376
CaO	0.00	0.00	0.00
TiO_2	0.35	0.33	0.30
MnO	0.00	0.06	0.04
FeO	1.64	1.24	1.69
Al_2O_3	35.85	35.71	34.80
SiO_2	46.91	46.31	46.58
K_2O	9.34	9.35	8.59
Na_2O	0.96	1.13	1.00
MgO	0.94	1.01	1.12
H_2O	4.56	4.52	4.49
Sum	100.55	99.66	98.61
Si	6.165	6.141	6.222
Al^{IV}	1.835	1.859	1.778
Al^{VI}	3.717	3.720	3.699
Ti	0.035	0.033	0.030
Fe	0.180	0.138	0.189
Mg	0.184	0.200	0.223
Mn	0.000	0.007	0.005
Ca	0.000	0.000	0.000
Na	0.245	0.291	0.259
K	1.566	1.581	1.463
H	4.000	4.000	4.000
O	24.000	24.000	24.000
w	1.810	1.872	1.722
x	4.116	4.097	4.145
Fe/Fe+Mg			

Table 5B

Core 142

Muscovite

Depth	345	696	799	1112	1151	1164	1203	1203	1265	1265
CaO	0.00	0.00	0.00	0.00	0.00	0.00	0.00	0.00	0.00	0.00
TiO_2	0.25	0.37	0.33	0.27	0.31	0.28	0.41	0.29	0.30	0.33
MnO	0.00	0.00	0.00	0.00	0.01	0.00	0.03	0.00	0.05	0.01
FeO	1.44	2.51	1.64	1.50	1.78	1.82	1.59	1.48	2.95	1.93
Al_2O_3	35.11	33.91	33.60	35.20	34.86	32.07	34.57	34.71	33.77	34.29
SiO_2	46.70	44.73	46.50	47.01	47.09	48.64	46.26	46.34	45.38	47.04
K_2O	8.32	8.89	9.44	8.77	8.62	9.52	9.02	8.91	8.96	9.41
Na_2O	1.39	1.14	0.91	0.82	0.44	0.71	0.95	1.00	0.88	1.10
MgO	0.82	1.43	1.18	1.05	1.12	1.71	1.16	0.99	2.15	1.13
H_2O	4.49	4.38	4.44	4.52	4.50	4.50	4.47	4.46	4.44	4.51
Sum	98.52	97.36	98.04	99.14	98.73	99.25	98.46	98.18	98.88	99.74
Si	6.227	6.113	6.278	6.235	6.264	6.476	6.205	6.222	6.117	6.250
Al^{IV}	1.771	1.887	1.722	1.765	1.736	1.524	1.795	1.778	1.883	1.750
Al^{VI}	3.747	3.573	3.624	3.736	3.729	3.507	3.669	3.713	3.481	3.619
Ti	0.025	0.038	0.034	0.027	0.031	0.028	0.041	0.029	0.030	0.033
Fe	0.161	0.287	0.185	0.166	0.198	0.203	0.178	0.166	0.333	0.214
Mg	0.163	0.291	0.237	0.208	0.222	0.339	0.232	0.198	0.432	0.222
Mn	0.000	0.000	0.000	0.000	0.001	0.000	0.003	0.000	0.006	0.001
Ca	0.000	0.000	0.000	0.000	0.000	0.000	0.000	0.000	0.000	0.000
Na	0.359	0.302	0.238	0.211	0.113	0.183	0.247	0.260	0.230	0.283
K	1.415	1.550	1.626	1.484	1.463	1.617	1.543	1.526	1.541	1.595
H	4.000	4.000	4.000	4.000	4.000	4.000	4.000	4.000	4.000	4.000
O	24.000	24.000	24.000	24.000	24.000	24.000	24.000	24.000	24.000	24.000
w	1.775	1.852	1.864	1.694	1.576	1.800	1.790	1.786	1.770	1.878
x	4.096	4.190	4.080	4.137	4.181	4.077	4.124	4.107	4.282	4.090
Fe/Fe+Mg	0.596	0.496	0.438	0.445	0.473	0.374	0.439	0.456	0.439	0.493

Table 6

Amphibole

Hornblende

Depth	862	862	862	977	977	1133	1133	1135	1144 (Core)
CaO	12.05	12.58	12.62	11.38	11.54	11.88	11.84	11.52	11.73
TiO_2	0.10	0.13	0.10	0.39	0.34	0.09	0.10	0.20	0.08
MnO	0.23	0.23	0.25	0.25	0.23	0.79	0.79	0.89	0.55
FeO	9.13	10.03	9.56	14.71	15.07	8.72	7.95	10.30	10.20
Al_2O_3	5.98	8.45	6.43	17.39	16.96	5.20	5.02	7.43	5.12
SiO_2	52.04	50.20	51.38	42.35	42.31	52.18	52.47	49.75	51.27
K_2O	0.00	0.05	0.04	0.33	0.30	0.03	0.00	0.07	0.02
Na_2O	0.57	0.80	0.52	1.70	1.71	0.70	0.66	0.97	0.68
MgO	16.84	15.61	17.11	8.57	8.62	17.34	18.70	14.84	17.61
H_2O	2.10	2.11	2.11	2.02	2.02	2.10	2.12	2.05	2.09
Sum	99.04	100.19	100.12	99.09	99.10	99.03	99.65	98.02	99.35
Si	7.425	7.142	7.293	6.269	6.279	7.458	7.427	7.253	7.361
Al^{IV}	0.575	0.858	0.707	1.731	1.721	0.542	0.573	0.747	0.639
Al^{VI}	0.431	0.558	0.368	1.302	1.245	0.334	0.265	0.530	0.227
Ti	0.011	0.014	0.011	0.043	0.038	0.010	0.011	0.022	0.009
Mn	0.028	0.028	0.030	0.031	0.029	0.096	0.095	0.110	0.067
Fe	1.089	1.193	1.135	1.821	1.870	1.042	0.941	1.256	1.225
Mg	3.581	3.310	3.620	1.891	1.907	3.694	3.945	3.225	3.768
Ca	1.842	1.917	1.919	1.805	1.835	1.819	1.796	1.800	1.804
K	0.000	0.009	0.007	0.062	0.057	0.005	0.000	0.013	0.004
Na	0.158	0.221	0.143	0.488	0.492	0.194	0.181	0.274	0.189
H	2.000	2.000	2.000	2.000	2.000	2.000	2.000	2.000	2.000
O	24.000	24.000	24.000	24.000	24.000	24.000	24.000	24.000	24.000
w	2.000	2.147	2.070	2.355	2.384	2.019	1.977	2.087	1.997
x	5.140	5.103	5.164	5.089	5.089	5.175	5.257	5.143	5.296
Fe/Fe+Mg	0.238	0.269	0.243	0.495	0.499	0.236	0.208	0.298	0.255

Table 6 (continued)

Amphibole

	Hornblende			Actinolite		Cummingtonite		
Depth	1144 (Core)	1144 (Core)	1144 (Core)	1144 (Core)	1144 (Core)	1144 (Rim)	1144 (Rim)	1144 (Rim)
CaO	11.95	11.43	11.55	10.78	11.79	0.96	1.03	0.65
TiO_2	0.12	0.11	0.12	0.03	0.03	0.01	0.00	0.00
MnO	0.57	0.74	0.71	0.86	0.60	2.40	2.15	2.02
FeO	10.14	10.16	10.61	9.97	9.18	20.10	18.51	15.54
Al_2O_3	5.68	4.48	6.17	2.34	2.87	0.32	0.31	0.44
SiO_2	51.31	52.48	51.21	52.74	54.33	53.70	54.05	56.29
K_2O	0.04	0.09	0.07	0.00	0.00	0.00	0.00	0.00
Na_2O	0.76	0.56	0.77	0.21	0.35	0.00	0.00	0.02
MgO	17.13	17.69	16.39	20.81	19.75	19.40	20.80	22.62
H_2O	2.10	2.10	2.09	2.10	2.14	2.04	2.06	2.12
Sum	99.80	99.84	99.69	99.84	101.04	98.93	98.91	99.70
Si	7.334	7.479	7.335	7.511	7.602	7.879	7.865	7.967
Al^{IV}	0.666	0.521	0.665	0.393	0.398	0.055	0.053	0.033
Al^{VI}	0.291	0.232	0.376	0.000	0.075	0.000	0.000	0.041
Ti	0.013	0.012	0.013	0.003	0.003	0.001	0.000	0.000
Mn	0.069	0.089	0.086	0.104	0.071	0.298	0.265	0.242
Fe	1.212	1.211	1.271	1.187	1.074	2.466	2.253	1.839
Mg	3.650	3.758	3.499	4.417	4.119	4.242	4.511	4.772
Ca	1.830	1.745	1.772	1.645	1.768	0.151	0.161	0.099
K	0.007	0.016	0.013	0.000	0.000	0.000	0.000	0.000
Na	0.211	0.155	0.214	0.058	0.095	0.000	0.000	0.005
H	2.000	2.000	2.000	2.000	2.000	2.000	2.000	2.000
O	24.000	24.000	24.000	24.000	24.000	24.000	24.000	24.000
w	2.048	1.916	1.999	1.703	1.862	0.151	0.161	0.104
x	5.235	5.301	5.245	5.712	5.343	7.008	7.029	6.895
Fe/Fe+Mg	0.260	0.257	0.279	0.226	0.218	0.395	0.358	0.304

Table 7A

Core 117

Plagioclase

Depth	654	1178	1223 (Rim)	1223 (Core)	1223 (Core)	1223 (Rim)	1223 Average	1238	1243
CaO	5.11	0.61	4.45	5.31	5.01	3.81	4.64	5.49	5.31
Fe_2O_3	0.00	0.00	0.29	0.26	0.22	0.16	0.22	0.11	0.00
Al_2O_3	23.12	19.45	23.93	25.11	24.78	23.96	24.44	25.04	23.54
SiO_2	63.01	67.78	61.93	60.43	61.79	62.47	61.65	60.52	62.00
K_2O	0.07	0.07	0.03	0.00	0.00	0.00	0.00	0.07	0.06
Na_2O	8.72	11.24	8.31	8.43	8.08	8.96	8.44	8.64	8.65
Sum	100.03	99.15	98.94	99.54	99.88	99.36	99.39	99.87	99.56
Si	2.787	2.987	2.763	2.695	2.733	2.773	2.741	2.694	2.760
Al^{IV}	1.205	1.010	1.237	1.305	1.267	1.227	1.259	1.306	1.235
Al^{VI}	0.000	0.000	0.020	0.014	0.025	0.026	0.022	0.007	0.000
Fe^{3+}	0.000	0.000	0.010	0.009	0.007	0.005	0.007	0.004	0.000
Ca	0.242	0.029	0.213	0.254	0.237	0.181	0.221	0.262	0.253
Na	0.748	0.960	0.719	0.729	0.693	0.771	0.728	0.746	0.746
K	0.004	0.004	0.002	0.000	0.000	0.000	0.000	0.004	0.003
O	8.000	8.000	8.000	8.000	8.000	8.000	8.000	8.000	8.000

Table 7B

Core 142

Plagioclase

Depth	345	345	696	862	870	977	977	1151	1232
CaO	3.28	3.18	4.31	5.73	4.35	4.21	5.23	4.78	3.92
Fe_2O_3	0.10	0.10	0.00	0.26	0.00	0.04	0.12	0.20	0.00
Al_2O_3	22.94	22.64	22.57	24.74	22.59	24.01	24.71	23.79	22.44
SiO_2	64.13	64.13	63.13	60.80	63.26	63.18	61.28	62.42	64.44
K_2O	0.00	0.00	0.06	0.07	0.08	0.00	0.03	0.02	0.06
Na_2O	9.27	9.25	9.45	7.73	9.18	8.99	8.32	8.60	9.58
Sum	99.72	99.30	99.52	99.33	99.46	100.43	99.69	99.81	100.44
Si	2.828	2.838	2.806	2.713	2.810	2.776	2.722	2.765	2.831
Al^{IV}	1.172	1.162	1.182	1.287	1.183	1.224	1.278	1.235	1.162
Al^{VI}	0.020	0.019	0.000	0.013	0.000	0.019	0.016	0.007	0.000
Fe^{3+}	0.003	0.003	0.000	0.009	0.000	0.001	0.004	0.007	0.000
Ca	0.155	0.151	0.205	0.274	0.207	0.198	0.249	0.227	0.185
Na	0.792	0.794	0.814	0.669	0.791	0.766	0.717	0.739	0.816
K	0.000	0.000	0.003	0.004	0.005	0.000	0.002	0.001	0.003
O	8.000	8.000	8.000	8.000	8.000	8.000	8.000	8.000	8.000

Table 8

Core 142

Clinozoisite

Depth	862	862	870	1232	1232
CaO	23.21	23.26	22.32	22.28	22.53
TiO_2	0.02	0.00	0.07	0.15	0.18
MnO	0.07	0.07	0.26	0.26	0.30
Fe_2O_3	2.07	1.77	7.43	5.75	6.01
Al_2O_3	32.75	32.96	26.42	29.11	29.00
SiO_2	39.47	39.86	38.53	38.60	40.28
MgO	0.05	0.05	0.00	0.07	0.00
H_2O	1.97	1.98	1.87	1.91	1.96
Sum	99.61	99.95	96.90	98.13	100.26
Si	3.004	3.019	3.079	3.023	3.084
Al^{IV}	0.000	0.000	0.000	0.000	0.000
Al^{VI}	2.938	2.941	2.488	2.687	2.616
Fe^{3+}	0.119	0.101	0.447	0.339	0.346
Mn	0.005	0.004	0.018	0.017	0.019
Ti	0.001	0.000	0.004	0.009	0.010
Mg	0.006	0.006	0.000	0.008	0.000
Ca	1.893	1.887	1.911	1.870	1.848
H	1.000	1.000	1.000	1.000	1.000
O	13.000	13.000	13.000	13.000	13.000
Ps	3	3	15	11	12

VITA

Walter T. Staten was born in San Francisco, California, on October 3, 1949. He attended Pepperdine College in Los Angeles, California, and Foothill Community College in Los Altos, California, receiving an Associate of Arts degree in 1971. Continuing his education, he attended Washington State University and California State University, Hayward, California, and received a Bachelor of Science degree in Geology in 1973. In the fall, 1974, he entered the graduate school of Virginia Polytechnic Institute and State University. Upon completion of graduate studies, he will begin employment with the Refractories Division of the Carborundum company.

Walter T. Staten

Walter T. Staten

A CHEMICAL STUDY OF THE SILICATE MINERALS OF THE GREAT GOSSAN LEAD AND SURROUNDING ROCKS IN SOUTHWESTERN VIRGINIA

by

Walter T. Staten

(ABSTRACT)

Samples of garnet-grade Ashe formation schists, gneisses, and amphibolites from two drill holes through the Great Gossan Lead in southwestern Virginia have been studied petrographically and chemically. Metamorphic temperatures determined from the muscovite-paragonite solvus, the muscovite-calcite-quartz system, and Fe-Mg distribution in biotite and garnet are approximately 400-460°C. Using the sphalerite geobarometer, metamorphic pressures were found to have been equal to or greater than 4 kbar.

Fine- to medium-grained garnet-chlorite-biotite-quartz-muscovite schists and gneisses predominate. Other lithologies include thin layers of hornblende amphibolite, sulfide ore, quartz veins, thin layers of hornblendic gneiss, marble lenses and minor solution cavities. The coarser-grained ore zone lithologies are dominated by chlorite, hornblende and actinolite-tremolite with cummingtonite rims, calcite, and quartz. Garnet-chlorite and garnet-biotite selvages are also occasionally found in the ore zone.

The ferromagnesian minerals show marked iron depletion within 2-5 feet of the sulfide ore. Ore zone chlorite and biotite show a significant increase in magnesium; garnets show a similar increase in manganese.

The cores of garnets from the ore zone show the influence of the ore even at the earliest stages of garnet growth, indicating that the ore was present prior to the peak of metamorphism. The distribution coefficients for Fe $\rightleftarrows$ Mg exchange reactions for garnet-biotite and garnet-chlorite also indicate that the ore and the surrounding rocks were metamorphosed together. Therefore, hypotheses for a synsedimentary or early hydrothermal origin for the ore are favored over those suggesting a post-metamorphic hydrothermal origin.